Inhalable Macromolecular Prodrugs of Ciprofloxacin for the Treatment of Pulmonary Intracellular Bacterial Infections

Debobrato Das

A dissertation

submitted in partial fulfillment of the

requirements for the degree of

Doctor of Philosophy

University of Washington

2017

Reading Committee:

Patrick Stayton, Chair

Daniel Ratner, Chair

Anthony Convertine

Program Authorized to Offer Degree:

Bioengineering

University of Washington

Abstract

Inhalable Macromolecular Prodrugs of Ciprofloxacin for the Treatment of Pulmonary Intracellular Bacterial Infections

Debobrato Das

Chair of the Supervisory Committee:
Professor Patrick Stayton
Professor Daniel Ratner
Department of Bioengineering

Alveolar intracellular bacterial infections, such as those caused by *Burkholderia pseudomallei* and *Francisella tularensis*, are one of the most challenging infectious disease settings where the appropriate treatment of these pulmonary pathogens remains an important unmet clinical need. In this thesis, we outline the design and development of an inhalable macromolecular prodrug technology against airborne *F. tularensis* (pulmonary tularemia). *Francisella* is an infectious bacterium with a high global burden, historical precedence of being weaponized for biological warfare, and is currently classified by the U.S. Centers for Disease Control and Prevention as a Tier 1 bioagent capable of mass public harm and casualty. The current standards of care for treating respiratory infections of *F. tularensis* relies on rigorous prolonged applications of oral and intravenous antibiotics. In greater than forty-percent of cases, these therapies clinically fail to clear the bacterial infection due to poor pulmonary biodistribution and sustained localized drug concentrations causing a high-rate of fatality and disease relapse.

Direct pulmonary drug delivery offers a unique opportunity to control drug concentrations at the site of bacterial persistence, and is gaining popularity as an attractive strategy for the treatment of pulmonary infections. Inhalable free-drug dispersions and liposomal based antibiotic formulations have been clinically exploited against bacteria such as *Pseudomonas aeruginosa* in cystic fibrosis patients, however, with limited success due to poor pulmonary pharmacokinetics brought on by rapid drug release, low drug encapsulation efficiencies, and complex formulations procedures that affect manufacturing scalability and reproducibility. To address these limitations, we have synthesized polymeric prodrugs with high-drug densities of a model antibiotic, ciprofloxacin, from polymerizable drug monomers that can provide rapid extended therapy against respiratory tularemia and reduce drug dosing.

Our macromolecular ciprofloxacin prodrugs deliver sustained release of antibiotics via ester hydrolysis from engineered chemically-labile drug-linkers, with the ability to control drug release kinetics with the choice of various linkers and polymer architecture. Specifically, ciprofloxacin polymeric prodrugs derived from a phenolic ester modified drug linker showed faster hydrolysis kinetics in human serum with 50% of the drug released within 5d, whereas constructs with an alkyllic ester linkage demonstrated similar release over 22d. Using a quantitative LC-MS approach, this difference in drug release was also captured *in vivo* with pulmonary drug half-lives of 9.3h and 15.6h from the phenol and alkyllic ester macromolecular prodrugs, respectively. Establishing appropriate *in vivo* antibiotic pharmacokinetic-pharmacodynamic profiles is critical for promoting therapeutic efficacy. We observed that having a slower alkyl-ester modified drug linker within these unimeric copolymer morphologies although provides improved stability, it fails to meet specific PK-PD thresholds necessary for efficacy. This was further supported by evaluations using lethal aerosol exposures of *F. tularensis* in murine challenge models where we

demonstrated enhanced survival rates with the endotrachaelly administered fast-releasing macromolecular prodrugs compared to slower-releasing variants and free drug controls.

Modifying the polymer architecture provided an alternative approach to alter and control drug release profiles. Systematic hydrolysis studies in human serum showed that diblock copolymers where the drug was segregated to a second hydrophobic segment had considerably slower release kinetics compared to the molecularly soluble unimeric species. This was independent of the drug-linker suggesting that degree of solvation near the esters is important to achieve and can vary the hydrolysis rates. Current iterations of these macromolecular prodrugs extend from these observations to create more complex architectures such as mannosylated radiant star nanoparticles that can actively target and bind alveolar macrophages, and has improved drug release kinetics, compared to the previous micelle-forming diblock copolymers. In addition, the incorporation of mannose targeting chemistry can provide potential dose-sparing properties to overcome drug resistance.

The manufacturing of these drug conjugates deviates from formulation based approaches and focuses on creative small-molecule synthetic strategies providing a highly-modular technology where the final macromolecular therapeutic can be engineered from a library of drugs, drug-linkers, and corresponding hydrophilic targeting moieties or solubilizers. These constructs characteristically afford an expanded and more versatile drug repertoire from conventional delivery vehicles, and the success of these macromolecular prodrugs stems from providing tunable, individualized drug release kinetics that control for *in vivo* PK parameters such as C_{max} and AUC. This thesis establishes inhalable macromolecular prodrugs synthesized from polymerizable prodrug monomers as a promising modular platform technology that can not only treat aerosolized *F. tularensis* but may also be applicable for other invasive alveolar intracellular bacteria.

TABLE OF CONTENTS

LIST OF FIGURES

LIST OF TABLES

ACKNOWLEDGEMENTS

The work presented in this thesis is a joint effort by numerous individuals part of the Stayton-Ratner and Skerrett research groups including but not limited to: Dr. Anthony Convertine for the design and development of many of the described prodrug constructs; Dr. Selvi Srinivasan for the synthesis of various drug monomers; Dr. Hye-nam Son and Brian Lee for their patience and help in doing animal PK/biodistribution and efficacy studies; Dr. Jasmin Chen for her previous work in mannosylated polymeric prodrugs; Abby Kelly and Ida Su for their support and assistance on many in vitro analytical methods; and Dale Whittington from UW Department of Medicinal Chemistry for expertise in quantitative LC/MS I would like to gratefully thank my advisors Dr. Patrick Stayton and Dr. Daniel Ratner for their support, mentorship, and guidance over the past four years, as well as Dr. Shawn Skerrett whose expertise in the biology and clinical collaboration was instrumental for the success of this project. I also thank my Supervisory Committee for their advice and valuable feedback on my research direction: Dr. Anthony Convertine, Dr. Suzie Pun, Dr. Shawn Skerrett, Dr. Bruce Montgomery, and Dr. Cole DeForest. This thesis was funded by the United States Defense Threat Reduction Agency (Grant #HDTRA1-13-1-0047) and the UW Molecular Medicine Training Program-Howard Hughes Medical Institute fellowship.

This page is

intentionally

left blank

CHAPTER 1. Introduction and Background

1.1 Pulmonary melioidosis and tularemia are highly-lethal infectious diseases

Lower-respiratory tract infections remain the leading cause of mortality from infectious diseases around the world.[1] Among these pathogens include the highly-lethal, gram-negative intracellular bacteria *Burkholderia pseudomallei* and *Francisella tularensis*, which cause pulmonary melioidosis and tularemia, respectively. Due to their ability to cause catastrophic diseases by an airborne route, coupled with low initial and readily acquirable doses, the U.S. Centers for Disease Control and Prevention (CDC) has classified these bacteria as Tier 1 (highly-virulent) biothreat agents capable of use in biochemical warfare and terrorism.[2–4] In the 1970s, researchers at the World Health Organization (WHO) utilized various modeling studies to predict the effects of mass airborne release of biothreats such as *F. tularensis* in the U.S. under relevant meteorological conditions and bacterium decay-rates in air.[5] For example, assuming the use of an antibiotic-sensitive *F. tularensis* strain, health officials at the WHO theorized that in a city with a population of 5 million, there would result in approx. 250,000 cases of life-threatening respiratory tularemia, with 3500 case-fatalities even with immediate antibiotic treatment.[2,3] In present day, where both melioidosis and tularemia infections have a worldwide presence and there is a significant concern for public health and safety, those that have an added high-risk for bacterial exposure remain to be troops of all nationalities that serve in areas with the widespread diseases.[2,4–8]

1.1.1 Etiology, prevalence, and virulence of Burkholderia pseudomallei

As the causative agent of melioidosis, *B. pseudomallei* is most common to southeast Asia (e.g. Thailand) and northern Australia (**Fig. 1.1A**).[8–11] The disease has an array of clinical presentations that can vary from acute septicemia to chronic focal pathology and latent infection, which can reactivate in host from tissue reservoirs.[4] Depending on the severity of the disease, melioidosis can mimic other infections such as glanders, typhoid fever, and tuberculosis. *B. pseudomallei* is found naturally in the environment in contaminated soil and water and, although, can have diverse routes of entry into the host, from ingestion through skin abrasions, inhalation of the microbe often times leads to the poorest prognosis.[4,9,12] Endemic respiratory melioidosis has an incident rate of approx. 50 cases per 100,000 with 40-50% fatality without treatment and 10% reoccurrence with treatment.[8,11] Moreover, *B. pseudomallei* is intrinsically resistant to many antibiotics including penicillin, cephalosporins, macrolides, rifamycins, colistin, and aminoglycosides.[4] The current standard of care for treating respiratory melioidosis typically starts with IV antimicrobial therapy with ceftazidime and meropenem for 10-14 days followed by 3-6 months of oral therapy with doxycycline.[4,13]

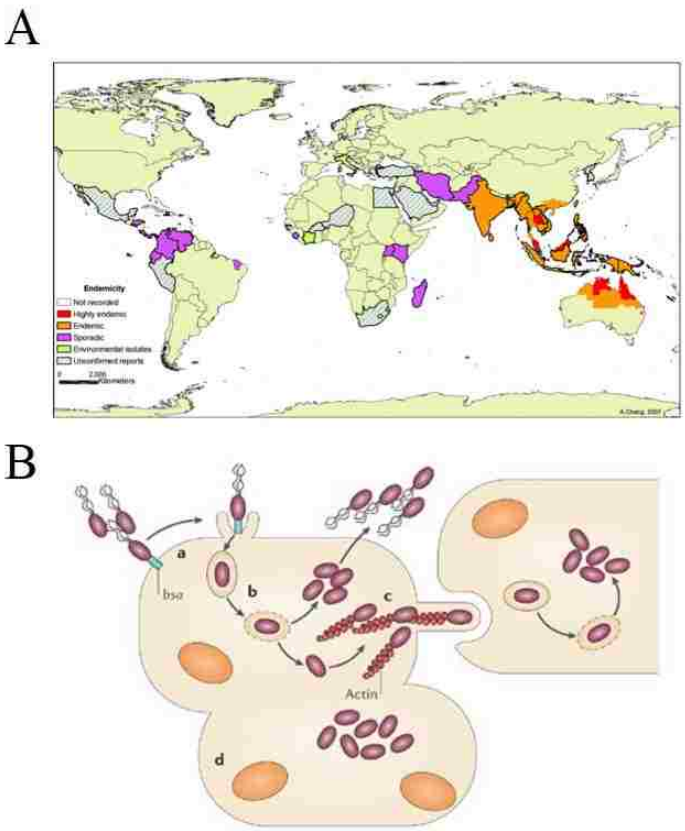

FIGURE 1.1. Epidemiology of respiratory melioidosis and the intracellular life-cycle of *Burkholderia pseudomallei*. (A) Pulmonary melioidosis is predominantly localized to southeast Asia, and parts of Africa, South America, and Australia. (B) Inhalation of *B. pseudomallei* results in the intracellular accumulation (*a*-*b*) and distribution (*c*-*d*) of the pathogen within alveolar macrophages. Virulence factors such as the expression of burkholderia secretion apparatus (bsa) and actin motor proteins helps the bacteria infect, replicate, and persist in phagocytic host immune cells. Figure modified from ref. [13].

B. pseudomallei is an aerobic, motile, non-spore forming bacillus that predominantly survives and replicates within macrophages, and uses multiple mechanisms to facilitate pathogenesis and bacterial dissemination (**Fig. 1.1B**).[14] One important virulence factor is a type III secretion system (TTSS) that functions as a molecular syringe and interacts with host cell membrane to inoculate bacterial effector proteins into a target cell's cytosol.[13,15–17] The TTSS gene cluster helps to make up the *Burkholderia* secretion apparatus (bsa), which encodes for proteins necessary for bacterial invasion and endosomal escape.[15,16] Intracellular *B. pseudomallei* can be propelled by inducing continuous polymerization of actin at one pole of the bacterial cell, which

results in the formation of membrane protrusions that can project into adjacent host cells, facilitating cell-to-cell bacterial migration.[14,18] In addition, *B. pseudomallei* produces an extracellular polysaccharide capsule [-3)-2-*O*-acetyl-6-deoxy-β-D-manno-heptopyranose-(1] that is capable of preventing opsonization and phagocytosis by limiting the deposition of C3b compliment factor on the bacterial surface.[19–21] Due to the native pathogen's high-replicative capacity in humans, a laboratory surrogate such as *B. thailandensis* is commonly used for research.[4,19,22] Although *B. thailandensis* naturally coexists with *B. pseudomallei* in the environment, the former bacterium rarely causes disease in humans, but has equal virulence to the wild-type *B. pseudomallei* in hamsters and mice.[13,23]

1.1.2 Etiology, prevalence, and virulence of Francisella tularensis

Pulmonary tularemia is a zoonotic infection that results from the inhalation of the infectious bacterium, *Francisella tularensis* and is present in several parts of the world, from the U.S. to most of Europe and Australia (**Fig. 1.2A**).[2] The pathogen can have varied modes of entry into a host from insect bites (e.g. ticks, deer flies, etc.), cutaneous contact with infected animal carcasses, and ingestion of contaminated food and water.[3,24] Nevertheless, inhalation of the viable organisms results in the most dangerous form of tularemia with a fatality rate of > 30% if untreated.[2,25] Pneumonic tularemia can have clinical presentations of ulcerative bronchitis, pulmonary hemorrahagic edema, suppurative necrosis of lung parenchyma, as well as potential granulomas.[26] Growth of *F. tularensis* in culture from pharyngeal swabs and sputum specimens provides definitive means of confirming a pulmonary tularemia diagnosis. Medical care for the respiratory form of this disease stems primarily from antibiotic eradication of *F. tularensis*, which can reduce mortality rates to approx. 4%.[7,27] Exhaustive oral and IV administrations lasting 3-4 weeks of

aminoglycosides (e.g. streptomycin and gentamicin), and fluoroquinolones (e.g. ciprofloxacin) are currently the standard of care for antibiotic therapy against pulmonary tularemia.[2,26,28,29]

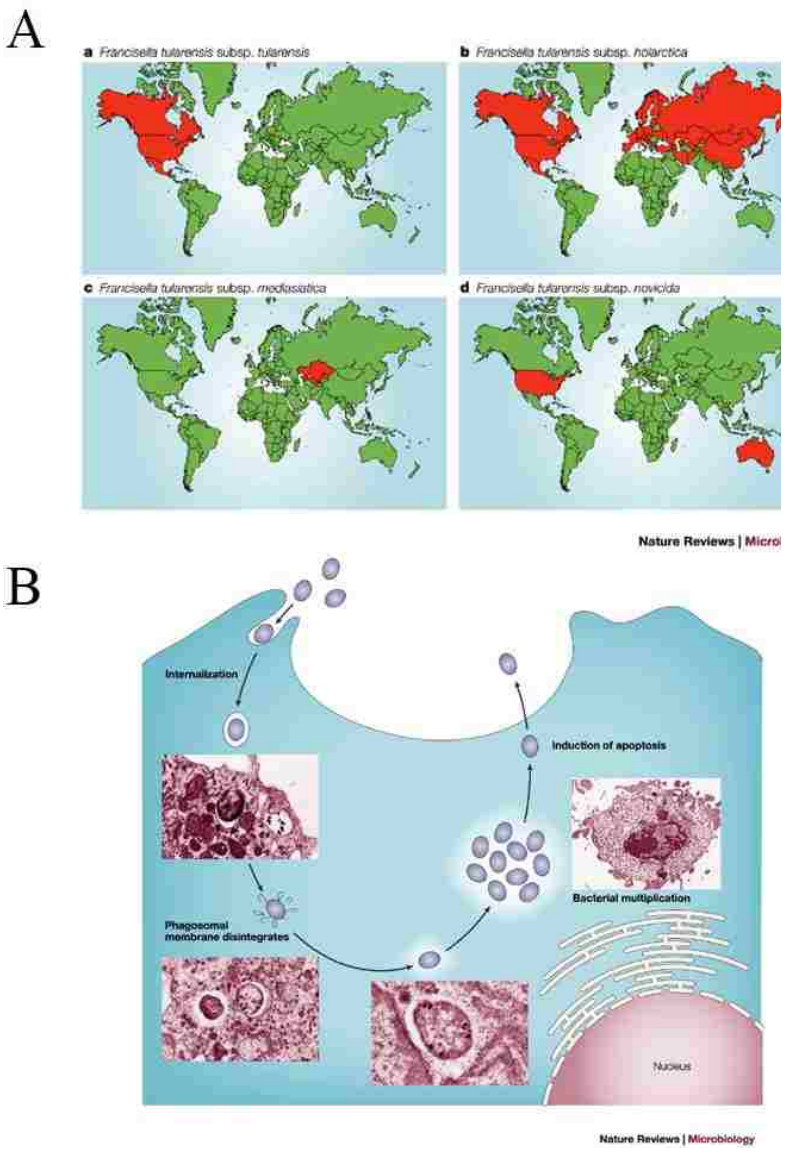

FIGURE 1.2. Epidemiology of respiratory tularemia and the intracellular life-cycle of *Francisella tularensis*. (A) Pulmonary tularemia has a global presence with the subsp. *tularensis* and *novicida* resulting in high number of lethal cases. (B) Similar to *B. pseudomallei*, inhaled *F. tularensis* targets host alveolar macrophages, resulting in the phagocytic internalization and intracellular accumulation of the pathogen. *F. tularensis* has a high replicative capacity, overpowering the immune cell and inducing apoptosis. Figure modified from ref. [2].

Similar to *B. pseudomallei*, the facultative intracellular pathogen *F. tularensis* predominantly targets host macrophages (**Fig. 1.2B**). After entry into the macrophage, the bacteria

are contained inside phagosomes, where by acidification of subcellular compartment has been hypothesized to be essential for *F. tularensis* replication.[30] Studies by electron and confocal microscopy have demonstrated that during the first 3-4 hours of infection, the pathogen is co-localized with late endosomal-lysosomal markers before being released into the cytoplasm for replication.[31] Although mechanisms behind endosomal escape remain to be elucidated, intracellular bacterial replication is known to be quite rapid with 1.5-2.5 $\log_{10}$ bacteria present per cell within 24 hours-post infection.[32,33] The infection cycle renews as the macrophage undergoes apoptosis, releasing large numbers of *Francisella* into the microenvironment.[34,35] Genomic and proteomic studies have helped to suggest the role of potential molecular regulators for intracellular bacterial survival and growth, but remain to be further explored as targets for therapeutic efficacy.[36] Moreover, known virulence factors such as bacterial lipopolysaccharide and protective capsule have been identified to be necessary for immune evasion and resistance.[37–40] Due to a low dose for infection (~10-20 cfu) and a high intracellular replicative capacity, most research into the biology of *F. tularensis* has been done using an atypical live vaccine strain (LVS-SchuS4), which is derived from a *F. tularensis* subsp. *holarctica* strain, and is attenuated in humans while retaining little virulence in mice.[2,41] In comparison, an alternative strain (U112) from *F. tularensis* subsp. *novicida*, which shares approx. 98% nucleotide identity with *F. tularensis subsp. tularensis*, is considered to be a more lethal surrogate model with higher virulence than LVS-SchuS4 in mice.[42–44]

1.2 The current oral and IV standards of care require improvement

The standard of care for treating pulmonary infectious melioidosis and tularemia is oral and IV antimicrobial therapies. However, many antibiotics administered orally or through IV

injection are limited by poor pharmacokinetics and biodistribution to the lungs, and can have associated systemic toxicity.[24,45,46] For instance, ciprofloxacin, which is a commonly prescribed oral fluoroquinolone used to treat pulmonary *F. tularensis*, has a bioavailability of only approx. 65% with a serum half-life of 4 h.[47] This is in comparison to doxycycline, part of the tetracycline family of drugs, which has a bioavailability of >90 % and serum half-life of 18 h. According to the U.S. Food and Drug Administration (FDA), about 40-50% of an orally administered ciprofloxacin dose is excreted by renal clearance as unchanged drug. Additionally, due to the vigorousness of these respiratory infections and the ability of the bacteria to evade natural immune responses, some antibiotics alone, such as ciprofloxacin or tetracycline, when administered orally or via IV are not able to clear the pathogens, resulting in high relapse rates of the disease.[8,13,45] Therefore, patients taking oral ciprofloxacin for pulmonary tularemia have to end up taking large amounts of drug (e.g. 500-750 mg capsules) more frequently (e.g. q12 h), and often times in combination with other drugs over extended periods of time (weeks-months).[48] Consequently, these intensive antibiotic treatment cycles can not only be slow-acting and inefficient, but also financially overwhelming for patients. For these reasons, there exists a clinical unmet need for new efficient drug formulations that improves on the current therapeutic standards by localizing and sustaining effective drug concentrations in the lungs, which can also potentially reduce patient burden.

1.3 Pulmonary drug delivery offers an attractive alternative for drug administration

Direct pulmonary drug delivery provides a convenient, efficient, non-invasive strategy to treat respiratory infections by localizing drugs to the site of bacterial persistence. The delivery of high drug concentrations directly to the disease site not only minimizes the risk of systemic side

effects, but also provides a rapid clinical response that bypasses therapeutic barriers, such as poor gastrointestinal absorption or the first-pass metabolism.[46] In this regard, pulmonary drug delivery can achieve similar or superior therapeutic effects at a fraction of the systemic dose. Inhalable forms of medications have existed for many years and have been clinically used as first-line therapy against lung conditions such as asthma and chronic obstructive pulmonary disease. Recently, the FDA has approved the use of inhalable antibiotics such as aztreonam (Cayston®, Gilead) and tobramycin (Tobi®, Novartis) for the treatment of pulmonary bacterial infections in cystic fibrosis patients.[49]

1.3.1 Aerosolization of antibiotics

Therapeutic efficacies of pulmonary drug delivery are dependent upon the dose deposited and its distribution within the lung.[46] Pulmonary infections from both *B. pseudomallei* and *F. tularensis* have been shown to start in the bronchioles of the lung and spread distally into the

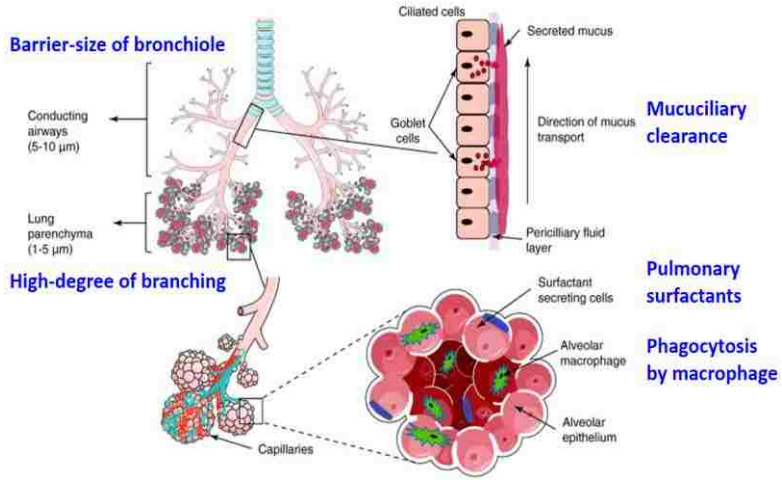

FIGURE 1.3. Lung physiology provides key barriers for pulmonary drug delivery. Inhalable antibiotic delivery systems must be able to achieve therapeutic concentrations of drug localized to deep lung parenchyma where there is high bacterial persistence. Drug formulations that successfully reach alveolar macrophages will overcome barriers including resistance-forming pulmonary anatomical features (bronchiole size and degree of branching), mucuciliary clearance, and the presence of potential molecular-disruptive surfactants. Figure modified from ref. [51].

smaller alveolar spaces before entering the blood and disseminating to other organs.[50,51] Aerosolization of antibiotics compared to intranasal instillations or intratracheal injections have been shown to access these deeper lung environments where the bacteria can preside and create a more well-distributed endotracheal delivery reflected in improved *in vivo* bactericidal activity.[52–54] It should be noted that in a diseased lung, mucus plugs in the bronchi and bronchioles may prevent appropriate aerosol deposition and is subsequently one of the main limitations of pulmonary antibiotic delivery.[46] In addition, airway geometry defined by progressive branching and narrowing, and relative lung humidity can encourage particle impaction upon aerosolization resulting in decreased deposition and distribution into the alveolar space (**Fig. 1.3**).[55] Current research in pulmonary drug delivery devices have sought to address these challenge by developing nebulizers/microsprayers that use pressure sensitive, high-velocity, aerosol streams that have a reduced probability of impaction to reach lung disease environments.[56]

1.3.2 Mechanisms of lung clearance

Deposited drugs after aerosolization can be cleared from the lungs, absorbed into the blood, or degraded via drug metabolism. Drug particles deposited in the conducting airways are primarily removed through mucuciliary clearance and, to a lesser extent, are absorbed through the airway epithelium into the blood and lymphatic system (**Fig. 1.3**).[46] Ciliated epithelium extends from the trachea to the terminal bronchioles. The airway epithelial goblet cells and submucosal glands secrete mucus composed of proteoglycans and glycoproteins forming a two-layer mucus coat over the ciliated epithelium: a low-viscosity periciliary layer covered by a high-viscosity gel layer.[57] Insoluble particles are trapped in the mucus gel layer and are moved toward the pharynx by the metachronous beating of cilia. In comparison, lipophilic and hydrophilic molecules can more

readily pass through the airway epithelium via passive transport or extracellular pathways (e.g. tight junctions, active transport, etc.), respectively.[58] Drugs deposited in the distal alveolar region can be phagocytosed and cleared by alveolar macrophages or directly absorbed into pulmonary circulation (**Fig. 1.3**).[55] The rate of drug absorption from the alveoli is dependent on size, as alveolar permeability is inversely related to the molecular weight of the absorbing species.[59] Lastly, drug metabolism can influence the therapeutic efficacy of inhaled drugs; however, all metabolizing enzymes found in the liver are found in a lower concentrations distributed throughout the conducting airways and alveoli.[60] For example, phase 1 cytochrome-450 (CYP450) enzymes are 20 times lower in the lung than in the liver.[46] Other enzymes include monooxygenase, aldehyde dehydrogenase, NADPH-CYP450 reductase, proteases (e.g. endopeptidase, cathepsin H, etc.) and esterase, which is specifically present in high concentration within alveolar macrophages.

1.4 Pulmonary delivery of free drug formulations have limited efficacy

Pharmaceutical companies have developed inhalable free drug formulations in efforts to address the therapeutic shortcomings of oral and IV administered antibiotics against pulmonary bacterial infections. In 1997, an inhalable solution formulation of the aminoglycoside antibiotic tobramycin (TOBI®; Novartis) became the first inhaled antibiotic to be approved by the FDA for the treatment of pulmonary infections caused by *Pseudomonas aeruginosa* in patients with cystic fibrosis.[49] The TOBI® solution for inhalation is formulated as an aqueous solution with the pH and salinity adjusted specifically for administration by a compressed air driven reusable aerosol unit.[61] Each single-use 5 mL ampule contains 300 mg tobramycin and 11.25 mg sodium chloride in sterile water. Sulfuric acid and sodium hydroxide are added to adjust the pH to 6.0, while nitrogen gas is used for sparging. At present, treatment with TOBI® involves using the nebulizer device to

administer the antibiotic over a 15-minute period twice daily.[49] The cationic polar molecule TOBI® does not readily cross the epithelial membrane in the lungs, and due to the noted variability of individual dosing and rapid pulmonary free drug clearance, the drug has poor accumulation in sputum and serum.[62] For example, after the first 300 mg dose of TOBI®, the average drug concentration in the sputum is about 1.2 µg/g and falls to approx. 1.1 µg/g after 20 weeks of therapy.[61] In 2010, the FDA approved the next inhalable antibiotic, aztreonam monobactam solution (Cayston®; Glidead) for treatment against also *P. aeruginosa* infections in cystic fibrosis patients.[49] A dose of Cayston® inhalable solution consists of a 3 mL vial containing lyophilized aztreonam (75 mg) and lysine (46.7 mg) in a 0.17% sodium chloride aqueous solution at pH 4.5-6. Administration of Cayston® uses an Altera nebulizer that is an improvement over the TOBI system because it decreases the dosing time from approx. 15 min to 3 min.[63] The efficacy of Cayston® following 28 days of therapy, however, was reported to be similar to that of TOBI®, with only 10% improvements in pulmonary function of subjects receiving the inhalable treatment against those receiving placebo controls.[64–66]

Inhalable free drug formulations are currently limited by the relative solubility of drugs in salt-form in the sputum, and poor drug pharmacokinetic properties in the pulmonary space (i.e. trafficking into epithelial tissue and rapid lung clearance).[67] This results in short respiratory half-lives and resident times of the inhaled drug, and the potential for sub-therapeutic dosing that can influence treatment efficacy.[68] Due to these challenges, current inhalable free drug formulations such as TOBI and Cayston require repeated daily dosing over months at a time, reducing patient adherence. Thus, new pulmonary drug delivery systems that improve on the limitations of administering free-drug formulations can have significant clinical impact for patients with persistent respiratory infections.

1.5 Drug encapsulating delivery systems

Encapsulation delivery vehicles (e.g. liposomes, polymer particles, etc.) have historically been used as potential drug carriers for a variety of active compounds including small molecule drugs and biologics, therapeutic proteins and vaccines, and diagnostic agents.

1.5.1 Liposomes for antibiotic delivery

Liposomes are colloidal systems, usually 0.05 – 5 μm in diameter composed primarily of a combination of synthetic or natural lipids (phospho- and sphingo-lipids) and other bilayer constituents such as cholesterol and hydrophilic polymer-lipid conjugates.[69] Due to the relative polarity of the lipid hydrophilic head groups and thermodynamic influences from the hydrophobic effect, liposomes can undergo spontaneous self-assembly under hydrated aqueous conditions to form unilamellar and multilamellar vesicles. Drugs with widely varying lipophilicities can subsequently be encapsulated in these constructs, either in the lipid bilayer or entrapped in the aqueous core of the liposome. Numerous procedures have been developed to prepare liposomal drug systems (e.g. reverse-phase evaporation, freeze-thaw, extrusion, etc.) and depend strongly on the co-solvents used and the physiochemical properties of the encapsulated drug.[70] These approaches often times yield difficulty in reproducibility and manufacturing scalability, and results in poor drug encapsulation efficiencies.[69,71] In addition to complex formulation methods, liposomes can also suffer from incomplete and burst drug release kinetics which may limit control over individual drug dosing and efficacy (**Fig. 1.4A**).[68,71]

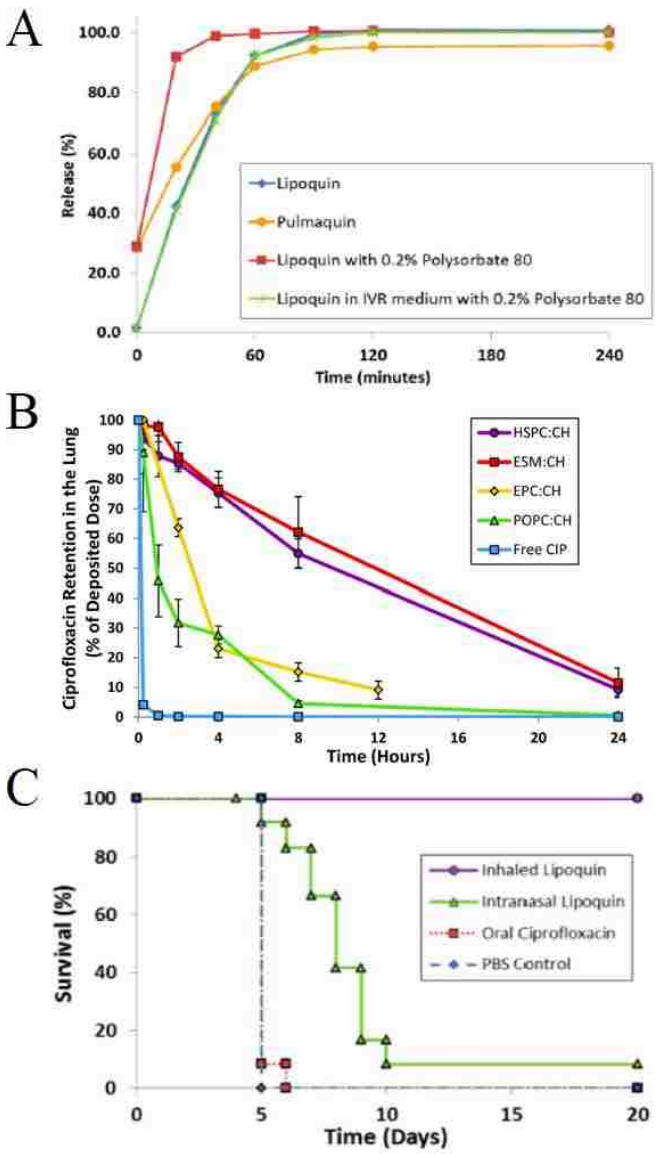

FIGURE 1.4. Key characteristics of clinically relevant inhalable liposomal ciprofloxacin formulations for the treatment against highly-infectious pulmonary agents. (A) *In vitro* drug release kinetics from liposomal ciprofloxacin variants demonstrates burst release of drug within 0-30 min, followed by continuous rapid release for 60-120 min in PBS, pH 7.4. (B) *In vivo* pulmonary retention times of aerosolized free and liposomal encapsulated ciprofloxacin shows significant improvement in drug half-lives of liposomal systems over free drug controls. (C) Therapeutic efficacy of oral ciprofloxacin (50 mg/kg), intranasally instilled liposomal ciprofloxacin (50 mg/kg), and aerosolized liposomal ciprofloxacin (50 mg/kg) against inhaled *F. tularensis* Schu S4 infection in mice (n = 12 for each group). The study depicts the importance of aerosol delivery of drug formulations as shown by the enhanced survival rates of mice treated with inhaled liposomal ciprofloxacin compared to oral and intranasal formulated drug controls. Figure modified from ref. [52].

The clinical applications of liposomes are well known and the initial success achieved with many liposome-based drugs has fueled further clinical investigations. For example, an inhalable liposomal ciprofloxacin (Aradigm) formulation is currently undergoing pre-clinical trials for localized treatment and prevention against pulmonary anthrax infections.[52] Ciprofloxacin for inhalation is an aqueous colloidal dispersion containing a mixture of ciprofloxacin hydrochloride and the corresponding ciprofloxacin base encapsulated in unilamellar liposomes at a drug concentration of 50 mg/mL. The average particle size of these liposomes is 75-120 nm. In comparison to free drug formulations, liposomal drug delivery systems can provide extended therapeutic half-lives with reduced overall drug dosing and potentially systemic toxicity. For instance, un-encapsulated ciprofloxacin is rapidly absorbed and cleared within 2 h after pulmonary administration (**Fig. 1.4B**).[52] In contrast, the use of excipient compounds, such as liposomes, increases respiratory drug residence times to approx. 24 h.[54] Proof-of-concept *in vivo* studies utilizing endotrachaelly administered liposomal ciprofloxacin for post-exposure prophylaxis against a *F. tularensis* LV-Schu4 strain demonstrated improved survival rates in mice compared to oral and aerosolized free drug and saline negative controls (**Fig. 1.4C**).[52,54] Moreover, others have also established enhanced therapeutic efficacy of liposomal ciprofloxacin over free drug formulations in other pulmonary pathogen models (e.g. *Pseudomonas aeruginosa*, *Coxiella burnetti*).[53,72]

Current research with liposomal delivery systems has focused on synthesizing immunoliposomes that function to increase drug accumulation in desired tissues and organs, as well as discovering liposome surface modification strategies that allow for implementing chemical reactive groups for enhanced therapeutic properties (e.g. antibody- and folate-mediated targeting).[71,73,74]

1.5.2 Polymer-drug encapsulated particles for antibiotic delivery

Polymer derived nano- and micro- particulate systems have been utilized in a variety of drug delivery applications including pulmonary administrations of antibiotics. Due to the highly variable and often times poor physiological stability properties of liposomal systems, polymer-drug encapsulated carriers offer an alternative approach to better control the delivery and release of drugs and minimize daily drug dosing.[75] In addition to potentially providing improved protection of the entrapped drug, polymer-drug encapsulated systems can also provide easier surface modification that allows for cellular targeting and transport through lung lining fluid.[68] For example, covalent modification of poly(sebacic acid) particles with high-density, low molecular weight polyethylene glycol has demonstrated faster penetration of human mucus in comparison to uncoated particles.[76]

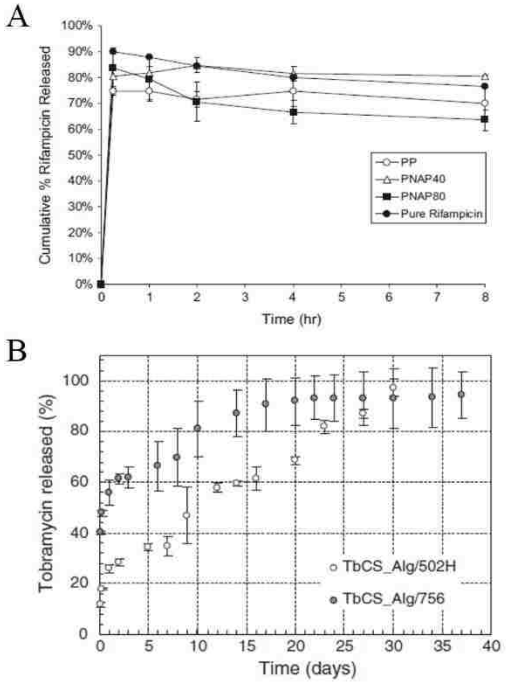

FIGURE 1.5. Representative drug release profiles from poly(lactic-co-glycolic) acid (PLGA) nanoparticles. (A) Cumulative drug release of rifampicin, a potent antibiotic for treating tuberculosis, from various porous PLGA particles demonstrates rapid burst release of drug within 0-30 minutes in PBS, pH 7.4. (B) Similar burst release kinetics was also observed from PLGA encapsulated tobramycin with 20-40% drug release within 0-1 day under physiological conditions. Figure modified from ref. [77,79].

Among the most commonly exploited polymeric nanomaterials for endotracheal delivery of antibiotics include poly(lactic-*co*-glycolic acid) (PLGA). In general, PLGA based polymeric constructs have generated significant research interests due to their favorable biocompatibility, composition dependent tunable degradation profiles, and the presence of modifiable end groups.[67] PLGA particles have traditionally been prepared by a combination of emulsion polymerization, solvent evaporation/extraction, or micro-droplet techniques.[68,77] Dry powder formulations of PLGA-antibiotic encapsulated carriers have been well studied for treating pulmonary infections. For example, porous PLGA microparticles containing <1 wt. % ciprofloxacin was synthesized using a version of emulsion polymerization and resulted in particles of approx. 10 μm that were capable of steady release of drug *in vitro* over 20 days.[78] In addition, PLGA loaded rifampicin particles (**Fig. 1.5A**), an anti-tuberculosis antibiotic, after intratracheal administration in pigs

demonstrated improved pulmonary half-lives (4 h) compared to oral (2.5 h) or IV (1.2 h) free drug formulations.[77] Still others have developed tobramycin (1-2 wt. %) loaded PLGA nanoparticles via a modified emulsion-solvent diffusion technique to demonstrate release properties for up to 25 days, and *in vitro* efficacy against *P. aeruginosa* planktonic cells (**Fig. 1.5B**).[79]

The disadvantages associated to drug encapsulation strategies stem from the difficulties and complexities of the preparation methods. Similar to the formulation of liposomal systems, the synthesis and development of polymer derived drug encapsulated particulates is associated to high-cost, inability to easily and reproducibly produce biologically-stable carriers, and low encapsulation efficiency with burst drug-release of many types of antibiotics (**Fig. 1.5**).[51,68,75,80] Alternative approaches using chemically-labile polymer-drug conjugation techniques have been explored to more readily create drug delivery systems with unique disease-responsive properties.

1.6 Polymeric drug conjugates offer advantages over encapsulated drug systems

Conjugation of drugs to polymer systems offer numerous advantages for simple, small molecule delivery, including the potential for sustained and controlled release of bioactives. Specifically, the drug release rate can be modulated based on the chemical bonds that link the active drug to the polymer (e.g. ester, hydrazine, acetal, amid, etc.), formulation properties of the polymer (e.g. powder, hydrogel, microspheres, etc.), and polymer chemical composition (e.g. non-bioactive polymer backbone or drug-linker molecules).[81] Additionally, by covalently linking the drug, higher drug loading is achieved compared to physical encapsulation and incorporation methods.[82]

1.6.1 Post-polymerization chemical conjugation of antibiotics to polymers

The chemical conjugation of small-molecule drugs to an existing polymer, post-polymerization, usually results in cleavable covalent bonds linking the antibiotic to the polymer backbone (**Fig. 1.6**).[83] Through this approach, it is also possible to add several different drugs and/or targeting moieties to the polymer construct. Fluoroquinolones, such as norfloxacin and ciprofloxacin, are among the well-investigated antibiotics for direct chemical conjugation strategies.[84] For example, norfloxacin has been covalently linked to dextran with tetrapeptide linkers, gly-phe-ala-leu and gly-phe-leu-gly, that are susceptible to degradation under lysosomal conditions.[85] The drug was coupled using trimethylsilyl-activated norfloxacin with subsequent reactions with pentafluorophenyl-activated peptides to create amide bond linked drug-peptide conjugates. Free drug was consequently released via enzymatic (cathepsin B) cleavage with 65% drug released within 24 h. Subsequent *in vivo* efficacy data maintained improved pulmonary bactericidal efficacy against *mycobacterium tuberculosis* compared to oral norfloxacin. In another example, norfloxacin polyester prodrugs were developed using ring-opening of cyclic esters.[86] Lactic acid and caprolactone homopolymer and copolymers were synthesized using glycerol, penthaerythritol, or polyethylene glycol as initiators to yield hydroxyl-terminated oligoesters with pendant arms. The antibiotic was conjugated post-polymerization to the free hydroxyl end groups of the polyesters through direct esterification. The result polymers were able to provide *in vitro* hydrolysis of free drug over five to seven days.

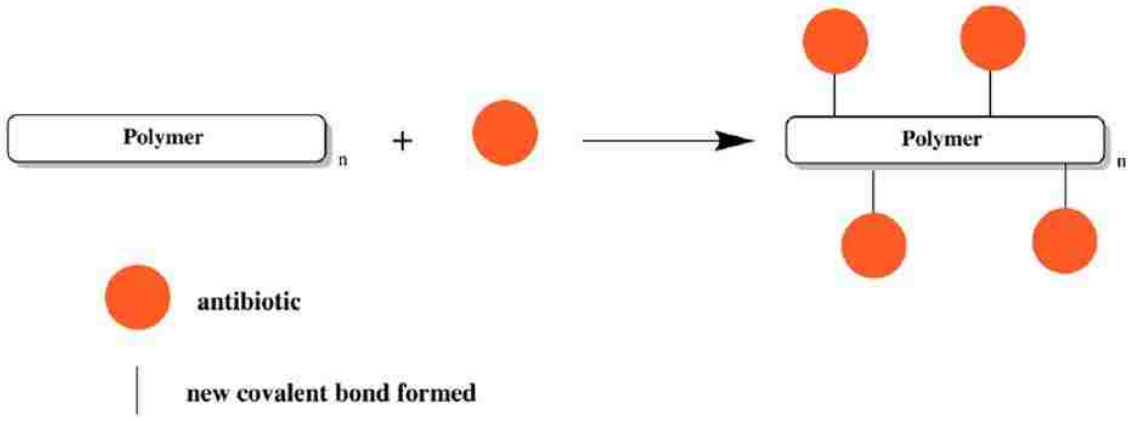

FIGURE 1.6. Direct conjugation of drugs to polymer scaffolds post-polymerization. Schematic representing post-polymerization conjugation of drug to create final bioactive polymeric prodrugs. Figure from ref. [81].

Similarly, cipfrofloxacin was conjugated to hydroxyl ends of polyesters with two, three, four or six arms.[87] The resulting ciprofloxacin-ester conjugate had a final drug content of 2-9 mol. % with polymer molecular weights of 6-11 kDa. Degradation was performed on the polymer-drug conjugates at 37C in aqueous buffer at pH 1, 4 and 7.4. The authors demonstrated that the use of polyethylene glycol as a hydrophilic initiator and rac-lactide as a low crystalline monomer resulted in the fastest release rate with 29% hydrolysis of ciprofloxacin after about 35 days at neutral pH. It was also found that lowering the pH to 1 increased the drug release to 37% over the same time period. In addition, others have used polyurethanes to conjugate ciprofloxacin using trimethylamine to create ester functionalized drug linkers.[88,89] The resulting polymers had molecular weights from 20-24 kDa and a molar mass dispersity of 1.6. Degradation studies were performed with and without cholesterol esterase in buffer at pH 7 to show twice the amount of drug released in the presence of the esterase. The enzyme-incubated samples were also able to demonstrate antibacterial activity against *P. aeruginosa* planktonic infection with minimum inhibitory concentrations comparable to free ciprofloxacin.

1.6.2 Polymerizable antibiotic monomers

In contrast to direct chemical conjugation of drugs to pre-made polymers, polymerizable antibiotic containing precursors is a creative alternative to create higher drug loaded polymeric prodrugs with sustained and controlled drug release properties (**Fig. 1.7A**).[81] For example, norfloxacin was reacted with a methacrylate to produce an acryl monomer that subsequently underwent a free radical polymerization to form the norfloxacin polymeric prodrug.[90] This synthesis was carried out by first reacting the antibiotic with glycidyl methacrylate in dimethylformamide to create the methacrylate quinolone monomer, which was subsequently treated to a free radical polymerization to form the drug-rich antibiotic polymer with molecular weight and molar mass dispersity of 42 kDa and 2.7, respectively. The antibiotic activity of the polyquinalone was evaluated against a variety of bacterial agents in PBS at physiological temperature via the shake flask test. Both the monomer and corresponding norfloxacin polymer displayed >98% reduction in bacterial planktonic cells. Similarly, norfloxacin was reacted with 3-(acryloyloxy)-2-hydroxypropyl methacrylate in dimethylformamide to yield another version of the antibiotic monomer (**Fig. 1.7B**).[91] Polymer constructs of the norfloxacin monomer with polyethylene glycol methyl ether methacrylate, was synthesized using free radical polymerization. The resulting homopolymer and copolymers had a molecular weight of 26 and 62 kDa, respectively, with molar mass dispersities of 1.7 and 1.8, respectively. *In vitro* bactericidal properties of the polymers and the antibiotic monomer was determined against *E. coli* and *S. aureus*, which showed 100% reduction for both bacterial strains.

In addition to fluoroquinolones, other family of drugs such as beta-lactams and aminoglycosides have also been utilized to create polymerizable antibiotic monomers. For

instance, gentamicin, an aminoglycoside, was chemically introduced into hyperbranched polymer networks using *N,N'*-methylenebisarcylamide dissolved in sodium bicarbonate.[92] The final branched polymer was linked by glycoside and amide bonds (molecular weight of 5.4 Da) that degraded only after 5 days at pH 5.5. Antibacterial efficacy using *E. coli* demonstrated 86% bacterial death after 12 h in LB broth.

Improving patient compliance and decreasing drug dosing remain a concern for current pulmonary antibiotic therapy.[46,68,93] Polymeric prodrugs as localized, controlled antimicrobial delivery systems can allow sufficiently high concentrations and extended release mechanisms to effectively eradicate persistent organisms.[81,87] The advantages of using prodrug monomers as oppose to direct conjugation of antibiotics stems from the greatly improved drug loading that is achieved using polymerizable precursors in synthesizing the final polymer. Moreover, free radical polymerization allows for a wider selection and easier incorporation of polymer attributes (e.g. pH responsiveness, targeting segments, etc.) that can have added benefits to creating antibiotic linked delivery systems.[94]

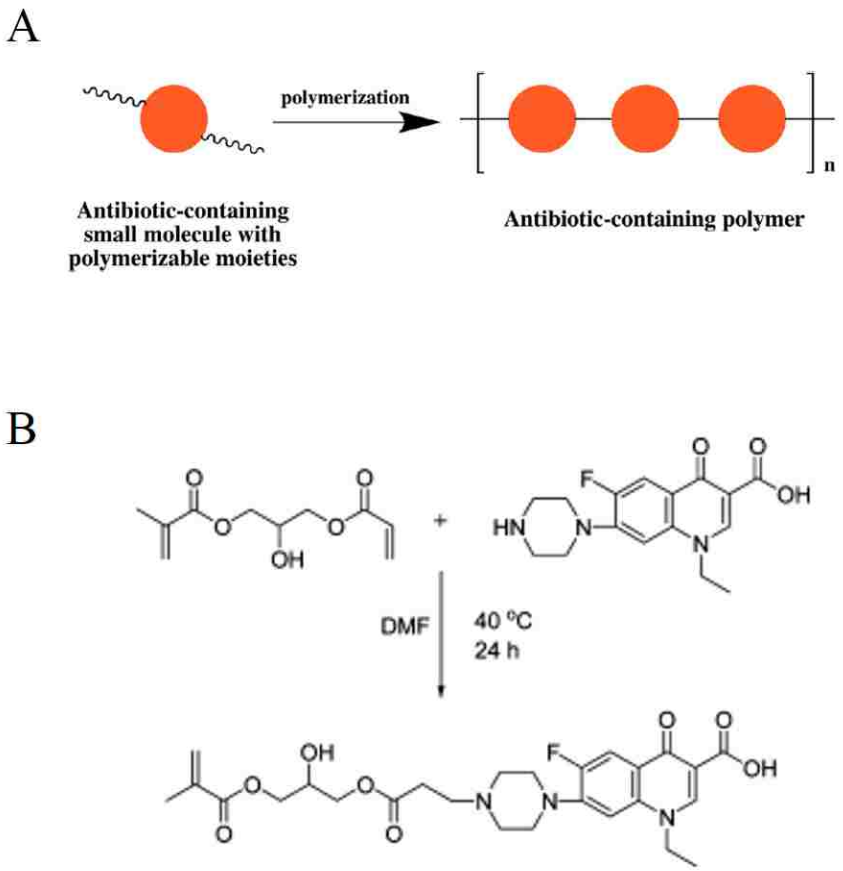

FIGURE 1.7. Polymerizable prodrug monomers to create polymeric prodrugs. (A) Schematic illustrating the use of antibiotic containing polymerizable monomer that can be used under free radical polymerization conditions to create drug-rich polymers. (B) A representative approach to synthesize polymerizable monomers of the antibiotic norfloxacin that can be polymerized into a polymer via the methacrylate backbone. Figure modified from ref. [81].

1.7 Reversible addition-fragmentation chain transfer polymerization is a robust, versatile, and highly-effective approach to develop polymeric prodrugs

Free radical polymerization utilizes reactive radical species as functional building blocks for polymer synthesis and remains one of the most widely employed techniques to create polymers for a variety of applications. Reversible addition-fragmentation chain transfer (RAFT) polymerization is a form of controlled free radical polymerization that proceeds via a degenerative chain transfer process where there is an equilibration between propagating polymer and dormant

radical species.[95] In contrast, techniques such as atom transfer radical polymerization (ATRP) and nitroxide mediated polymerization (NMP) establish equilibrium by reversible termination of the propagating polymer chain through redox reactions with a metal halide salt or a nitroxide end-cap, respectively.[96] The RAFT process is unique and advantageous in that it can be used with a wide range of monomers and reaction conditions, and in each case provides high control over polymer molecular weight and molar mass dispersities. For example, RAFT provides good control over the polymerization of vinyl esters and vinylamides, where NMP and ATRP typically provide minimal control.[96,97] Additionally, RAFT is compatible with a wide variety of reaction media, being routinely applied in organic solution, aqueous solution, and in dispersed phase.[98]

1.7.1 RAFT is a 'living' process

RAFT is an example of a living polymerization, where chain termination and transfer reactions are limited, so as to allow for the preparation of block copolymers and complex architectures. In an ideal living polymerization, chains are initiated at the beginning, grow at the same rate, and survive the polymerization without termination.[96] It is necessary for living radical polymerization to prevent or suppress processes that would otherwise terminate chains irreversibly. In the case for RAFT, this only becomes possible in the presence of reagents (e.g. reversible chain transfer agents) that react with the propagating radicals so that the majority of the chains are maintained in the dormant form.[99] In general, the degenerative chain transfer that occurs in RAFT polymerization is facilitated by a thiocarbonylthio chain transfer agent (RAFT CTA) that is functionally swapped between growing polymer chains. The effective control over molecular weight and molar mass dispersity arises through rapid equilibration of chains with respect to the polymerization rate where all chains have an equal opportunity to grow.[98] Upon completion of a

RAFT polymerization, the majority of polymer chains will possess a thiocharbonylthio end-group, with the overall process able to be viewed as an insertion of monomer units between the S-R bond of the RAFT CTA (**Fig. 1.8A**). The conserved raft end-group, often termed a macro-RAFT chain transfer agent (macroCTA) facilitates the synthesis of block copolymers via subsequent polymerization cycles with secondary monomer species.[95,96]

1.7.2 Mechanism behind RAFT

The RAFT mechanism begins with the formation of an initiator derived radical (I^O) that propagates with monomer (M) to give a polymer radical (P_n^O) (**Fig. 1.8B**). In an ideal RAFT polymerization reaction, P_n^O is efficiently reacted with the RAFT agent (1) after which the intermediate (3) fragments to give the macroCTA (2) and the expelled radical (R^O), which reinitiates polymerization.[95–97] The initialization of the RAFT process concludes when the original RAFT agent and corresponding radicals are consumed. In a well-controlled RAFT polymerization, the reaction moves into main equilibrium rapidly to allow for maximal equilibration of the growing chains and giving resulting polymers low dispersity.[98] Termination of the RAFT process for a given polymer occurs when two growing polymers come together to form a dead polymer chain. When developing reaction conditions for RAFT, three ratios must be taken into consideration: (1) $[M]_O$:$[RAFT]_O$, (2) $[RAFT]_O$:$[I]_O$, and (3) $[M]_O$:$[I]_O$ ratios.

(1) $[M]_O$:$[RAFT]_O$ is the degree of polymerization and determines the theoretical number average molar mass. This is a theoretical value since it assumes there are no undesired reactions, such as termination or irreversible chain transfer. A defined $[M]_O$:$[RAFT]_O$ ratio allows for the preparation of polymers with targeted molar mass.[96,99]

(2) $[RAFT]_O:[I]_O$ is the ratio of initial raft agent to initiator. It provides control over the polymerization by affecting the ratio of dormant chains to dead chain ends.[97]

(3) $[M]_O:[I]_O$ is the ratio of initial total monomer to initiator ratio and influences the rate of polymerization.[95,98]

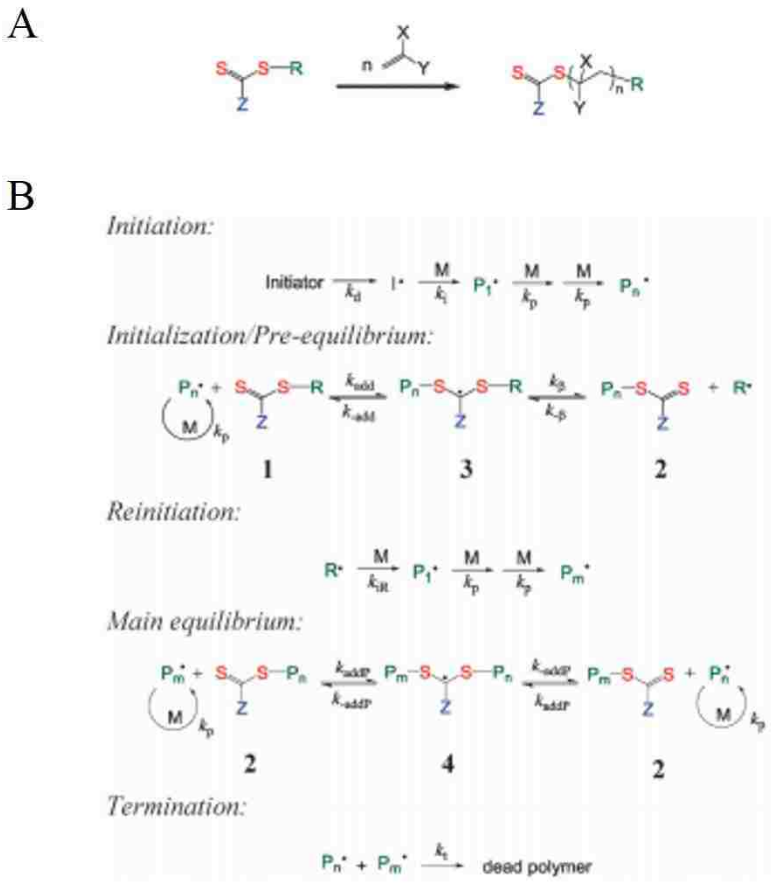

FIGURE 1.8. Overview of reversible-addition fragmentation chain transfer (RAFT) polymerization. (A) Scheme for the overall outcome of the RAFT process. Upon completion of RAFT polymerization, the majority of polymer chains will possess a thiocarbonylthio end-group with an overall process able to be viewed as an insertion of monomers between the S-R bond of the RAFT agent to give the final polymer with predetermined properties. (B) Schematic illustrating the equilibria of RAFT polymerization. The RAFT process provides high degree of versatility for monomer choice and high control over final polymer molecular weight and composition. Figure modified from ref. [96].

1.7.3 Using RAFT to produce antibiotic polymers

The RAFT polymerization of polymeric prodrugs have been utilized by other groups in the past. For example, Smith et al employed RAFT technique in DMSO to polymerize copolymers incorporating the broad spectrum antiviral, Ribavirin, with the addition of poly(N-(2-hydroxypropyl) methacrylamide), PHPMA as a therapeutic alternative against co-infections of HIV and the hepatitis C virus.[100] The authors observed fine control over the size and molecular weight distributions over varied target degree of polymerizations of their HPMA polymeric constructs with a maximum Ribavirin composition of 23 mol. %. In addition, others have utilized RAFT polymerization to create antimicrobial polymers containing well defined cationic residues that mimic natural antimicrobial peptides to bactericidal properties against vigorous strains of methicillin resistant *S. aureus*, *S. epidermidis*, and *C. albicans*.[101]

The polymer chemistry synthesis detailed herein improves and extends the versatility of RAFT to create innovative drug delivery platform-strategy of polymeric prodrugs capable of releasing drug with varying sustained release profiles, and consequently providing engineering guidelines for the intracellular delivery of a variety of potential chemically amenable antibiotics. The uniqueness of the current work stems from the development of polymerizable ciprofloxacin prodrug monomers that are used to synthesize new biocompatible polymeric prodrugs with distinct and well-defined materials and biological properties.

1.8 REFERENCES

1. Skyberg, J. A. *et al.* Nasal acai polysaccharides potentiate innate immunity to protect against pulmonary Francisella tularensis and Burkholderia pseudomallei infections. *PLoS Pathog.* **8,** (2012).
2. Oyston, P. C., Sjostedt, A. & Titball, R. W. Tularaemia: bioterrorism defence renews interest in Francisella tularensis. *Nat Rev Microbiol* **2,** 967–978 (2004).
3. Dennis, D. T. *et al.* Tularemia as a Biological weapon. *JAMA* **285,** 2763 (2001).
4. Cheng, A. C. & Currie, B. J. Melioidosis: epidemiology, pathophysiology, and management. *Clin. Microbiol. Rev.* **18,** 383–416 (2005).
5. World health Organization. *Health aspects of chemical and biological weapons.* (WHO, Geneva, 1970)
6. Wuthiekanun, V. *et al.* Detection of Burkholderia pseudomallei in soil within the Lao People's Democratic Republic. *J. Clin. Microbiol.* **43,** 923–924 (2005).
7. Petersen, J. M. & Schriefer, M. E. Tularemia: emergence/re-emergence. *Vet. Res.* **36,** 455–467 (2005).
8. Maharjan, B. *et al.* Recurrent melioidosis in Patients in Northeast Thailand Is Frequently Due to Reinfection Rather than Relapse. *J. Clin. Microbiol.* **43,** 6032–6034 (2005).
9. Currie, B. J. *et al.* The epidemiology of melioidosis in Australia and Papua New Guinea. *Acta Trop.* **74,** 121–127 (2000).
10. Lewis, E. R. G. *et al.* The art of persistence-the secrets to Burkholderia chronic infections. *Pathog. Dis.* **74,** 170–170 (2016).
11. Parry, C. M. *et al.* Melioidosis in Southern Vietnam: Clinical Surveillance and Environmental Sampling. *Clin. Infect. Dis.* **29,** 1323–1326 (1999).
12. Rainfall Data.
13. Wiersinga, W. J., van der Poll, T., White, N. J., Day, N. P. & Peacock, S. J. Melioidosis: insights into the pathogenicity of Burkholderia pseudomallei. *Nat. Rev. Microbiol.* **4,** 272–82 (2006).
14. Reckseidler, S. L., DeShazer, D., Sokol, P. A. & Woods, D. E. Detection of Bacterial Virulence Genes by Subtractive Hybridization: Identification of Capsular Polysaccharide of Burkholderia pseudomallei as a Major Virulence Determinant. *Infect. Immun.* **69,** 34–44 (2001).
15. Stevens, M. P. *et al.* An Inv/Mxi-Spa-like type III protein secretion system in Burkholderia pseudomallei modulates intracellular behaviour of the pathogen. *Mol. Microbiol.* **46,** 649–659 (2002).
16. Rainbow, L., Hart, C. A. & Winstanley, C. Distribution of type III secretion gene clusters in Burkholderia pseudomallei, B. thailandensis and B. mallei.
17. Ulrich, R. L. *et al.* Role of quorum sensing in the pathogenicity of Burkholderia pseudomallei. *J. Med. Microbiol.* **1840,** 1053–1064 (2016).
18. Stevens, M. P. *et al.* Identification of a bacterial factor required for actin-based motility of Burkholderia pseudomallei. *Mol. Microbiol.* **56,** 40–53 (2005).
19. Hoppe, I. *et al.* Characterization of a murine model of melioidosis: comparison of different strains of mice. *Infect. Immun.* **67,** 2891–900 (1999).
20. Steinmetz, I., Rohde, M. & Brenneke, A. B. Purification and Characterization of an Exopolysaccharide of Burkholderia (Pseudomonas) pseudomallei. *Infect. Immun.* **63,** 3959–3965 (1995).

21. Stevens, M. P. *et al.* Attenuated virulence and protective efficacy of a Burkholderia pseudomallei bsa type III secretion mutant in murine models of melioidosis. doi:10.1099/mic.0.27146-0
22. Leakey, A. K., Ulett, G. C., Hirst, R. G. & Leakey, A. K. BALB/c and C57Bl/6 mice infected with virulent Burkholderia pseudomallei provide contrasting animal models for the acute and chronic forms of human melioidosis. *Microb. Pathog.* **24,** 269–275 (1998).
23. Thibault, F. M., Valade, E. & Vidal, D. R. Identification and Discrimination of Burkholderia pseudomallei, B. mallei, and B. thailandensis by Real-Time PCR Targeting Type III Secretion System Genes. *J. Clin. Microbiol.* **42,** 5871–5874 (2004).
24. Ellis, J., Oyston, P. C. F., Green, M. & Titball, R. W. Tularemia. *Clin. Microbiol. Rev.* **15,** 631–646 (2002).
25. Tarnvik, A. Nature of Protective Immunity to Francisella tularensis. *Rev. Infect. Dis.* **11,** 440–451
26. HILLMAN, C. C. TULAREMIA. *J. Am. Med. Assoc.* **108,** 538 (1937).
27. Staples, J. E., Kubota, K. A., Chalcraft, L. G., Mead, P. S. & Petersen, J. M. Epidemiologic and Molecular Analysis of Human Tularemia, United States, 1964–2004. *Emerg. Infect. Dis.* **12,** 1113–1121 (2006).
28. Johansson, A. *et al.* Scandinavian Journal of Infectious Diseases In Vitro Susceptibility to Quinolones of Francisella tularensis subspecies tularensis In Vitro Susceptibility to Quinolones of Francisella tularensis subspecies tularensis. *Scand J Infect Dis* **34,** 327–330 (2002).
29. Ikaheimo, I., Syrjälä, H., Karhukorpi, J., Schildt, R. & Koskela, M. In vitro antibiotic susceptibility of Francisella tularensis isolated from humans and animals. *J. Antimicrob. Chemother.* **46,** 287–290 (2000).
30. Kirimanjeswara, G. S., Olmos, S., Bakshi, C. S. & Metzger, D. W. Humoral and cell-mediated immunity to the intracellular pathogen Francisella tularensis. *Immunol. Rev.* **225,** 244–55 (2008).
31. Lindgren, H. *et al.* Factors affecting the escape of Francisella tularensis from the phagolysosome. *J. Med. Microbiol.* **53,** 953–958 (2004).
32. Elkins, K. L., Leiby, D. A., Winegar, R. K., Nacy, C. A. & Fortier, A. H. Rapid Generation of Specific Protective Immunity to Francisella tularensis. *Infect. Immun.* **60,** 4571–4577 (1992).
33. Fortier, A. H. *et al.* Growth of Francisella tularensis LVS in Macrophages: the Acidic Intracellular Compartment Provides Essential Iron Required for Growth. *Infect. Immun.* **63,** 1478–1483 (1995).
34. Lai, X.-H., Golovliov, I. & Sjostedt, A. Francisella tularensis Induces Cytopathogenicity and Apoptosis in Murine Macrophages via a Mechanism That Requires Intracellular Bacterial Multiplication. *Infect. Immun.* **69,** 4691–4694 (2001).
35. Lai, X.-H. & Sjostedt, A. Delineation of the Molecular Mechanisms of Francisella tularensis-Induced Apoptosis in Murine Macrophages. *Infect. Immun.* **71,** 4642–4646 (2003).
36. Elkins, K. L., Cowley, S. C. & Bosio, C. M. Innate and adaptive immune responses to an intracellular bacterium, Francisella tularensis live vaccine strain. *Microbes Infect.* **5,** 135–142 (2003).
37. Fortier, A. H. *et al.* Life and death of an intracellular pathogen: Francisella tularensis and the macrophage. *Immunol. Ser.* **60,** 349–61 (1994).

38. Sandstrom, G., Lofgren, S. & Tarnvik2, A. A Capsule-Deficient Mutant of Francisella tularensis LVS Exhibits Enhanced Sensitivity to Killing by Serum but Diminished Sensitivity to Killing by Polymorphonuclear Leukocytes. *Infect. Immun.* 1194–1202 (1988).
39. Ancuta, P., Pedron, T., Girard, R., Sandstr, G. & Chaby, R. Inability of the Francisella tularensis Lipopolysaccharide To Mimic or To Antagonize the Induction of Cell Activation by Endotoxins. *Infect. Immun.* **64,** 2041–2046 (1996).
40. Fulop, M., Mastroeni, P., Green, M. & Titball, R. W. Role of antibody to lipopolysaccharide in protection against low- and high-virulence strains of Francisella tularensis. *Vaccine* **19,** 4465–4472 (2001).
41. Karlsson, J. *et al.* Sequencing of the *Francisella tularensis* Strain Schu 4 Genome Reveals the Shikimate and Purine Metabolic Pathways, Targets for the Construction of a Rationally Attenuated Auxotrophic Vaccine. *Microb. Comp. Genomics* **5,** 25–39 (2000).
42. Vinogradov, E., Conlan, W. J., Gunn, J. S. & Perry, M. B. Characterization of the lipopolysaccharide O-antigen of Francisella novicida (U112). *Carbohydr. Res.* **339,** 649–654 (2004).
43. Santic, M., Molmeret, M. & Abu Kwaik, Y. Modulation of biogenesis of the Francisella tularensis subsp. novicida-containing phagosome in quiescent human macrophages and its maturation into a phagolysosome upon activation by IFN-γ. *Cell. Microbiol.* **7,** 957–967 (2005).
44. Rick Lyons, C. & Wu, T. H., Animal Models of Francisella tularensis Infection. *Ann. N. Y. Acad. Sci.* **1105,** 238–265 (2007).
45. Maurin, M., Mersali, N. F. & Raoult, D. Bactericidal activities of antibiotics against intracellular Francisella tularensis. *Antimicrob. Agents Chemother.* **44,** 3428–3431 (2000).
46. Labiris, N. R. & Dolovich, M. B. Pulmonary drug delivery. Part I: Physiological factors affecting therapeutic effectiveness of aerosolized medications. *Br. J. Clin. Pharmacol.* **56,** 588–599 (2003).
47. MacGregor, R. R. & Graziani, A. L. Oral administration of antibiotics: a rational alternative to the parenteral route. *Clin. Infect. Dis. An Off. Publ. Infect. Dis. Soc. Am.* **24,** 457–467 (1997).
48. US FDA, Prescribing information - CIPRO ® (ciprofloxacin hydrochloride) [online].
49. O'Sullivan, B. P., Yasothan, U. & Kirkpatrick, P. Inhaled aztreonam. *Nat. Rev. Drug Discov.* **9,** 357–358 (2010).
50. Lazdunski, A. M., Ventre, I. & Sturgis, J. N. Regulatory circuits and communication in Gram-negative bacteria. *Nat. Rev. Microbiol.* **2,** 581–592 (2004).
51. Sou, T. *et al.* New developments in dry powder pulmonary vaccine delivery. *Trends Biotechnol.* **29,** 191–198 (2011).
52. Cipolla, D., Blanchard, J. & Gonda, I. Development of liposomal ciprofloxacin to treat lung infections. *Pharmaceutics* **8,** 1–31 (2016).
53. Norville, I. H. *et al.* Efficacy of liposome-encapsulated ciprofloxacin in a murine model of Q fever. *Antimicrob. Agents Chemother.* **58,** 5510–5518 (2014).
54. Hamblin, K. A. *et al.* Liposome Encapsulation of Ciprofloxacin Improves Protection against Highly Virulent Francisella tularensis Strain Schu S4. *Antimicrob. Agents Chemother.* **58,** 3053–3059 (2014).
55. Lippmann, M., Yeates, D. B. & Albert, R. E. Deposition, retention, and clearance of inhaled particles. *Br. J. Industr. Med.* **37,** 337–362 (1980).

56. DOLOVICH, M. New Propellant-Free Technologies under Investigation. *J. Aerosol Med.* **12,** S–9–S–17 (1999).
57. Itoh, H., Smaldone, G. C., Swift, D. L. & Wagner, H. N. Mechanisms of aerosol deposition in a nasal model. *J. Aerosol Sci.* **16,** 529–534 (1985).
58. Sanchis, J., Dolovich, M., Rossman, C. & Newhouse, M. Lung clearance in patients with airways obstruction. *Bull. Physiopathol. Respir. (Nancy).* **9,** 325–37 (1972).
59. Pavia ', D., Thomson2, M. L., Clarke ', S. W. & Shannon2, H. S. Effect of lung function and mode of inhalation on penetration of aerosol into the human lung. *Thorax* **32,** 194–197 (1977).
60. Folkesson, H. G. *et al.* Alveolar epithelial clearance of protein. *J. Appl. Physiol.* **80,** 1431–45 (1996).
61. Novartis. Prescribing information – Tobi, *Novartis Pharmaceutical Corporation website* [online], http://www.pharma.us.novartis.com/product/pi/pdf/tobi.pdf (2010)
62. Burns, J. L. *et al.* Effect of Chronic Intermittent Administration of Inhaled Tobramycin on Respiratory Microbial Flora in Patients with Cystic Fibrosis. *J. Infect. Dis.* **179,** 1190–1196 (1999).
63. Weber, A., Smith, A., Williams-Warren, J., Ramsey, B. & Covert, D. S. Nebulizer delivery of tobramycin to the lower respiratory tract. *Pediatr. Pulmonol.* **17,** 331–339 (1994).
64. Retsch-Bogart, G. Z. *et al.* Efficacy and Safety of Inhaled Aztreonam Lysine for Airway Pseudomonas in Cystic Fibrosis*.
65. McCoy, K. S. *et al.* Inhaled Aztreonam Lysine for Chronic Airway *Pseudomonas aeruginosa* in Cystic Fibrosis. *Am. J. Respir. Crit. Care Med.* **178,** 921–928 (2008).
66. Gibson, R. L. *et al.* Microbiology, safety, and pharmacokinetics of aztreonam lysinate for inhalation in patients with cystic fibrosis. *Pediatr. Pulmonol.* **41,** 656–665 (2006).
67. Cook, R. O., Pannu, R. K. & Kellaway, I. W. Novel sustained release microspheres for pulmonary drug delivery. *J. Control. Release* **104,** 79–90 (2005).
68. Pilcer, G. & Amighi, K. Formulation strategy and use of excipients in pulmonary drug delivery. *Int. J. Pharm.* **392,** 1–19 (2010).
69. Torchilin, V. P. Recent advances with liposomes as pharmaceutical carriers. *Nat. Rev. Drug Discov.* **4,** 145–160 (2005).
70. Vemuri, S. & Rhodes, C. T. Preparation and characterization of liposomes as therapeutic delivery systems: a review. *Pharm. Acta Helv.* **70,** 95–111 (1995).
71. Sharma, A. & Sharma, U. S. Liposomes in drug delivery: Progress and limitations. *Int. J. Pharm.* **154,** 123–140 (1997).
72. Webb, M. S. *et al.* Antibacterial Efficacy against an In Vivo Salmonella typhimurium Infection Model and Pharmacokinetics of a Liposomal Ciprofloxacin Formulation Antibacterial Efficacy against an In Vivo Salmonella typhimurium Infection Model and Pharmacokinetics of a Lipos. *Antimicrob. Agents Chemother.* **42,** 45–52 (1998).
73. Woodle, M. C. Controlling liposome blood clearance by surface-grafted polymers. *Adv. Drug Deliv. Rev.* **32,** 139–152 (1998).
74. Klibanovl, A. L., Maruyamal, K., Torchilin, V. P. & Huangl, L. Amphipathic polyethyleneglycols effectively prolong the circulation time of liposomes. **268,** 235–237 (1990).
75. Ungaro, F., D'Angelo, I., Miro, A., La Rotonda, M. I. & Quaglia, F. Engineered PLGA nano- and micro-carriers for pulmonary delivery: Challenges and promises. *J. Pharm.*

Pharmacol. **64,** 1217–1235 (2012).
76. Tang, B. C. *et al.* Biodegradable polymer nanoparticles that rapidly penetrate the human mucus barrier. *Proc. Natl. Acad. Sci. U. S. A.* **106,** 19268–19273 (2009).
77. Sung, J. C. *et al.* Formulation and pharmacokinetics of self-assembled rifampicin nanoparticle systems for pulmonary delivery. *Pharm. Res.* **26,** 1847–1855 (2009).
78. Yang, Y. *et al.* Development of highly porous large PLGA microparticles for pulmonary drug delivery. *Biomaterials* **30,** 1947–1953 (2009).
79. Ungaro, F. *et al.* Dry powders based on PLGA nanoparticles for pulmonary delivery of antibiotics: Modulation of encapsulation efficiency, release rate and lung deposition pattern by hydrophilic polymers. *J. Control. Release* **157,** 149–159 (2012).
80. Arnold, M. M., Gorman, E. M., Schieber, L. J., Munson, E. J. & Berkland, C. NanoCipro encapsulation in monodisperse large porous PLGA microparticles. *J. Control. Release* **121,** 100–109 (2007).
81. Stebbins, N. D., Ouimet, M. A. & Uhrich, K. E. Antibiotic-containing polymers for localized, sustained drug delivery. *Adv. Drug Deliv. Rev.* **78,** 77–87 (2014).
82. Prudencio, A. *et al.* Polymeric prodrugs of ampicillin as antibacterial coatings. *J. Bioact. Compat. Polym.* **29,** 208–220 (2014).
83. Roseeuw, E. *et al.* Polymeric prodrugs of antibiotics with improved efficiency. *J. Mater. Sci. Mater. Med.* **10,** 743–746 (1999).
84. Adhami, Z. N., Wise, R., Weston, D. & Crump, B. The pharmacokinetics and tissue penetration of norfloxacin. *J. Antimicrob. Chemother.* **13,** 87–92 (1984).
85. Coessens, V., Schacht, E. H. & Domurado, D. Synthesis and in vitro stability of macromolecular prodrugs of norfloxacin. *J. Control. Release* **47,** 283–291 (1997).
86. Sobczak, M., Witkowska, E., Olędzka, E. & Kolodziejski, W. Synthesis and Structural Analysis of Polyester Prodrugs of Norfloxacin. *Molecules* **13,** 96–106 (2008).
87. Sobczak, M. Synthesis and characterization of polyester conjugates of ciprofloxacin. *Eur. J. Med. Chem.* **45,** 3844–3849 (2010).
88. Woo, G. L. Y. *et al.* Biological characterization of a novel biodegradable antimicrobial polymer synthesized with fluoroquinolones. *J. Biomed. Mater. Res.* **59,** 35–45 (2002).
89. Woo, G. L. Y., Mittelman, M. W. & Santerre, J. P. Synthesis and characterization of a novel biodegradable antimicrobial polymer. *Biomaterials* **21,** 1235–1246 (2000).
90. Dizman, B., Elasri, M. O. & Mathias, L. J. Synthesis, Characterization, and Antibacterial Activities of Novel Methacrylate Polymers Containing Norfloxacin. *Biomacromolecules* **6,** 514–520 (2005).
91. Moon, W.-S. *et al.* Antimicrobial activity of a monomer and its polymer based on quinolone. *J. Appl. Polym. Sci.* **90,** 1797–1801 (2003).
92. Chen, M. *et al.* Multifunctional Hyperbranched Glycoconjugated Polymers Based on Natural Aminoglycosides. *Bioconjug. Chem.* **23,** 1189–1199 (2012).
93. Samad, A., Sultana, Y. & Aqil, M. Liposomal drug delivery systems: an update review. *Curr. Drug Deliv.* **4,** 297–305 (2007).
94. Yang, M. & Santerre, J. P. Utilization of Quinolone Drugs as Monomers: Characterization of the Synthesis Reaction Products for Poly(norfloxacin diisocyanatododecane polycaprolactone). *Biomacromolecules* **2,** 134–141 (2001).
95. Moad, G. *et al.* Living free radical polymerization with reversible addition – fragmentation chain transfer (the life of RAFT).
96. Keddie, D. J. A guide to the synthesis of block copolymers using reversible-addition

fragmentation chain transfer (RAFT) polymerization. *Chem. Soc. Rev.* **43,** 496–505 (2014).
97. Chiefari, J. *et al.* Living Free-Radical Polymerization by Reversible Addition-Fragmentation Chain Transfer: The RAFT Process.
98. Moad, G., Chong, Y. K., Postma, A., Rizzardo, E. & Thang, S. H. Advances in RAFT polymerization: the synthesis of polymers with defined end-groups. (2005). doi:10.1016/j.polymer.2004.12.061
99. Mayadunne, R. T. A. *et al.* Living Radical Polymerization with Reversible Addition-Fragmentation Chain Transfer (RAFT Polymerization) Using Dithiocarbamates as Chain Transfer Agents. doi:10.1021/ma9906837
100. Kryger, M. B. L., Wohl, B. M., Smith, A. a a & Zelikin, A. N. Macromolecular prodrugs of ribavirin combat side effects and toxicity with no loss of activity of the drug. *Chem. Commun. (Camb).* **49,** 2643–5 (2013).
101. Michl, T. D. *et al.* RAFT-derived antimicrobial polymethacrylates: elucidating the impact of end-groups on activity and cytotoxicity. *Polym. Chem.* **5,** 5813 (2014).

CHAPTER 2. Objectives

Inhalable biothreats including *Burkholderia pseudomallei* and *Francisella tularensis* are of great clinical concern to public health and safety due to the aggressive *in vivo* replicative capacity of the pathogens. The current standard of care for treating these highly-infectious pulmonary bacteria are limited to oral and IV formulations of antibiotics that can have poor drug biodistribution to the lungs, require rigorous, prolonged drug dosing cocktails, and is clinically often times associated to disease relapse. In contrast, direct pulmonary drug delivery offers an exclusive, non-invasive, opportunity to provide localized therapy to the site of bacterial infection. Although inhalable free-drug formulations have been developed to address some of the shortcomings of oral and IV drug delivery, these systems have low pulmonary half-lives that fail to provide sustained therapy. For this reason, pulmonary delivery of free drug can require repeated self-administered dosing, and is associated to a high patient burden (low compliance). Historically, encapsulated drug systems, such as liposomes and polymeric nanoparticles, have been exploited to improve the pharmacokinetics of free drug by increasing *in vivo* drug residence times and decreasing drug clearance. Polymeric prodrugs, where the antibiotic has been incorporated into the polymer via a polymerizable group, offer an attractive alternative to encapsulated drug systems by enhancing drug loading, utilizing sophisticated drug-linkage chemistries for disease-specific applications, and improving manufacturing scalability. Controlled free-radical polymerization using polymerizable prodrug monomers is a creative strategy to engineer new inhalable antibiotic therapies consisting of drug-rich delivery vehicles with tunable drug release properties. To understand and evaluate the potential clinical impact of inhalable polymeric prodrugs derived from

polymerizable drug monomers against lethal highly-infectious pulmonary *F. tularensis* and *B. pseudomallei*, this thesis defines the following specific objectives:

1. To develop unimeric polymeric prodrug carriers that demonstrate tunable drug release behavior and bioactivity in an *in vitro* infectious bacterial co-culture model.
2. To demonstrate *in vivo* antibiotic efficacy in a highly-lethal aerosol challenge model, and establish the pharmacokinetics and biodistribution properties of resulting polymeric prodrug conjugates.
3. To develop and evaluate polymeric particulate morphologies for drug release, *in vivo* pharmacokinetics and biodistribution, and bioactivity against an established aerosol challenge model.

In meeting these objectives, this thesis develops a new class of antibiotic polymerizable prodrug monomers that can be used in reversible-addition fragmentation chain transfer (RAFT) polymerization technique to create new inhalable bioactive polymeric prodrugs of various architectures. These resulting constructs are unique in their ability to provide sustained drug release, have predetermined high-drug loading and polymer composition, and does not require the need for post-polymerization conjugation steps. In addition, the versatility of RAFT allows for the potential application and incorporation of a broad range of antibiotics targeting diverse diseases.

CHAPTER 3. RAFT polymerization of ciprofloxacin prodrug monomers for the controlled intracellular delivery of antibiotics*

*Provided as published: Das D., Srinivasan S., Kelly A.M., Chiu D.Y., Daugherty B.K., Ratner D.M., Stayton P.S., Convertine A.J. *Polymer Chemistry.* 7(4);826-37 (2016).

ABSTRACT

Prodrug monomers derived from the antibiotic ciprofloxacin were synthesized with phenolic or aliphatic esters linking the drug to a polymerizable methacrylate group. RAFT polymerization of these monomers exhibited linear pseudo-first-order kinetic and M_n vs. conversion plots and low Đ values throughout the polymerization. Prodrug monomers were then copolymerized with polyethyleneglycol methacrylate (O950) to yield hydrophilic copolymers with narrow Đ values. A poly(O950) macroCTA was also synthesized and chain extended with the antibiotic monomers to form diblock copolymers. The resultant copolymers and diblock copolymers were characterized via combination of ^{1}H and ^{19}F NMR and found to contain 16-17 and 30-35 wt.% Ciprofloxacin, respectively. DLS measurements suggest that the copolymers remain unimeric between pH 5.6-7.4 while the diblock copolymers form nanoparticles with diameters between 30-40 nm at physiological pH. Drug release kinetics were measured in human serum via HPLC. Copolymers containing Ciprofloxacin linked via phenolic esters showed faster hydrolysis rates with 40% drug released at 120h, whereas copolymers with the corresponding aliphatic ester linkages showed only 10% drug release over the same period. Diblock copolymers with a discrete ciprofloxacin block and a poly(O950) stabilizing block self-assemble into micelles greatly reducing hydrolysis rates for both ester linked drugs. *In vitro* toxicity measurements in

RAW 264.7 cells showed the copolymers to be nontoxic up to 20 mg/mL following a 24h incubation period. Co-culture efficacy was determined using *Burkholderia thailandensis* where an MIC of 0.6 and 6 mM were determined for the phenyl and aliphatic ester linked polymeric prodrugs, respectively.

3.1 Introduction

Respiratory melioidosis is an infectious disease found worldwide that is caused by the bacterium *Burkholderia pseudomallei*. Clinically, this disease presents as localized lung ulcerations with abscess formations and if left untreated can progress and disseminate into the bloodstream affecting all major organ systems. Mortality rates for these infections can be as high as 40% even with optimal antibiotic treatment.[4] The recommended treatment for this disease suffer from a number of significant limitations including: low therapeutic efficacy, poor drug biodistribution, and unfavorable pharmacokinetics.[5-7] A prodrug pulmonary delivery vehicle would enable controlled antibiotic release at a target site, and would help to lower dosing, decrease toxicity, prevent bacterial resistance.[8] Various pharmaceutical carriers (*e.g.* liposomes) are currently being developed to increase the stability and pharmacokinetic properties of administered drugs.[9-12] Liposomes, which are composite structures made primarily of lipids, are among well-investigated drug carriers for the delivery of water soluble drugs. For example, Wong et al. established the utility of Ciprofloxacin loaded di-palmitoyl-phosphatidylcholine liposomes after IV administration *in vivo* for increased circulation lifetime, which resulted in enhanced antibacterial activity against *Francisella tularensis* and improved delivery to key tissue systems including the liver and spleen. [13]

Despite their wide spread clinical use liposomal delivery systems are limited by low encapsulation efficiency for a number of important drugs and often require complex formulation procedures that are challenging to manufacture.[4,7,8,14,15] In contrast, polymer-drug conjugates can be synthesized with large amounts of the covalently linked prodrug without the need for formulation.[4,8] These polymeric prodrugs can designed to incorporate a range of sophisticated linkage chemistries or responsive self-immolation properties enabling the development of disease-specific release strategies.[16] A variety of polymer architectures have been evaluated for use as drug scaffolds including linear polymers, hyperbranched structures (e.g. dendrimers and hyperbranched polymers), and polymer brushes.[17-23] For example, Sanchez et al. prepared a library of poly-L-glutamic acid (PGA)-doxycycline (Doxy) conjugates through post-polymerization modifications of PGA carboxyl side chains into ester and amide functionalized drug linkages in efforts to investigate fibril deposits associated to familial amyloid polyneuropathy.[24] The authors demonstrated *in vitro* controlled release of drug from degradable ester modified PGA-Doxy conjugates with approximately 40% drug release within 16 days compared to the non-degradable amide alternative, which remained unaffected. Consequently, due to the stability of the amide linker employed, the study presented that IV administration *in vivo* of the PGA-amide-Doxy system was capable of having improved biodistribution compared to pure polymer negative controls and thereby may provide enhanced sustained therapy against amyloid polyneuropathy.

Polymerizable prodrug monomers provide an attractive route by which drug conjugates can be prepared directly without the need for post polymerization conjugation reactions. In this approach the therapeutic agent is linked to a polymerizable group via a hydrolytic or enzymaticly cleavable linkage. This approach has been employed by Dizman and coworkers to prepare copolymers containing methacrylated PEG and an antibacterial, Norfloxacin using conventional

free radical polymerization.[25] The resultant copolymers demonstrated functional efficacy at a polymer concentration of 25 mg/mL in an *in vitro* planktonic setting with a 100% reduction of bacterial load compared to no treatment. Reversible addition-fragmentation chain transfer (RAFT) polymerization is a versatile controlled living radical polymerization technique that enables the synthesis of polymers with predetermined molecular weights, complex architectures, and low molar mass dipsersities.[26] Moreover, RAFT technique has been employed by a variety of groups to prepare polymeric prodrugs with controlled molecular weights and low heterogeneity.[27] For example, Smith et al. utilized RAFT to copolymerize macromolecular prodrugs of the broad spectrum antiviral, Ribavirin, with the addition of poly(N-(2-hydroxypropyl) methacrylamide) (HPMA), as a therapeutic alternative against co-infections of HIV and the hepatitis C virus.[28] The authors observed fine control over the size and molecular weight distributions over varied target degree of polymerizations of their HPMA polymeric constructs with a maximum Ribavirin composition of 23 mol. %.

In this paper, we describe the use of RAFT polymerization to produce well-defined polymeric prodrugs of ciprofloxacin, an antibiotic used to treat many Gram negative bacteria, including Burkholderia pseudomallei, from monomeric drug precursors **(Scheme 1)**. The ability to incorporate ciprofloxacin with varied drug linker designs, and in controlled composition and steric relation to other comonomers can result in notable delivery advantages. We demonstrate copolymer and diblock copolymer designs that exhibit high drug loading and interesting mechanisms for controlling drug carrier architecture, solubility, drug release kinetics, and antibacterial efficacy.

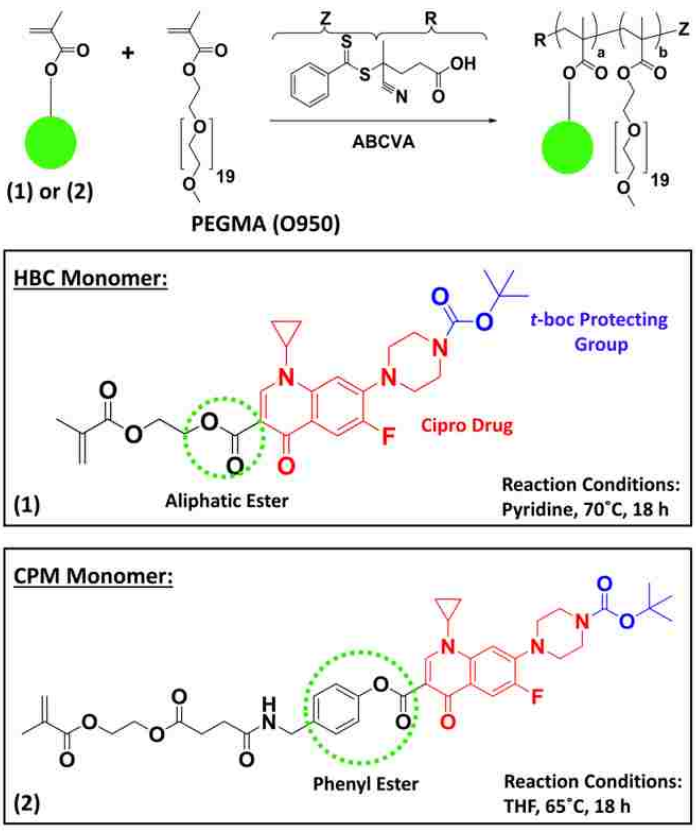

SCHEME 3.1. Synthetic strategy for the preparation of (1) poly(O950-*co*-HBC) and (2) poly(O950-*co*-CPM) via RAFT polymerization. The resultant copolymers contain aliphatic (1) and phenyl (2) esters linking the ciprofloxacin prodrugs to the polymer backbone. Cleavage of the *T*BOC protecting groups was accomplished by dissolving the copolymers in neat TFA for 2 h at 25 ^{o}C.

3.2 Experimental details

3.2.1 Materials

Chemicals and all materials were supplied by Sigma-Aldrich unless otherwise specified. Sodium trifluoroacetate was purchased from TCI America. Recombinant human butyrylcholinesterase (BChE) was obtained from R&D systems. PEGMA 950 (Aldrich) (30 g) was purified as described previously.[29] Spectra/Por regenerated cellulose dialysis membranes (6-8 kDA cutoff) where obtained from Fisher Scientific. G-25 prepacked PD10 columns were obtained from GE Life Sciences. MTS cytotoxicity kits were obtained from Promega. Unless otherwise stated, RAW 264.7 cells, murine derived macrophages (ATCC), were maintained in Dulbecco's modified eagle medium (DMEM) containing L-glutamine

(Gibco), 4.5g/L glucose, 10% fetal bovine serum (FBS, Invitrogen), and 1% penicillin-steptomycin (Gibco) at 37 °C and 5% CO_2.

3.2.2 Synthesis of (hydroxyethyl)methacrylate-boc-ciprofloxacin (HBC)

To 20 g (60 mmol) of ciprofloxacin in 350 mL of dioxane:water (1:1) was added 90 mL of 1N NaOH, followed by 20 g (91.6 mmol) of di-tert-butyl dicarbonate. The reaction mixture was stirred at room temperature for 17 h. The white precipitate obtained was filtered, washed with water and then with acetone. The product was dried under high vacuum overnight. Yield = 25.14 g (96.5 %). ^{1}H NMR (300 MHz, $CDCl_3$) δ 1.20 (m, 2H), 1.40 (m, 2H), 1.49 (s, 9H), 3.29 (t, J = 5.0 Hz, 4H), 3.54 (m, 1H), 3.67 (t, J = 5.0 Hz, 4H), 7.37 (d, J = 7.1 Hz, 2H), 7.99 (d, J = 12.9 Hz, 1H), 8.73 (s, 1H).

The resulting boc protected ciprofloxacin[30] 10.35 g (24 mmol), N,N,N',N'-tetramethyl-O-(1*H*-benzotriazol-1-yl)uronium hexafluorophosphate (HBTU) 22.8 g (0.16 mol) and N,N-dimethylpyridin-4-amine (DMAP) 292 mg (2.4 mmol) were taken in 500 mL of CH_2Cl_2 and cooled to 0 ^{0}C. N,N-diisopropylethylamine 21 mL (0.12 mol) was added, followed by 2-hydroxylethyl methacrylate 11.7 g (90 mmol). After 10 min at 0 ^{0}C, the solution was stirred at room temperature for 16 h. The reaction mixture was washed with brine (2 X 200 mL) and the organic phase was dried over anhydrous sodium sulfate. After evaporation of the solvent, the product HEMA-Boc-Ciprofloxacin (HBC) was precipitated in ether, and then purified by column chromatography using 5 % methanol in chloroform. Yield = 10.85 g (83.1 %). δ 1.13 (m, 2H), 1.30 (m, 2H), 1.48 (s, 9H), 1.94 (s, 3H), 3.20 (t, J = 4.8 Hz, 4H), 3.42 (m, 1H), 3.64 (t, J = 4.8 Hz, 4H), 4.50 (m, 4H), 5.58 (s, 1H), 6.15 (s, 1H), 7.29 (d, J = 7.0 Hz, 1H), 8.0 (d, J = 13.1 Hz, 1H), 8.47 (s, 1H). MS (ESI, m/z): calc. for $C_{28}H_{34}FN_3O_7$ (M): 543.6, found: 544.5 $[M+1]^+$, 566.4 $[M+Na]^+$and 582.2 $[M+K]^+$ **(Fig. 3.1)**.

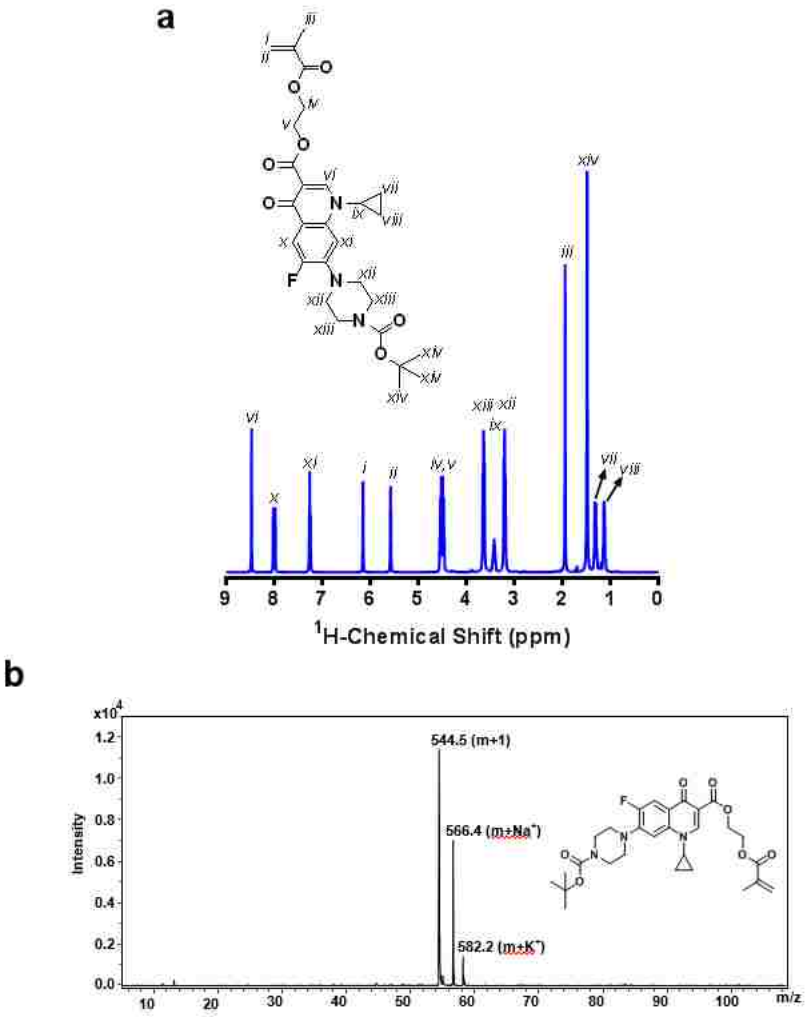

FIGURE 3.1. Representative (a) ^{1}H NMR and (b) mass spectroscopy of synthesized HEMA-Boc-Ciprofloxacin (HBC) monomer. Proton NMR scans were conducted in $CDCl_3$ at 500 MHz. Successful preparation of the indicated chemical structure was confirmed by the appearance of resonances associated with the tert-butyl group, residues from 2-hydroxyethyl methacrylate, and the parent drug. Mass spectroscopy was used as supporting data to validate the chemical structure of the resulting product (dominant species) by matching the molecular weight (544.5 m/z) of what is theoretically expected.

3.2.3 Synthesis of Ciprofloxacin-(phenol)methacrylate (CPM)

Mono-2-(methacryloyloxy)ethyl succinate 9.2 g (50 mmol) dissolved in 150 mL of CH_2Cl_2 was cooled to 0 ^{0}C. To this solution, *N*-hydroxysuccinimide 4.72 g (41 mmol) and *N*-*N*′-dicyclohexylcarbodimide 9.06 g (44 mmol) were added. After 15 min, the ice bath was removed and the reaction mixture was stirred at room temperature for 16 h. The byproduct dicyclohexylurea

was filtered off, and the filtrate was concentrated to 40 mL by evaporating the solvent under reduced pressure. This solution containing the activated NHS ester was directly added to 6.15 g (50 mmol) of 4-(aminomethyl)phenol pre-dissolved in 30 mL *N*,*N*-dimethylformamide, followed by 13.94 mL (0.1 mol) of trimethylamine. After stirring for 6 h at RT, the reaction mixture was diluted with 200 mL of CH_2Cl_2, and washed with water (2 X 100 mL). The organic layer was dried over anhydrous sodium sulfate and concentrated under reduced pressure. The thick residue obtained was treated with 100 mL ether, and vigorously stirred for 15 min. Then 75 mL of hexane was added, and again stirred well for 10 min. The solvent was carefully decanted and the process was repeated one more time. The product obtained was further purified by flash column chromatography using 5 % methanol in chloroform. Overall yield for two steps: 10.16 g (76 %). ^{1}H NMR (300 MHz, $CDCl_3$) δ 1.93 (s, 3H), 2.50 (t, J = 6.7 Hz, 2H), 2.72 (t, J = 6.7 Hz, 2H), 4.30 (s, 4H), 4.34 (d, J = 5.6 Hz, 2H), 5.59 (m, 1H), 6.08 (t, J = 5.6 Hz, 1H), 6.12 (s, 1H), 6.30 (s, 1H), 6.75 (d, J = 8.5 Hz, 2H), 7.09 (d, J = 8.5 Hz, 2H). MS (ESI, m/z): calc. for $C_{17}H_{21}NO_6$ (M): 335.4, found: 358.8 $[M+Na]^+$ and 693.8 $[2M+Na]^+$.

Boc protected ciprofloxacin (as synthesized from above)[30] 2.15 g (5 mmol) and N,N-dimethylpyridin-4-amine (DMAP) 610 mg (5 mmol) were taken in 250 mL of CH_2Cl_2 and cooled to 0 ^{0}C. To this solution, N,N,N',N'-tetramethyl-O-(1*H*-benzotriazol-1-yl)uronium hexafluorophosphate (HBTU) 4.74 g (12.5 mmol) was added, followed by N,N-diisopropylethylamine 3.5 mL (20 mmol). After 10 min at 0 ^{0}C, the reaction mixture was stirred at RT for 30 min, and then cooled back to 0 ^{0}C. The phenolic monomer 1.68 g (5 mmol) was introduced and the reaction was continuously stirred at 0 ^{0}C for 20 min, and then at RT for 16 h. The reaction mixture was filtered and the filtrate was washed with water (100 mL) and brine (100 mL). The organic phase was dried over anhydrous sodium sulfate and the solvent was evaporated

under reduced pressure. The residue was precipitated in ether, and then purified by column chromatography using 30 % tetrahydrofuran in chloroform containing 0.1 % triethylamine. Yield = 2.45 g (65.4 %). ^{1}H NMR (300 MHz, $CDCl_3$) δ 1.18 (m, 2H), 1.35 (m, 2H), 1.5 (s, 9H), 1.94 (s, 3H), 2.52 (t, J = 6.7 Hz, 2H), 2.73 (t, J = 6.7 Hz, 2H), 3.33 (t, J = 4.9 Hz, 4H), 3.45 (m, 1H), 3.65 (t, J = 4.9 Hz, 4H), 4.32 (s, 4H), 4.44 (d, J = 5.7 Hz, 2H), 5.58 (m, 1H), 6.12 (s, 1H), 6.18 (t, J = 5.5 Hz, 1H), 7.15 (d, J = 8.5, 2H), 7.29 (two doublets merged, 3H), 8.05 (d, J = 13.1 Hz, 1H), 8.63 (s, 1H). MS (ESI, m/z): calc. for $C_{39}H_{45}FN_4O_{10}$ (M): 748.8, found: 750.1 $[M+1]^+$ and 771.8 $[M+Na]^+$ **(Fig. 3.2)**.

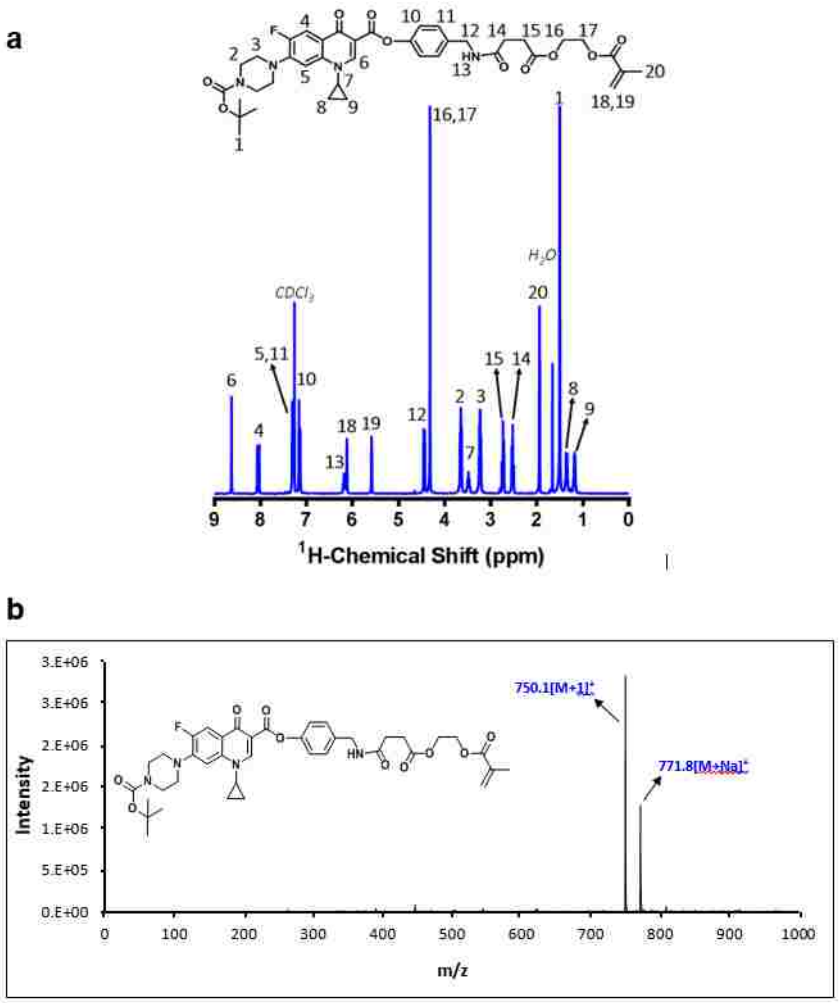

FIGURE 3.2. Representative (a) ^{1}H NMR and (b) mass spectroscopy of synthesized Ciprofloxacin Phenyl Methacrylate (CPM) monomer. Proton NMR scans were conducted in $CDCl_3$ at 500 MHz. Successful preparation of the indicated chemical structure was confirmed by the appearance of resonances associated with the tert-butyl group (1), residues from the (aminomethyl) phenolic group (10-13), and the parent drug (2-6). Mass spectroscopy was used as supporting data to validate the chemical structure of the resulting product (dominant species) by matching the molecular weight (750.1 m/z) of what is theoretically expected.

3.2.4 Kinetic evaluation of HBC

Kinetic evaluation of HBC was conducted with 4-cyano-4-(phenylcarbonothioylthio)pentanoic acid (CTP) and 4,4′-Azobis(4-cyanovaleric acid) (ABCVA) as the RAFT chain transfer agent and initiator respectively in acetic acid at 70 °C. The initial monomer to CTA to initiator ($[M]_o$:$[CTA]_o$:$[I]_o$) ratio was 25:1:0.2. In order to understand the influence of the degree of polymerization (DP) on the evolution of molecular weight, RAFT polymerizations of HBC were conducted under similar reaction conditions with

$[CTA]_o$:$[I]_o$ ratio of 5:1 and $[M]_o$:$[CTA]_o$ ratios of 12.5, 25, 50, and 100. Individual polymerization solutions were transferred to a septa-sealed vial and purged with nitrogen for 20 minutes. After the allotted time, the polymerization vials were transferred to a preheated water bath at 70 ^oC and allowed to polymerize for 2.5 h. Following polymerization, the individual vials were quenched by exposure to oxygen by opening the septa seal and immersing the vials in ice. The polymerizations were evaluated for monomer conversion via ^1H NMR in C_2D_6OS by comparing the HBC vinyl resonances at δ = 6.1 and 5.7 ppm to ester resonances at δ = 4.4 and 4.1 ppm.

3.2.5 RAFT copolymerization of PEGMA 950 (O950) and HBC

The RAFT copolymerization of poly(O950-*co*-HBC) was conducted in pyridine with CTP and ABCVA as the CTA and initiator respectively with $[M]_o$:$[CTA]_o$ and $[CTA]_o$:$[I]_o$, equal to 25:1 and 10:1. To a 100 mL round-bottom flask was added CTP (112.6 mg, 403 μmol), ABCVA (11.3 mg, 40.3 μmol), HBC (1.25 g, 2.62 mmol), O950 (7.08 g, 7.46 mmol), and pyridine (40.67g). The solution was then septa sealed and purged with nitrogen for 60 minutes. The round-bottom flask was then transferred to a preheated water bath at 70 ^oC and allowed to polymerize for 18 hours. The polymeization solution was then precipitated in ether and the resultant polymer was dried in vacuo for 48 h. The final molecular weight and Đ, as measured by GPC, and molar composition of poly(O950-*co*-HBC) was 13.1 kDa, 1.08, and 72:28 O950:HBC (74:26 feed), respectively. This corresponded to a 16 wt. % Ciprofloxacin incorporation. Copolymer compositions was determined by both ^1H NMR and ^{19}F NMR. Briefly, analysis by ^{19}F NMR used sodium trifluoroacetate ($C_2F_3NaO_2$) as an internal standard where 1.5 uL of a 10 mg/mL solution of $C_2F_3NaO_2$ was added to 1 mL of a 20 mg/mL polymer solution in C_2D_6OS and molar composition was determined by comparing the three fluorine resonances from the internal standard at δ = -73.4 ppm against the single fluorine resonances from Ciprofloxacin containing copolymer

at δ = -124.5 ppm. Molar compositions were also analyzed by ^{1}H NMR in $CDCl_3$ by comparing the HBC (9H) *t*-boc resonances at δ = 1.52 ppm to the O950 (3H) methoxy at δ = 3.4 ppm. Both methods of drug quantification were in good agreement and resulted in similar drug composition. For the purpose of this study, values obtained by ^{19}F NMR are being reported for all polymer systems.

3.2.6 RAFT copolymerization of O950 and CPM.

The RAFT copolymerization of poly(O950-*co*-CPM) was conducted in THF with CTP and ABCVA as the CTA and initiator respectively with $[M]_o$:$[CTA]_o$, $[CTA]_o$:$[I]_o$, equal to 25:1 and 10:1, similar to the polymerization of poly(O950-*co*-HBC). To a 25 mL round-bottom flask was added CTP (38.8 mg, 139 μmol), ABCVA (3.89 mg, 13.9 μmol), CPM (1.00 g, 1.34 mmol), O950 (2.03 g, 2.14 mmol), and THF (14.15g). The solution was then septa sealed and purged with nitrogen for 30 minutes. The round-bottom flask was then transferred to a preheated water bath at 65 ^{o}C and allowed to polymerize for 18 hours. The polymerization solution was then precipitated in ether and dried in vacuo for 48 h. The final molecular weight and Đ, as measured by GPC and molar composition of poly(O950-*co*-CPM) was 11.8 kDa, 1.09, and 64:36 O950:CPM (80:20 feed), respectively (16.7 wt. % Ciprfloxacin in the final copolymer). Similar to poly(O950-*co*-HBC), the copolymer composition of poly(O950-*co*-CPM) was determined by both ^{19}F NMR and, independently, by ^{1}H NMR, as previously described above.

3.2.7 Synthesis of poly(O950) via RAFT

The synthesis of a poly(O950) macroCTA was conducted in DMSO with CTP and ABCVA as the CTA and initiator respectively with $[M]_o$:$[CTA]_o$, $[CTA]_o$:$[I]_o$, equal to 25:1 and 10:1.[29] To a 50 mL round-bottom flask was added CTP (82.34 mg, 2.95 μmol), ABCVA (8.26 mg, 29.5

μmol), O950 (7.00 g, 7.37 mmol), and DMSO (28 g). The solution was then septa sealed and purged with nitrogen for 60 minutes. The round-bottom flask was then transferred to a preheated water bath at 70 ºC and allowed to polymerize for 18 hours. The transparent solution was then precipitated in ether six times, solvent decanted, and product collected and dried in vacuo. The resulting polymer had a molecular weight and Đ of 17.5 kDa and 1.12, respectively.

3.2.8 Synthesis of poly[(O950)-b-(HBC)] and poly[(O950)-b-(CPM)] via RAFT

The RAFT polymerization of poly[(O950)-*b*-(HBC)] from a poly(O950) macroCTA (17.5 Da, 1.12 Đ) was conducted in acetic acid with $[M]_o$:$[mCTA]_o$, $[mCTA]_o$:$[I]_o$ equal to 25:1 and 5:1. To a 25 mL round-bottom flask was added O950 mCTA (644 mg, 36.8 μmol), ABCVA (2.06 mg, 7.36 μmol), HBC (0.5 g, 0.92 mmol), and acetic acid (2.64 g). The solution was then septa sealed and purged with nitrogen for 30 minutes. The round-bottom flask was then transferred to a preheated water bath at 70 ºC and allowed to polymerize for 2.5 hours. The solution was then precipitated in ether for six times, solvent decanted, and product collected, dried in vacuo, and lyophilized over 48 h. The final molecular weight, Đ, and composition of poly[(O950)-*b*-(HBC)] was 48 kDa and 1.27, respectively, corresponding to DPs for each blocks of 18 and 56 respectively (34 wt. % ciprofloxacin in the final copolymer). Similar to the copolymers, the diblock compositions were determined by both ^{1}H NMR and ^{19}F NMR. Briefly for ^{19}F NMR analysis, 3 uL of a 10 mg/mL solution of $C_2F_3NaO_2$ was added to 1 mL of 20 mg/mL diblock polymer solution in C_2D_6OS and molar composition was determined again by comparing the three fluorine resonances from the internal standard at δ = -73.4 ppm against the single fluorine resonances from Ciprofloxacin diblock polymer at δ = -124.5 ppm. In addition, ^{1}H NMR in $CDCl_3$ was used to again compare the HBC (9H) *t*-boc resonances at δ = 1.52 ppm to the O950 (3H) methoxy at δ =

3.4 ppm. Analogous to the copolymers, values obtained from ^{19}F NMR are being reported for both diblocks.

The RAFT polymerization of poly[(O950)-*b*-(CPM)] utilized the same O950 mCTA homopolymer (Mn = 17.5 kDa, Đ = 1.12) as the one used in the synthetic strategy for the polymerization of poly[(O950)-*b*-(HBC)], as noted above. This reaction was conducted in THF with $[M]_o$:$[mCTA]_o$, $[mCTA]_o$:$[I]_o$ equal to 25:1 and 10:1. To a 10 mL round-bottom flask was added O950 mCTA (455 mg, 26.7 μmol), ABCVA (0.75 mg, 2.67 μmol), CPM (0.5 g, 0.67 mmol), and THF (2.55 g). The solution was then septa sealed and purged with nitrogen for 30 minutes. The round-bottom flask was then transferred to a preheated water bath at 65 ºC and allowed to polymerize for 18 hours. The final copolymer was subsequently isolated as detailed above. The final molecular weight, Đ, and composition of poly[(O950)-*b*-(CPM)] was 41.8 kDa and 1.35, respectively, corresponding to DPs for each blocks of 18 and 32 respectively (30 wt. % ciprofloxacin in the final copolymer).

3.2.9 Deprotection and purification of copolymer and diblock systems

Postpolymerization removal of the TBOC protecting groups, present on HBC and CPM residues, was conducted in neat trifluoroacetic acid (TFA) and 1:1 $CHCl_3$:TFA, respectively at a polymer concentration of 50 mg/mL . The reaction was allowed to proceed at 25ºC for 2h after which time the solution was precipitated in ether. The product was collected and dried in vacuo for 48 h. In order to remove any excess TFA salts that might be present, the polymers were redisolved in molecular grade water and dialyzed against first 250 mM and then 10 mM NaH_2PO_4 at pH 7.4 with repeated buffer changes (2-3x) over two days. The polymers were then frozen and lyophilized before further purification via PD-10 desalting column (GE Life Sciences) followed by lyophilization for an additional 48 h.

3.2.10 Gel permeation chromatography (GPC)

Absolute molecular weights and polydisperity indices were determined using using Tosoh SEC TSK-GEL α-3000 and α-e4000 columns (Tosoh Bioscience, Montgomeryville, PA) connected in series to an Agilent 1200 Series Liquid Chromatography System (Santa Clara, CA) and Wyatt Technology miniDAWN TREOS, 3 angle MALS light scattering instrument and Optilab TrEX, refractive index detector (Santa Barbara, CA). HPLC-grade DMF containing 0.1 wt.% LiBr at 60 ^{o}C was used as the mobile phase at a flow rate of 1 ml/min.

3.2.11 Characterization of copolymer and diblock micelles

Dynamic light scattering (DLS) studies of the block copolymers were conducted using a Malvern Instruments Zetasizer Nano series instrument equipped with a 22 mW He-Ne laser operating at 632.8 nm. Solutions of the copolymer and diblock were prepared in the pH range capturing the endosomal trafficking pathway (7.4, 7.0, 6.6, 6.2, 5.8, 5.2, and 4.6) with either 100 mM sodium phosphate or acetate buffer with 150 mM NaCl at a polymer concentration of 0.5 mg/mL. The resulting solutions were filtered with 0.22 μm filters prior to measurement, and mean diameter was defined as the ± half peak width. All measurements were performed in triplicate comparing the copolymer to the diblock. The polymer micelles were analysed for zeta potential, using a ZetaPALS detector, at 1 mg/mL polymer concentration as a function of pH (7.4, 7.0, 6.6, 6.2, 5.8, and 5.2) with either 10 mM sodium phosphate or acetate buffer.

3.2.12 Analysis of Ciprofloxacin by high-performance liquid chromatography

The HPLC analysis of Ciprofloxacin was carried out with an Agilent 1260 Quaternary HPLC Pump, Agilent 1260 Infinity Standard Automatic Sampler, Agilent 1260 Infinity Programmable Absorbance Detector, and Agilent ChemStation software for LC system (Palo Alto, CA). Both ciprofloxacin hydrochloride (Sigma Aldrich) and liquid Sera Human from AB blood donor (Sigma Aldrich) were purchased and used as received. The analyte was separated at ambient

temperature using a Zorbax RX-C_{18} (4.6 x 150 mm; 5 µm) analytical column (Agilent Technologies, CA).

The UV detector was operated at 277 nm, and the mobile phase consisted of 2% aqueous acetic acid and acetonitrile (84:16) v/v, as described elsewhere.[31] The flow rate was set at 1.0 mL/min and sample injection volume at 20 µL. A stock solution of Ciprofloxacin was prepared in deionized water at 10 mg/mL. Working solutions of Ciprofloxacin for standard curves were diluted from stock solution using the mobile phase to the listed concentrations of 200 µg/mL, 100 µg/mL, 50 µg/mL, 25 µg/mL, 12.5 µg/mL, 6.25 µg/mL, 3.12 µg/mL, and 1.56 µg/mL.

Each listed solution above was diluted with a 1:1 v/v ratio of either mobile phase:deionized water or mobile phase:human serum to create a final Ciprofloxacin standards of 100 µg/mL, 50 µg/mL, 25 µg/mL, 12.5 µg/mL, 6.25 µg/mL, 3.12 µg/mL, 1.56 µg/mL, and 0.78 µg/mL for pharmaceutical and biological analysis, respectively. Both non-serum (mobile phase:deionized water) and serum standards were subsequently treated with 50% acetonitrile (v/v) to promote protein precipitation. Serum standards were centrifuged at 12,000g for 15 minutes and supernatants were collected and filtered using a 0.45µm low protein binding filter before HPLC analysis. Non-serum standards were analyzed without the need for centrifugation. All standards were processed using a gradient HPLC elution profile, where the mobile phase transitioned to 100% acetonitrile over 15 minutes, followed by 10 minutes of column washing with acetonitrile and water and 5 minutes of equilibration with mobile phase.

3.2.13 Drug release from polymeric prodrugs

The drug release from polymer conjugates was carried out in serum at 37 ˚C at a polymer concentration of 6 mg/mL. Sample time points were collected on a regular basis. Quantification of total Ciprofloxacin in the polymer conjugates was measured by taking 6 mg/mL of polymer and dissolving it in

10% aq. H_2SO_4 for 48 h at 25 ˚C, denoted by Peak(H_2SO_4). The HPLC with a gradient elution profile was used to quantify amount of drug released using the same instrument parameters set forth for drug standards. A 1:1 dilution of serum sample to 2% aqueous acetic acid and acetonitrile (84:16) v/v was conducted, followed by another 1:1 dilution with acetonitrile. The resulting samples were vortexed and centrifuged at 12,000g for 15 minutes. Supernatants were collected and filtered using a 0.45µm low protein binding filter before running on the HPLC. Percent (%) drug released was subsequently quantified using the formula: % Drug Released = [Peak(t_x) – Peak(t_0)]/[Peak(H_2SO_4)], where t_x and t_0 are the peaks resolved by the HPLC at time x and zero, respectively.

3.2.14 In vitro cytotoxicity measurements

The cytotoxicity of the prodrug copolymers and diblocks were evaluated in RAW 264.7 cells using the CellTiter 96AQueous One Solution Cell Proliferation Assay (MTS) (Promega Corp., Madison, WI). RAW cells were seeded in DMEM (Gibco, Life Technologies, Grand Island, NY) containing 1% pen/strep and 10% fetal bovine serum (FBS) at a density of 50,000 cells/well in 96-well plates and allowed to adhere for 18 h at 37 °C with 5% CO_2. After incubation, polymers diluted in supplemented DMEM at a concentration of 40 mg/mL total polymer were added to cells in triplicate wells in a 1:1 dilution, then serially diluted down the plate (20 mg/mL-9.77 µg/mL), and cells were incubated for 24 hours. After the allotted time, cells were evaluated using the CellTiter MTS assay according to the manufactures instructions. The absorbance at 490 nm was evaluated using a Tecan Safire 2 microplate reader. MTS reagent alone was used as a negative control and all treatments were compared to untreated cells as a positive control to acquire percentage viability. All experiments were carried out in triplicate wells on duplicate days.

3.2.15 In vitro co-culture activity using a B. thailandensis infection model

To evaluate the *in vitro* efficacy of the polymer systems, RAW 264.7 murine macrophage cells were seeded into 48 well plates at a density of 500,000 cells/mL in 250 µL of antibiotic free DMEM (Gibco) + 10% FBS and allowed to adhere for 18 h at 37 °C with 5% CO_2. After 18 hours, RAW cells were infected with *Burkholderia thailandensis* (E264) at early log phase (OD_{600}=0.2) at a MOI of 5, and incubated for 1 hour. Growth media was then replaced with fresh DMEM containing 10% FBS and 250 µg/mL Kanamycin to remove extracellular bacteria and cells were incubated for another hour. Media was then replaced with unsupplemented DMEM containing varying concentrations of HBC copolymer (20-3000 µg/mL), CPM copolymer (1-2000 µg/mL), or free drug (0.01-100 µg/mL) into triplicate wells per treatment. Cells were incubated an additional 22 hours. After incubation, cell media was aspirated, cells were washed three times with 1x PBS, and lysed with 100 µL of PBS + 0.1% Triton X-100 (Sigma Aldrich, St. Louis, MO). Lysates were pooled by treatment, serially diluted, and plated onto triplicate LB agar plates at multiple10x dilutions, and incubated for 24 hours. After 24 hours colony forming units (CFU) were counted. Data represented as CFU/well vs. Ciprofloxacin dose. All experiments were repeated on duplicate days.

3.3 Results and discussion

3.3.1 Synthesis of monomer prodrugs HBC and CPM

Synthetic illustration of methacrylate Ciprofloxacin prodrug monomers HBC and CPM carrying aliphatic and phenyl ester linkages respectively **(Scheme 3.2)**. Using HBC and CPM, the Ciprofloxacin loading of the polymer prodrug can be controlled precisely by manipulating the molar ratio of the drug monomers during polymerization. Boc Ciprofloxacin[30] was effectively

conjugated to monomers via aliphatic or phenolic hydroxyl group using benzotriazole based uronium coupling reagent HBTU.

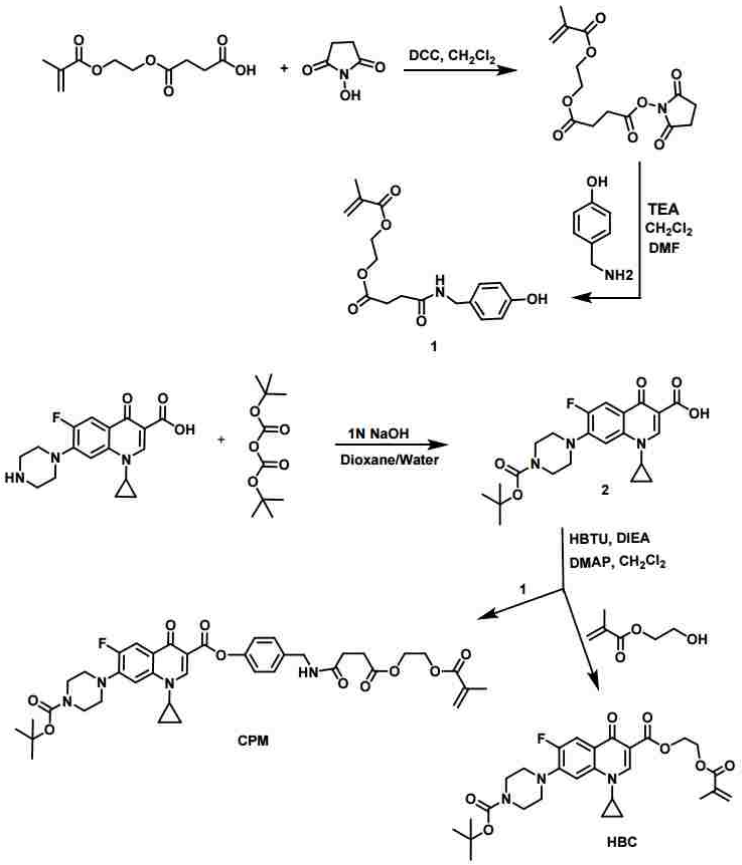

SCHEME 3.2. Synthesis of (1) butanoic acid, 4-[(4-hydroxyphenyl)methylamino]-4-oxo, 1-(2-methacryloyloxy)ethyl ester, (2) Boc Ciprofloxacin, and resulting prodrug monomers, HBC and CPM.

3.3.2 Kinetic evaluation of HBC

In order to understand the polymerization behavior of the bulky methacrylate-based prodrug monomers kinetics studies were conducted with HBC. In these studies, HBC was polymerized at 70 ^{o}C in acetic acid using the dithiobenzoate-based RAFT agent CTP and ABCVA as initiator respectively. Following a short induction period (~20 min) polymerization proceeds with linear pseudo-first order

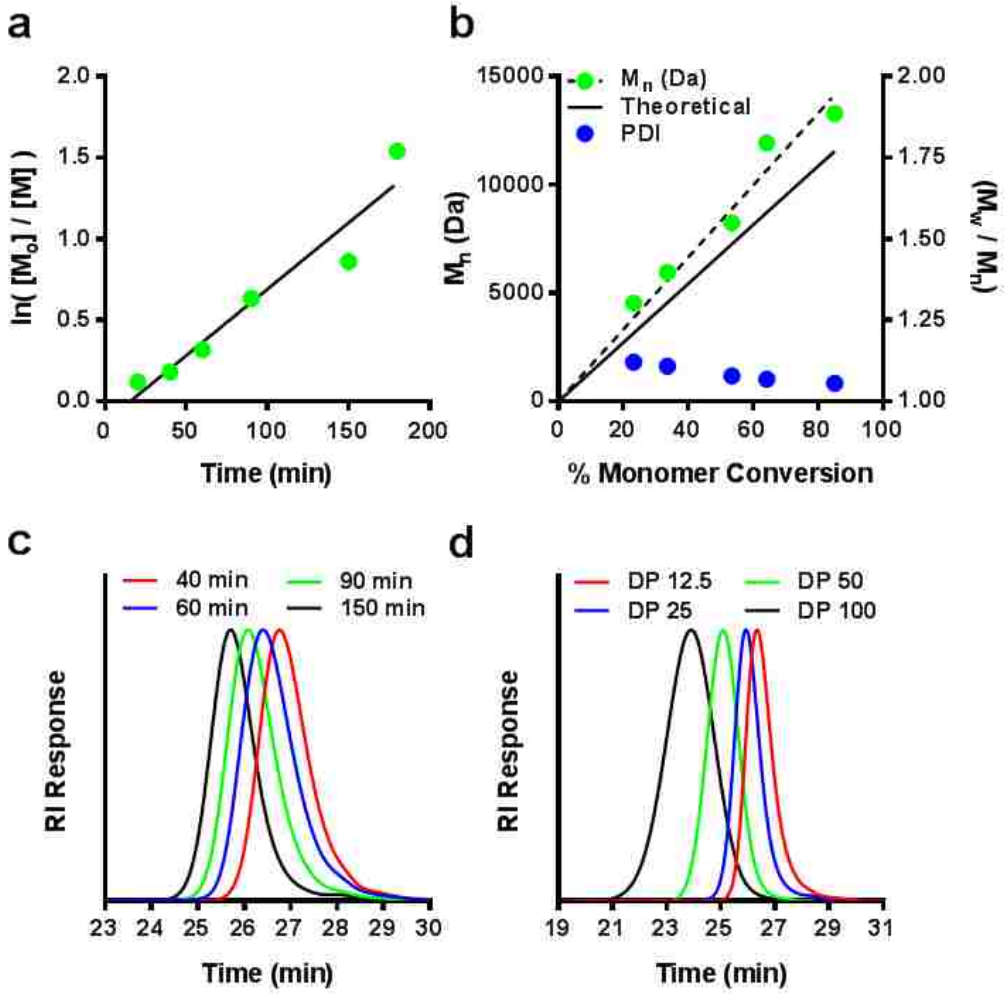

Figure 3.3. Kinetic analysis of the RAFT polymerization of HBC**.** (a) Pseudo first order rate plot, (b) Mn and Đ vs. conversion, and (c) RI traces showing the evolution of molar mass with time for $[M]_o$:$[CTA]_o$:$[I]_o$ equal to 25:1:0.2 at 70 °C with CTP and ABCVA as the chain transfer agent and initiator respectively. (d) Molecular weight distributions for the RAFT polymerization of HBC conducted at initial $[M]_o$/$[CTA]_o$ ratios of 12.5, 25, 50, and 100 at a fixed initial $[M]_o$ and $[CTA]_o$/$[I]_o$ ratio 20 wt% and 10 respectively. M_n (Da) and Đ values for the series were determined to be: DP 12.5 (7650/1.09), DP 25 (12000/1.07), DP 50 (26300/1.08), and DP 100 (52400/1.15). Absolute molecular weight values were determined by SEC equipped with inline laser light scattering detectors. Monomer conversion was determined by ^{1}H NMR by comparison of the vinyl resonances normalized to the total ester region relative prepolymerization values.

kinetics **(Fig. 3.3A)** suggesting that radical termination reactions remain low throughout the course of the polymerization. Evaluation of the M_w/M_n and M_n vs. conversion plots illustrates the controlled nature of HBC under polymerizations these conditions. As shown in **Fig. 3.3B**, M_n versus conversion plot remains linear up to relatively high monomer conversion (~80%) with low

molar mass dispersities and good agreement with the theoretical molecular weights. For example, polymerization of HBC for 40 min results in 23 % monomer conversion with experimental and theoretical molecular weights of 4.5 and 3.2 kDa, respectively, and a Đ of 1.12, while at 3 hours 85% conversion is reached with an M_n of 13.3 kDa ($M_{n\ theory}$ of 12.2 kDa) with a Đ of 1.06. Given the close agreement between the theoretical and experimental molecular weights under these conditions, it is likely that degradative chain transfer reactions are not occurring to a significant extent. Analysis of the MWDs shows that the peaks are unimodal and symmetric with a clear shift to lower elution volumes as a function of reaction time **(Fig. 3.3C)**. Narrow and symmetric MWDs were also observed for the polymerization of HBC targeting a range of DPs between 12.5 and 100 with a slight increase in the molar mass dispersity (Đ ~1.15 at 64% conversion) for polymerizations targeting a DP of 100 **(Fig. 3.3D)**. The lack of significant low molecular weight tailing in the MWDs coupled with low Đs and subsequent blocking experiments provide strong evidence supporting the controlled nature of these polymerizations despite the steric bulkiness of the ciprofloxacin monomer.

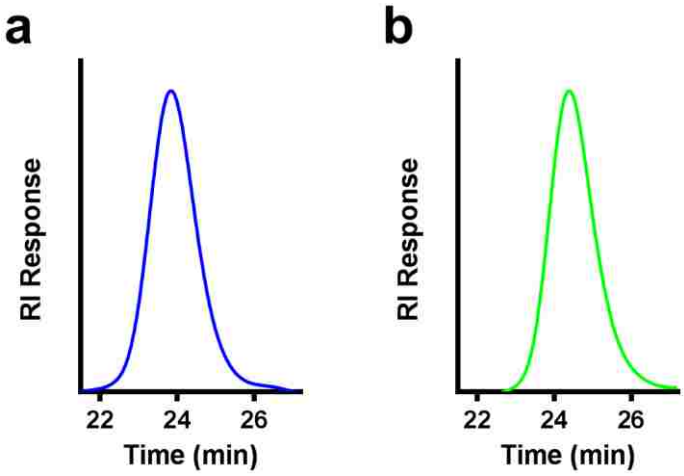

FIGURE 3.4. RI traces as measured by GPC showing molecular weight distributions of the copolymers (a) poly(O950-*co*-HBC) and (b) poly(O950-*co*-CPM). The RAFT polymerization of the copolymers were conducted in pyridine (blue) and THF (green), respectively, with $[M]_o$:$[CTA]_o$:$[I]_o$ equal to 25:1:0.1, and had a M_n of 13.1 and 11. 8 kDa with a Đ of 1.08 and 1.09, respectively.

3.3.3 RAFT copolymerization of HBC and CPM

Shown in **Scheme 1.**, is the synthetic strategy for the preparation of hydrophilic PEGMA-based copolymers with Ciprofloxacin linked to the polymer backbone via aliphatic (HBC) and phenyl ester (CPM) groups. Based on the favorable kinetic profile for HBC the RAFT copolymerization of this monomer with O950 was conducted at the same target $[M]_o/[CTA]_o$ and $[CTA]_o/[I]_o$ ratios (i.e. 25:1 and 5:1) **(Scheme 1)**.

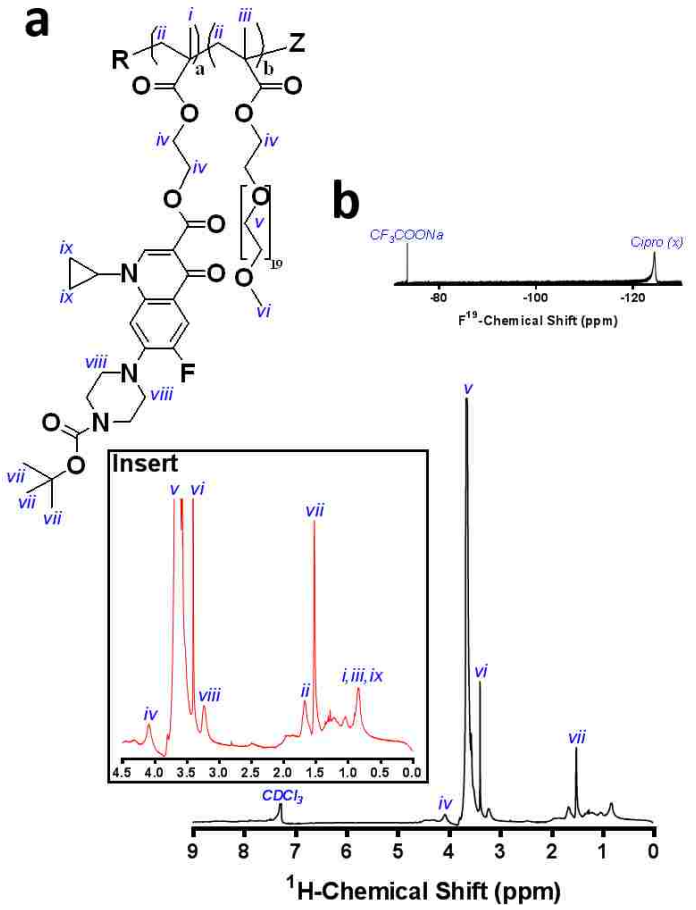

FIGURE 3.5. Representative (a) ^{1}H NMR and (b) ^{19}F NMR spectrum of poly(O950-*co*-HBC) in $CDCl_3$ and C_2D_6SO respectively with assignment of key resonances associated with the comonomers. Copolymer composition was determined by comparing the HBC (9H) *T*BOC resonances at δ = 1.52 ppm to the O950 (3H) methoxy resonance at δ = 3.4 ppm. ^{19}F NMR was conducted in C_2D_6SO using sodium trifluoroacetate ($C_2F_3NaO_2$) (0.11 μM) as an internal standard. Integration of the ciprofloxacin resonance at δ = -124.5 ppm (1F) relative to the internal standard at δ = -73.4 ppm (3F) was used to calculate the final polymer copolymer composition.

A molar feed ratio of O950 to HBC of 74:26 (mol:mol) was selected to prevent the hydrophobic HBC residues from inducing self-assembly of the copolymers into nanoparticles at physiological pH values. After isolation of the polymer via precipitation in ether, the M_n and Đ as measured by GPC **(Fig. 3.4A)** were determined to be 13.1 kDa and 1.08, respectively **(Table 3.1).** Copolymer composition was determined by both ^{1}H NMR **(Fig. 3.5A)** and ^{19}F NMR **(Fig. 3.5B)** with the latter technique yielding a molar composition of 72% O950 and 28% HBC (16 wt.% Ciprofloxacin). Key copolymer resonances **(Fig. 3.5A)** include the characteristic (9H) TBOC protective groups at $\delta = 1.52$ ppm

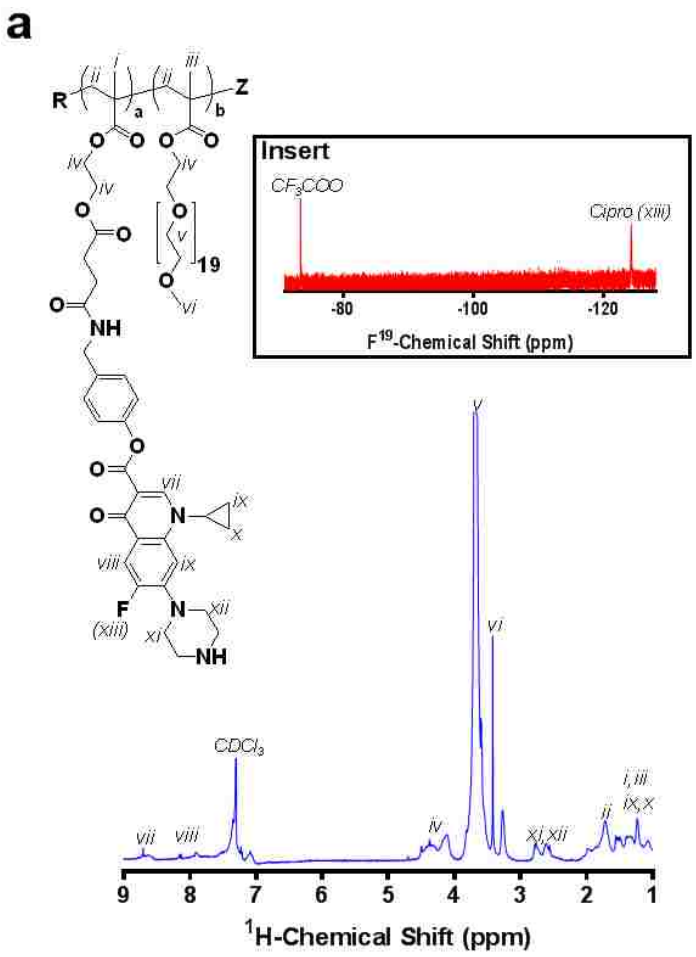

FIGURE 3.6. Representative ^{1}H NMR and ^{19}F NMR (insert) spectrum of poly(O950-*co*-CPM) in $CDCl_3$ and C_2D_6OS respectively with assignment of the characteristic resonances associated with the comonomers. Copolymer composition was determined by comparing the HBC (9H) *T*BOC resonances at δ = 1.52 ppm to the O950 (3H) methoxy resonance at δ = 3.4 ppm. Successful deprotection of copolymer systems was quantitatively indicated by the later disappearance of the characteristic *T*BOC resonance. ^{19}F NMR was conducted in C_2D_6SO using sodium trifluoroacetate ($C_2F_3NaO_2$) (0.11 µM) as an internal standard. Integration of the ciprofloxacin resonance at δ = -124.5 ppm (1F) relative to the internal standard at δ = -73.4 ppm (3F) was used to calculate the final polymer copolymer composition.

(sharp), the (3H) O950 methoxy residues at δ = 3.4 ppm (sharp), and the polymer backbone alkyl esters at δ = 4.1 ppm (sharp to broad). To produce the therapeutically active form of the polymeric prodrug, the tBOC protecting groups were removed using neat TFA at 25 ^{o}C for 2 h. Quantitative tBOC removal of was confirmed by ^{1}H NMR by following the disappearance of the sharp (9H) resonance at δ = 1.52 ppm. The synthesis of poly(O950-*co*-CPM) was conducted under conditions

similar to those employed for HBC except that the temperature was reduced to 65 ^{o}C to minimize the potential for cleavage of the more labile phenyl ester linkages. Because of the greater solubility of the CPM monomer in organic solvents it was possible to conduct polymerizations in THF. Similar to the polymerization of poly(O950-*co*-HBC), a feed ratio of 80:20 (mol:mol) O950:CPM was selected to prevent association of the hydrophobic CPM residues and subsequent formation of self-assembled nanoparticles. Copolymer composition (via ^{19}F NMR) was determined to be 64 mol % O950 and 36 mol % (80 mol % O950 and 20 mol % CPM feed) **(Fig. 3.6)** with M_n and Đ values, as measured by GPC **(Fig. 3.4B),** of 11.8 kDa and 1.09, respectively **(Table 3.1).**

TABLE 3.1. Summary of composition, molecular weights, and molar mass dispersity for statistical copolymers of HBC and CPM with O950.

Poly. #	O950 (feed)	O950 (exp.)	HBC (feed)	HBC (exp.)	CPM (feed)	CPM (exp.)	M_n (kDa)	dndc	Đ	Drug (wt.%)
1	74	65	26	35	-	-	13.1	0.061	1.08	16
2	80	64	-	-	20	36	11.8	0.093	1.09	16.7

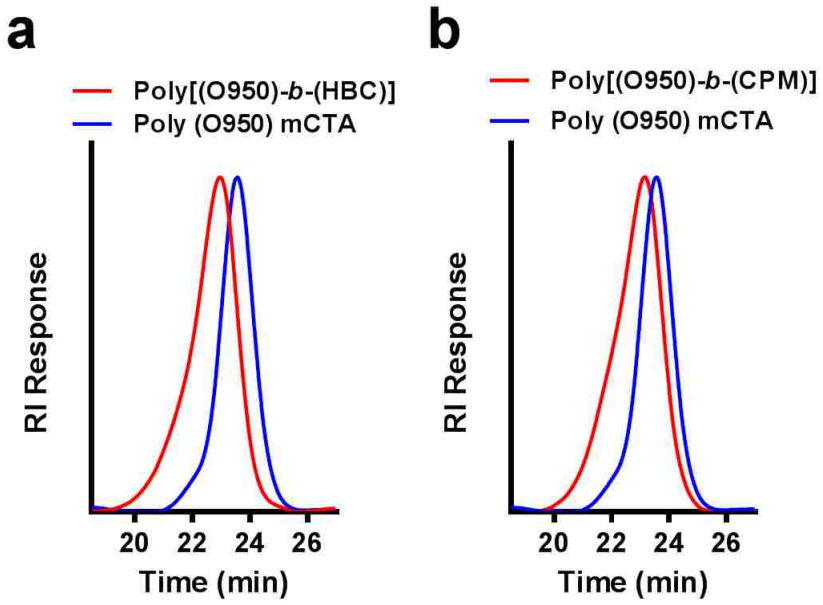

FIGURE 3.7. SEC chromatograms supporting the formation of (a) poly[(O950)-*b*-(HBC)] and (b) Poly[(O950)-*b*-(CPM)] from a poly(O950) mCTA (M_n of 17.5 kDa with a M_w/M_n of 1.12). The poly(O950) macroCTA was prepared by polymerizing O950 at 70 °C for 18 h in DMSO with CTP and ABCVA as the CTA and initiator with $[M]_o$ and $[M]_o$:$[CTA]_o$:$[I]_o$ = 20 wt. % and 25:1:0.1 respectively. Block copolymers of (a) HBC and (b) CPM were conducted in acetic acid and THF, respectively, with a $[M]_o$:$[CTA]_o$:$[I]_o$ equal to 25:1:0.2 for Poly[(O950)-*b*-(HBC)] (M_n of 48 kDa with a M_w/M_n of 1.27) and a $[M]_o$:$[CTA]_o$:$[I]_o$ equal to 25:1:0.1 for Poly[(O950)-*b*-(CPM)] (M_n of 41.8 kDa with a M_w/M_n of 1.35).

3.3.4 RAFT diblock polymerizations of HBC and CPM

Diblock copolymers where the hydrophobic prodrug monomer residues are localized in a discrete block stabilized in aqueous solution by a hydrophilic poly(O950) segment were also prepared in order to establish the effect of this morphology on the resultant drug release profiles. This architecture could be advantageous in drug delivery applications because it allows polymers with prodrug contents greater than 50 wt % to be synthesized. The diblock copolymers were synthesized by first preparing a poly(O950) macroCTA (M_n = 17.5 kDa, Đ = 1.12) **(Table 3.2)** from which HBC and CPM were polymerized targeting a DP of 25. The formation of the desired poly[(O950)-*b*-(HBC)] and poly[(O950)-*b*-(CPM)] diblock copolymers was confirmed by the clear shift in the MWD to shorter elution volumes and lack of significant homopolymer impurity

(Fig. 3.7). Based on ^{19}F NMR the block ratios for poly[(O950)-*b*-(HBC)] and poly[(O950)-*b*-(CPM)] were determined to be 18:56 (34 wt.% Ciprofloxacin) and 18:32 (30 wt.% drug) **(Fig. 3.8)**. Molecular weight, composition, and molar mass dispersity values for these materials are summarized in **Table 3.2**.

TABLE 3.2. Summary of composition, molecular weights, and molar mass dispersity values for diblock copolymers of HBC and CPM prepared from a poly(O950) macroCTA.

	1st block (O950 mCTA)			**2nd block (HBC Core)**		**2nd block (CPM Core)**		**Complete Polymer**				
Poly. #	**M_n (kDa)**	**Đ**	**DP**	**M_n (kDa)**	**DP**	**M_n (kDa)**	**DP**	**M_n (kDa)**	**dndc**	**Block ratio**	**Đ**	**Drug (wt.%)**
3	17.5	1.12	18	-	-	-	-	17.5	0.060	-	1.12	-
4	17.5	1.12	18	30.5	56	-	-	48	0.080	1.74	1.27	34
5	17.5	1.12	18	-	-	24.3	32	41.8	0.087	1.39	1.35	30

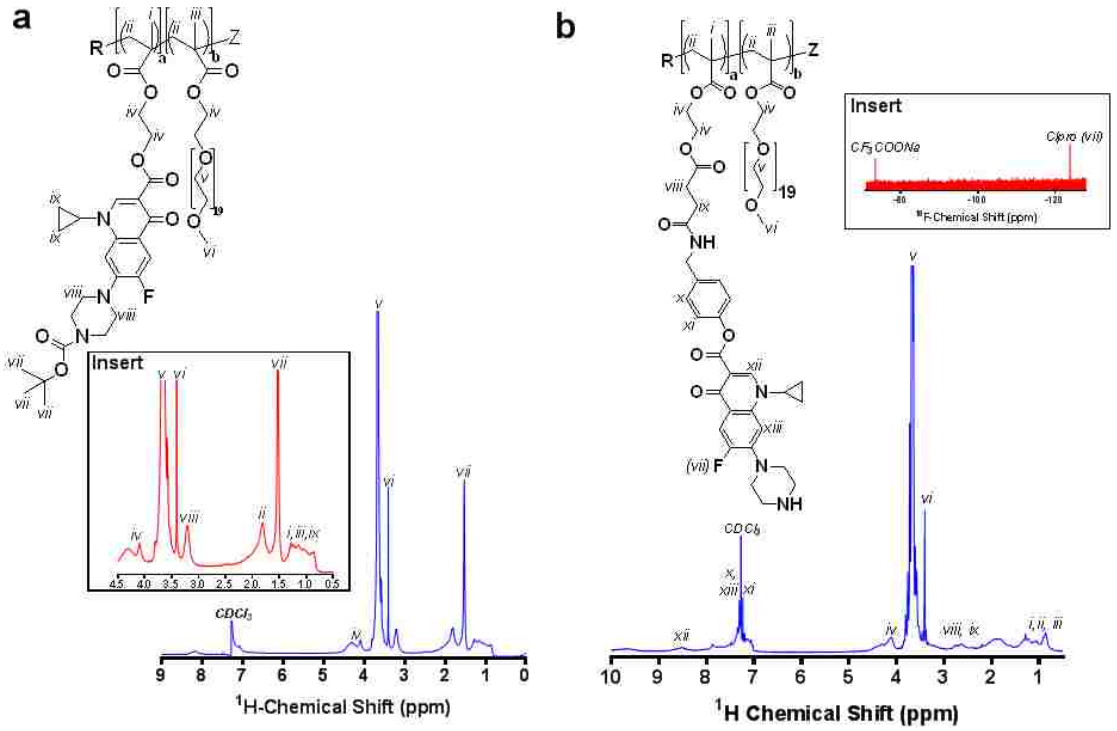

FIGURE 3.8. Representative NMR spectrums of (a) poly[(O950)-*b*-(HBC)] and (b) poly[(O950)-*b*-(CPM)] diblocks in $CDCl_3$ with assignment of the characteristic resonances associated with the monomers. Diblock compositions were determined by comparing the HBC (9H) *T*BOC resonances at δ = 1.52 ppm to the O950 (3H) methoxy resonance at δ = 3.4 ppm. Additionally, ^{19}F NMR was conducted in C_2D_6SO using sodium trifluoroacetate ($C_2F_3NaO_2$) (0.22 μM) as an internal standard. Integration of the ciprofloxacin resonance at δ = -124.5 ppm (1F) relative to the internal standard at δ = -73.4 ppm (3F) was used to calculate the final polymer

3.3.5 Aqueous solution studies for Ciprofloxacin containing copolymers and diblock copolymers

The aqueous morphologies of both the copolymer and diblock copolymer architectures were evaluated under physiologically relevant conditions. At a pH of 7.4 and 7.0, where the deprotected Ciprofloxacin residues should be predominately deprotonated and therefore hydrophobic in nature, hydrodynamic diameters of 37.4 ± 1.85 and 40.7 ± 2.01 nm are observed for poly[(O950)-*b*-(HBC)]. Similar particle sizes were observed for poly[(O950)-*b*-(CPM)] (30.8 ± 2.14 and 29.5 ± 3.83) at these pH values. The observed particle sizes are consistent with the formation of spherical core-shell nanoparticles where poly(O950) segments forming a hydrophilic corona around a dehydrated polymeric prodrug core.[29,32,33] The observed differences in size between the two diblocks at higher pH values may be attributed

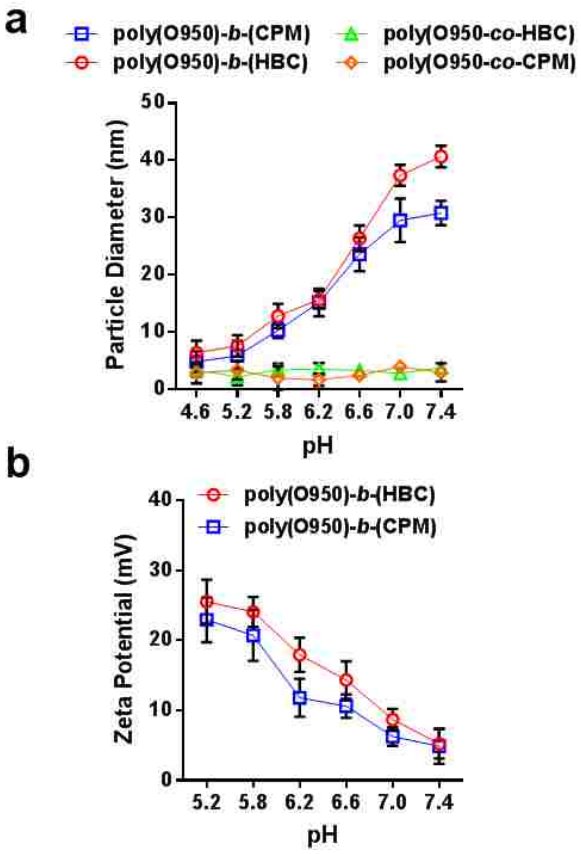

FIGURE 3.9. Aqueous size and charge measurements for statistical copolymers and diblock copolymers containing ciprofloxacin prodrug residues. (a) Hydrodynamic diameter (D_h) and (b) zeta potentials measurements as a function of pH. Buffers were prepared using 100 mM sodium phosphate or acetate with 150 mM NaCl for particle size measurements and 10 mM sodium phosphate for zeta potential measurements; all buffers were titrated to the appropriate pH. Polymer concentrations were made at 0.5 mg/mL and 1 mg/mL for DLS and zeta potential, respectively, and filtered using 0.22 µm filter before running experiments.

to slightly longer HBC block relative to CTPM (i.e. DP of HBC block of 56 vs. 32 for CPM) **(Table 3.2)**.[34] Reduction of the solution pH to 5.2 results in a significant decrease in hydrodynamic diameter to around 5-8 nm for both diblock copolymers **(Fig. 3.9A)**. This behavior is likely caused by an increase in the protonation state of the secondary amines present on Ciprofloxacin residues in the polymer core. The resultant increase in positive charge along the polymer backbone destabilizes the micellar core via charge-charge repulsion while increasing the hydrophilicity of the core-forming segment. These sizes are consistent with molecularly dissolved unimers and do not change significantly upon further reduction of the solution pH **(Fig. 3.9A)**. Zeta potential

measurements for these materials at pH 7.4 were determined to be slightly positive with values of 5.24 ± 2.1 mV and 4.85 ± 2.5 mV observed for poly[(O950)-*b*-(HC)] and poly[(O950)-*b*-(CPM)] respectively **(Fig. 3.9B)**. Decreasing the pH to 5.2 increases the zeta potential to 26.56 ± 3.14 mV for poly[(O950)-*b*-(HC)] and 22.96 ± 3.21 for poly[(O950)-*b*-(CPM)] **(Fig. 3.9B)** supporting an increase in the protonation state of the copolymer at lower pH values.

3.3.6 Release kinetics of Ciprofloxacin from copolymers and diblock copolymers quantified by HPLC

HPLC was used to quantify drug release by detecting free drug as a function of time normalized to amount of drug present during initial incubation. This in turn was standardized to the total available drug in the system as quantified by dissolving a known amount of polymer in 10% aq. H_2SO_4 for 48 h at 25 ˚C. Using a Ciprofloxacin standard curve, the total amount of drug in the polymers was validated against compositional values obtained from ^{19}F NMR. In these studies, it was observed that free Ciprofloxacin elutes at approximately 1.59 ± 0.04 min, as supported by representative tandem mass spectrometry **(Fig. 3.10)** with a limit of detection of 0.39 µg/mL. Hydrolysis rates in human serum were determined for both of the deprotected monomers (ie. HBC and CPM) prior to their incorporation into copolymers as shown in **Fig. 3.11A,B**. These studies suggest that the respective rates of hydrolysis for the aliphatic (HBC) and phenyl (CPM) ester linked drugs are not significantly affected by the presence of serum proteins. A significant difference in the relative hydrolysis rates for these monomers was observed with CPM showing nearly 50 % drug release at 24 hours while HBC required 120 h to reach this value **(Fig. 3.11A)**. This apparent difference likely arises from the improved hydrolytic susceptibility of CPM's phenyl ester functionality, which is known to form a resonance-stabilized phenoxide as a leaving group.[35]

Butyrylcholinesterase (BChE) is a human enzyme generated by the liver that freely circulates in the blood to facilitate the breakdown of many drugs.[36,37] The addition of increasing concentrations of BChE

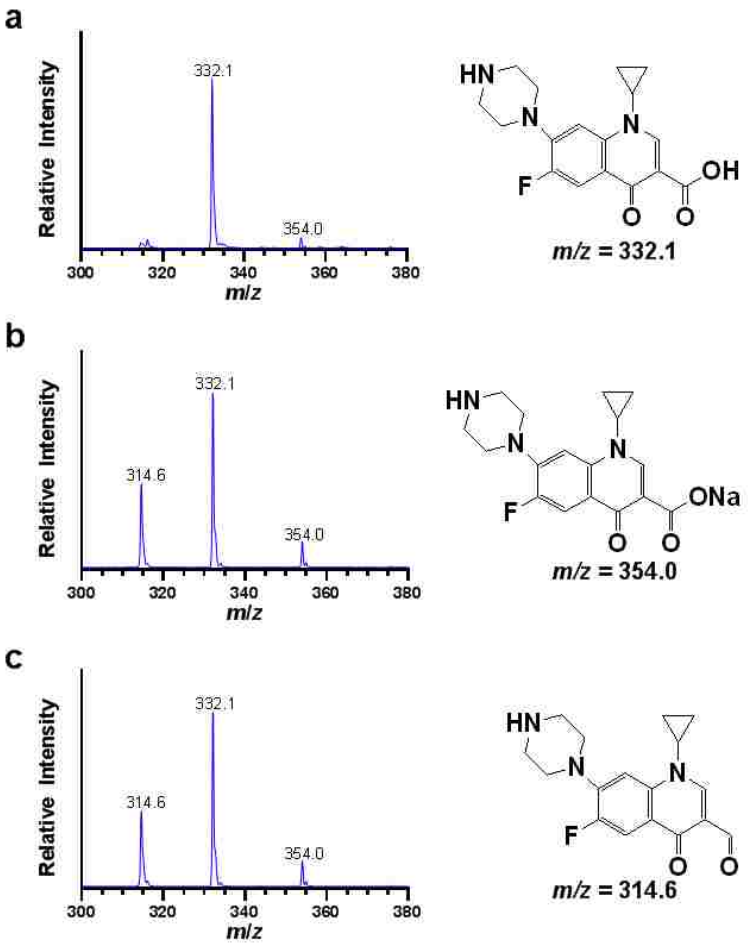

FIGURE 3.10. The peaks associated to (a) free drug elution and representative drug release in serum from example polymer systems, (b) poly(O950-*co*-HC) (24 d) and (c) poly[(O950)-*b*-(HC)] (20 d), was isolated using HPLC and confirmed through mass spectroscopy. The appearance of the dominant peak (332.1 m/z) from the polymer samples suggests an appropriate peak selection for monitoring drug release.

to solutions of the prodrug monomer in buffer enhances hydrolysis of both types of ester bonds as noted by the enhanced pseudo-first order release profiles for HC and CPM monomers **(Fig. 3.11A,B)**. Interestingly, without the enzyme present, the release transitions from an apparent first order kinetics to near zero-order for the deprotected HBC monomer suggesting not only slower

drug release, but also that this particular monomer is more responsive to a natural esterase than the more labile phenolic ester monomer (CPM) **(Fig. 3.11A)**. It is important to note that in the presence of serum, where the concentration of the enzyme is much higher than those tested in buffer, the drug release profile from the monomers are similar to that observed in buffer alone (no BChE), suggesting that enzyme mediated hydrolysis may not be the predominant

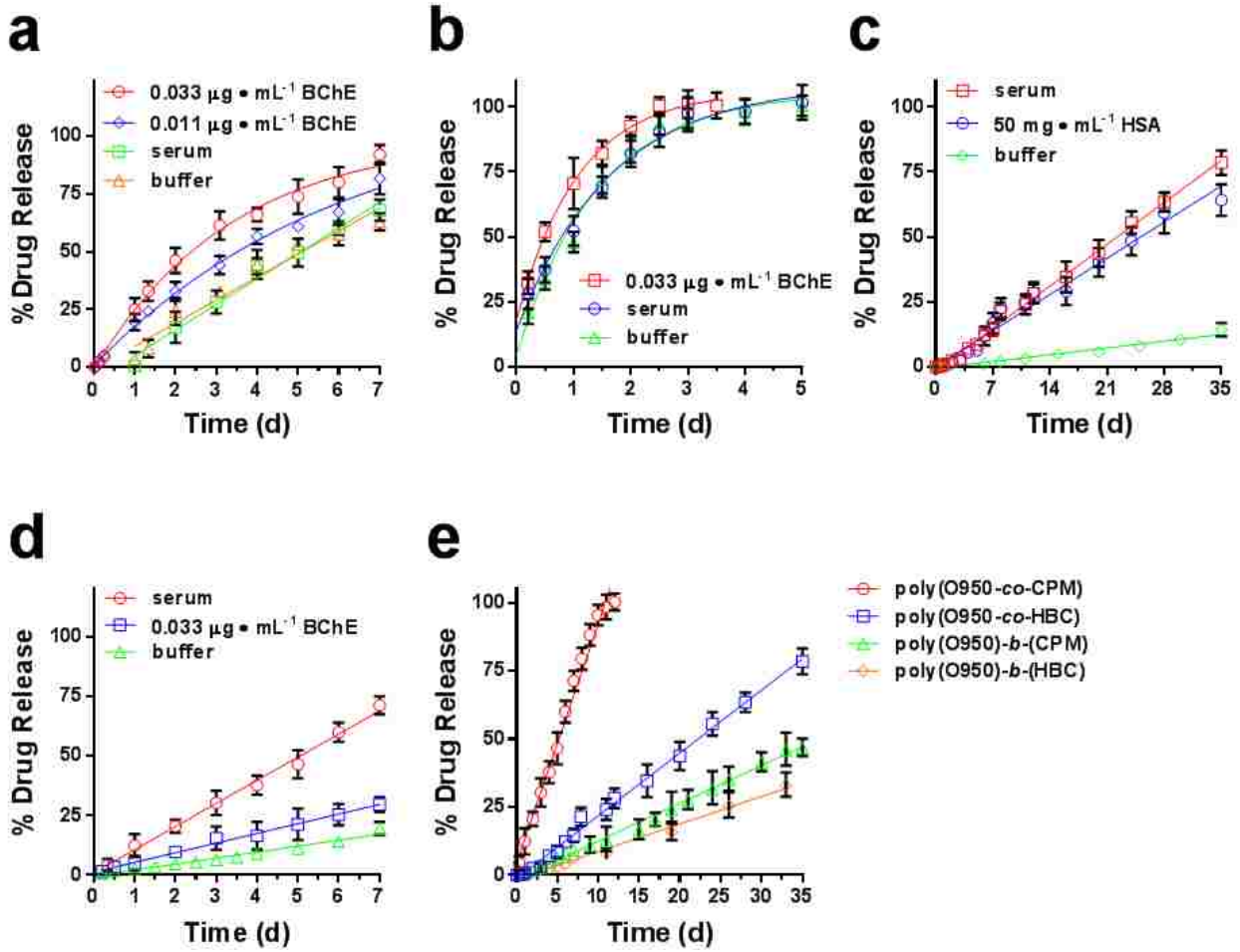

FIGURE 3.11. Drug release kinetics measured by high purification liquid chromatography as a function of time of (a) HC monomer in the presence of varying amounts of Butyrylcholinesterase (BChE) and 100% human serum, (b) CPM monomer in the presence of BChE and serum, (c) poly(O950-*co*-HC) in serum, pH 7.4 buffer, and human serum albumin, (d) poly(O950-*co*-CPM) in serum and in the presence of BChE, (e) and cipro containing statistical copolymers and block copolymers in 100% serum. All drug release studies were conducted at 37 ˚C and free drug detection was quantified using an elution gradient profile at 277 nm. All studies were conducted with deprotected monomers and polymers. Free ciprofloxacin was extracted from the aqueous samples using acetonitrile as an organic phase precipitation technique, and HPLC analysis was conducted using a mobile phase consisting of 2% aq. acetic acid:acetonitrile (84:16 v/v/).

mechanism of drug release from the monomer in a physiological setting. Although the release profiles of poly(O950-*co*-HBC) in serum and buffer are near zero-order, the kinetics of hydrolysis and subsequent release of free drug were observed to be faster in serum than buffer **(Fig. 3.11C)**. In efforts to probe this observation, the copolymers were incubated in buffer with the addition of 50 mg/mL human serum albumin (HSA) and assayed for free drug as a function of time. In these studies, the inclusion of the protein was shown to improve release kinetics to rates similar to those observed in serum **(Fig. 3.11C)**. This observation is hypothesized to arise from the association of the unimeric copolymer with proteins found in serum (e.g. human serum albumin) to produce polymer conformations with improve solvation of the pendent ester bonds. Similar release kinetics for ester linked Ciprofloxacin-polymer conjugates have been observed by a number of groups.[38,39] For example, Sobczak and coworkers observed approximately 20-25% Ciprofloxacin release over 35 days from multi-armed and star shaped homopolymers of poly(ϵ-caprolactone) and polylactide that were end-functionalized with between 3-8 mol % of drug.[39]

The addition of BChE to poly(O950-*co*-CPM), in buffer resulted in a slight increase in the hydrolysis rate relative to buffer alone **(Fig. 3.11D)**. This increase was, however, not as large as samples incubated in serum suggesting the importance of serum proteins in facilitating ester hydrolysis for polymer backbone-linked drugs. These findings suggest that the presence of enzyme alone may not be sufficient to significantly improve hydrolysis rates for esters found within low dielectric environments, such as the case with many polymer backbones.[40] In contrast, the large increase in drug release observed for monomers incubated with the enzyme **(Fig. 3.11A,B)** can be attributed to the lack of a polymerized chemical backbone, which may allow for BChE to access to the esters groups promoting faster cleavage rates than the observed in serum. Comparison of

copolymers containing phenyl- (CPM) and aliphatic- (HBC) esters showed that poly(O950-*co*-CPM) hydrolyzed more rapidly than poly(O950-*co*-HBC) with approximately 50 % drug release observed at 120 h and 21 days respectively. In both cases however incorporation of the ester-linked drug into copolymers resulted in a substantial decrease in hydrolysis rates relative to the parent monomers **(Fig. 3.11C,D)**.

The effect of polymer architecture on drug release behavior was also evaluated by synthesizing diblock copolymers consisting of a hydrophilic poly(O950) corona forming segment and a hydrophobic poly(HBC) or poly(CPM) core forming segment. As shown in **Fig. 3.11E**, sequestration of the prodrug residues to a hydrophobic micellar core results in a significant decrease in ester hydrolysis rates relative to the molecularly soluble constructs. Interestingly, the apparent difference in hydrolysis kinetics between the HBC and CPM copolymers is much greater than those observed for the analogous diblock copolymers. It is important to note that although the rate of drug release from the diblocks are much slower than the copolymers, the total drug content for diblocks are greater (30 wt.% drug for poly[(O950)-*b*-(HBC)] and 34 wt. % drug for poly[(O950)-*b*-(CPM)] vs. 16 wt. % drug for poly(O950-*co*-HC) and 16.7 wt.% drug for poly(O950-*co*-CPM)) **(Table 3.2)**. Consequently, there is a larger quantity of drug released from the diblock over a longer period of time as compared to the copolymer.

3.3.7 In vitro polymer toxicity and efficacy

The biocompatibility of the polymeric prodrugs was established in RAW 264.7 cells. In these studies, cells were incubated with varying concentrations of the copolymer and diblock copolymer prodrugs for 24 hours. No notable (< 80% cell viability) toxicity was observed for both the poly(O950-*co*-HBC) and poly(O950-*co*-CPM) even at polymer concentrations of 20 mg/mL

(**Fig. 3.12A)**. In contrast, the diblock copolymer constructs demonstrated dose dependent toxicity with RAW cell viability falling below 80% at polymer concentrations exceeding approximately 1 mg/mL **(Fig. 3.13)**. This toxicity is likely a result of interactions of the lightly charged poly(ciprofloxacin) segments with cell membranes upon internalization and subsequent acidification of endosomal compartments. This phenomenon has been previously reported for other positively charged systems such as cationic polystyrene nanospheres (~40-50 nm), which have been elicited to promote an apoptotic pathway in RAW 264.7 cells.[41]

Based on the copolymers' lack of toxicity in RAW cells even at elevated concentrations **(Fig. 3.12A)**, poly(O950-*co*-HBC) and poly(O950-*co*-CPM) were selected for further studies to evaluate efficacy using a coculture challenge assay with *Burkholderia thailandensis* infected RAW 264.7 cells **(Fig. 3.12A)**. Here *B. thailandensis* was used as a surrogate model for the evaluation of *B. pseudomallei* infectivity.[42] The coculture challenge assay was able to capture the full dose response curve of free Ciprofloxacin, consistent with literature indicating a minimum inhibitory concentration (MIC) of 10 μg/mL or 0.03 mM.[43, 44] Evaluation of poly(O950-*co*-HBC) in this assay yields an MIC of 2000 μg/mL (6 mM) which is consistent with hydrolysis studies where approximately 1-2% drug release is observed at 24 h in 100% serum **(Fig. 3.11C)**. In contrast, coculture studies conducted with poly(O950-*co*-CPM) resulted in a 10-fold reduction in

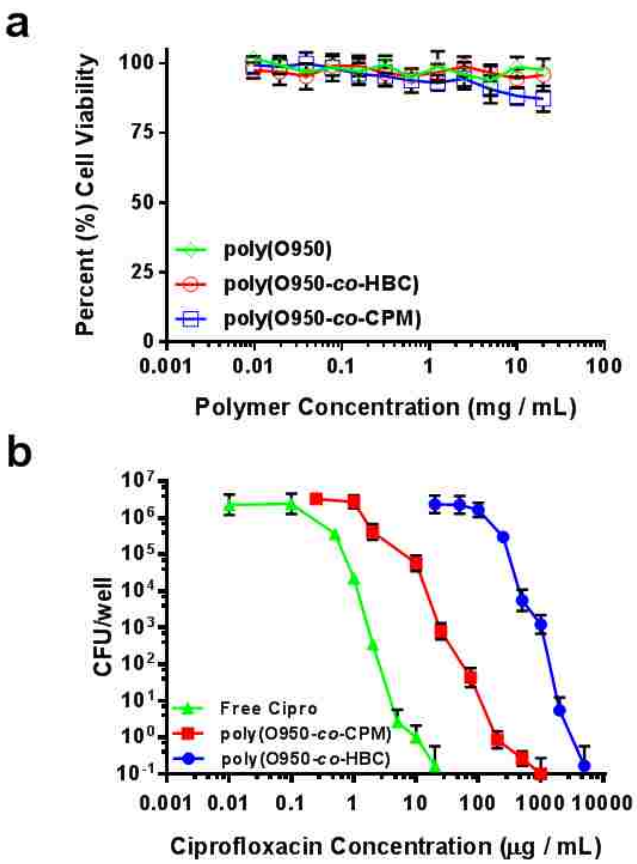

FIGURE 3.12. *In vitro* toxicity and efficacy using RAW 264.7 cells representing (a) MTS results for varying concentrations of Poly(O950-*co*-HC) and Poly(O950-*co*-CPM) compared to PEGMA 950 mCTA (negative control), and (b) co-culture assay with cells treated with varying concentrations of both copolymers and free Ciprofloxacin (positive control) following infection with *B. thailandensis* to determine antibacterial efficacy. Polymer concentrations ranged from 20 mg/mL to 3.7 µg/mL, and toxicity was evaluated with the CellTiter 96AQueous One Solution Cell Proliferation Assay according to manufacturer's protocol.

the MIC of 200 µg/mL (0.6 mM) **(Fig. 3.12B)**. These results are consistent with trends observed in the drug release studies and suggest that the phenyl ester linked Ciprofloxacin provides superior antibiotic activity in vitro as a result of higher drug cleavage rates **(Fig. 3.11D)**.

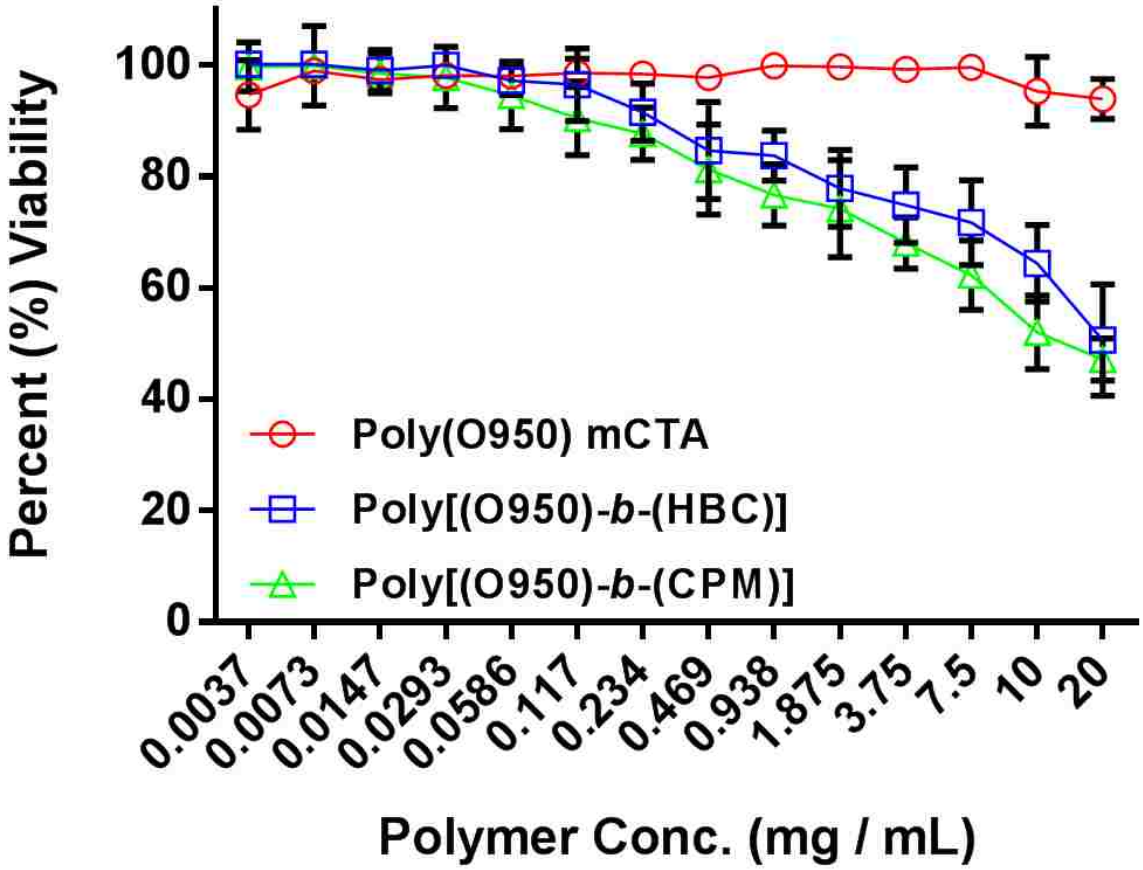

FIGURE 3.13. RAW 264.7 cell viability in the presence of both diblocks was quantified using a MTS assay over a wide polymer dose range (mg/mL). After 24 h, both polymer diblocks exhibit a dose dependent toxicity with cell viability measured below 80% with polymer concentrations greater than ca. 1 mg/mL.

3.4 Conclusion

Methacrylate-based prodrug monomers were synthesized from the antibiotic Ciprofloxacin and then incorporated into copolymers and diblock copolymers using RAFT polymerization. Linear pseudo first order kinetics were observed for the homopolymerization HBC and both monomers showed narrow and symmetric molecular weight distributions over a range of target DPs between 12 and 100. Prodrug monomers were then either copolymerized with polyethylene glycol methacrylate (O950) to yield hydrophilic copolymers or chain extend from poly(O950) macroCTAs to yield diblock copolyemrs. The resultant copolymers and diblock copolymers contained 16 and 34 % drug respectively. DLS and zeta potential measurements were employed to evaluate the pH-dependent aqueous solution properties of these

constructs. At physiological pH values the diblock copolymer constructs yielded hydrodynamic diameters that are consistent with micelles, which disassembled upon a reduction in the solution pH to 6.6. In contrast, the copolymers formed molecular dissolved unimers with particle sizes that were largely independent of the solution pH. Copolymers containing Ciprofloxacin linked via phenolic esters showed faster hydrolysis rates with 40% drug released at 120h, whereas copolymers with the corresponding aliphatic ester linkages showed only 10% drug release over the same period. Diblock copolymers with a discrete ciprofloxacin block showed greatly reducing hydrolysis rates for both ester-linked drugs. In vitro toxicity measurements in RAW 264.7 cells showed the copolymers to be nontoxic up to 20 mg/mL following a 24h incubation period. Co-culture efficacy was determined using Burkholderia thailandensis where an MIC of 0.6 and 6 mM were determined for the phenyl ester and aliphatic ester linked polymeric prodrugs respectively.

3.5 Acknowledgements

This work was funded by the Defence Threat Reduction Agency (Grant #HDTRA1-13-1-0047).

3.6 REFERENCES

1. P. Russell, SM Eley, J. Ellis, M. Green, DL. Bell, DJ. Kenny and RW. Titball, J. *Antimicrob. Chemoth.*, 2000, **45**, 813
2. R. Garrafo, D. Jambou, RM. Chichmanian, S. Ravoire and P. Lapalus, *Antimicrob. Agents. Ch.*, 1991, **35**, 2215
3. M. Brunner, U. Hollenstein, S. Delacher, D. Jager, R. Schmid, E. Lackner, A. Georgopoulos, HG. Eichler and M. Muller, *Antimicrob. Agents. Ch.*, 1999, **43**, 1307
4. WJ. Wiersinga, BJ. Curie and SJ. Peacock, *N. Engl. J. Med.*, 2012, **367**, 1035
5. H. Kranz and R. Bodmeier, *Int. J. Pharm.*, 2007, **332**, 107
6. ND. Stebbins, MA. Ouimet and KE. Uhrich, *Adv. Drug. Deliver. Rev.*, 2014, **78**, 77
7. VP. Torchilin, Annu. *Rev. Biomed. Eng.*, 2006, **8**, 343
8. KE. Uhrich, *Chem. Rev.*, 1999, **99**, 3181
9. EM. Hetrick and MH. Schoenfisch, *Chem. Soc. Rev.*, 2006, **35**, 780
10. P. Wu and DW. Grainger, *Biomaterials*, 2006, **27**, 2450
11. J. Kost and R. Langer, *Adv. Drug. Deliver. Rev.*, 2012, **64**, 327
12. S. Davaran, J. hanaee and A. Khosravi, *J. Control Release*, 1999, **58**, 279
13. JP. Wong, H. Yang, KL. Blasetti, G. Schnell, J. Conley and LN. Schofield, *J. Control. Release*, 2003, **92**, 265
14. DA. Edwards, J. Hanes, G. Caponetti, J. Hrkach, A. Ben-Jebria, ML. Eskey, J. Mintzes, D. Deaver, N. Lotan, and R. Langer, *Science*, 1997, **276**, 1868

15. RB. Greenwald, CW. Gilbert, A. Pendri, CD. Conover, J. Xia and A. Martinez, *J. Med. Chem.*, 1996, **39**, 424
16. Y. Zhang, L. Ma, X. Deng and JJ. Chen. *Polym. Chem.*, 2013, **4**, 224
17. J. Khandare and T. Minko, *Prog. Polym. Sci.*, 2006, **31**, 359
18. ER. Kenawy, SD. Worley and R. Broughton, *Biomacromolecules*, 2007, **8**, 1359
19. X. Li, Q. Wu, F. Zhang and XF. Lin, *J. Appl. Polym. Sci.*, 2008, **108**, 431
20. M. Kuzuya and SI. Kondo, *Chem. Pharm. Bull.*, 1991, **39**, 3018
21. M. Kryger, BM. Wohl, AA. Smith and AN. Zelikin, *Chem. Commun.*, 2013, **49**, 2643
22. Y. Cao and W. He, *Acta Biomater.*, 2013, **9**, 4558
23. DD. Lane, DY. Chiu, FY. Su, S. Srinivasan, HB. Kern, OW. Press, PS. Stayton and AJ. Convertine, *Polym. Chem.*, 2015, **6**, 1286
24. I. Conejos-Sanchez, I. Cardoso, M. Oteo-Vives, E. Romero-Sanz, A. Paul, AR. Sauri, MA. Morcillo, MJ. Saraiva and MJ. Vicent, *J. Control. Release.*, 2015, **198**, 80
25. B. Dizman, MO. Elasri and LJ. Mathias, *Biomacromolecules*, 2005, **6**, 514
26. DJ. Keddie, *Chem. Soc. Rev.*, 2014, **43**, 496
27. RT. Mayadunne, E. Rizzardo, J. Chiefari, YK. Chong, G. Moad and SH. Thang, *Macromolecules*, 1999, **32**, 6977
28. AA. Smith, K. Zuwala, MB. Kryger, BM, Wohl, C. Guerrero-Sanchez, M. Tolstrup, A. Postma and AN. Zelikin, *Chem. Sci.*, 2015, **6**, 264
29. D. Roy, GY. Berguig, B. Ghosn, DD. Lane, S. Braswell, PS. Stayton and AJ. Convertine, *Polym. Chem.*, 2014, **5**, 1791
30. U. Tehler, JH. Fagerberg, R. Svensson, M. Larhed, P. Artursson and CAS. Bergstrom. *J. Med. Chem.*, 2013, **56**, 2690
31. SS. Wu, CY. Chein and YH Wen, *J. Chromatogr. Sci.*, 2008, **46**, 490
32. GY. Berguig, AJ. Convertine, S. Frayo, HB. Kern, E. Procko, D. Roy, S. Srinivasan, DH. Margineantu, G. Booth, MC. Palanca-Wessels, D. Baker, D. Hockenbery, OW. Press and PS. Stayton, *Mol. Ther.*, 2015, **5**, 907
33. AJ. Convertine, BS. Lokitz, Y. Vasileva, LJ. Myrick, CW. Scales, AB. Lowe and CL. McCormick, *Macromolecules*., 2006, **39**, 1724
34. L. Zhang and A. Eisenberg. *Macromolecules*., 1999, **32**, 2239
35. RW, Taft, *J. Am. Chem. Soc.*, 1952, **74**, 3120
36. SP. Browne, EA. Slaughter, RA. Couch, EM. Rudnic and AM. McLean, *Biopharm. Drug. Dispos.*, 1998, **19**, 309
37. I. Manoharan, R. Boopathy, S. Darvesh and O. Lockridge, *Clinica. Chimica. Acta.*, 2007, **378**, 128
38. GL. Woo, MW. Mittelman and JP. Santerre, *Biomaterials*, 2000, **21**, 1235
39. M. Sobczak, *Eur. J. Med. Chem.*, 2010, **45**, 3844
40. PV. Wetering, NJ Zuidam, MJ. Steenbergen, OA Houwen, WJM. Underberg and WE Hennink. *Macromolecules*., 1998, **31**, 8063
41. T. Xia, M. Kovochich, M. Lion, JI. Zink and AE. Nel. *ACS Nano*., 2008, **2**, 85
42. A. Haraga, E. West, MJ. Brittnacher, SJ. Skerrett and SI. Miller, *Infect. Immun.*, 2008, **75**, 5402
43. FM. Thibault, E. Hernandez, DR. Vidal, M. Girardet and JD. Cavallo, *J. Antimicrob. Chemother.*, 2004, **54**, 1134
44. RL Ulrich, D. DeShazer, TA. Kenny, MP. Ulrich, A. Moravusova, R. Opperman, S. Bavari, RL. Bowlin, DT. Moir and RG. Panchal. *Appl. Envrion. Microbiol.*, 2013, **79**, 5830

CHAPTER 4. Synthesis of zwitterionic, hydrophobic, and amphiphilic polymers *via* RAFT polymerization induced self-assembly (PISA) in acetic acid*

*Provided as published: Das D., Gerboth G., Postma A, Srinivasan S., Kern H., Chen J., Ratner D.M., Stayton P.S., Convertine A.J. *Polymer Chemistry.* 7(39);6133-43 (2016).

ABSTRACT

Polymerization induced self-assembly (PISA) in acetic acid was employed to polymerize the hydrophilic sulfobetaine monomer 2-(*N*-3-sulfopropyl-*N*,*N*-dimethyl ammonium)ethyl methacrylate (DMAPS) and the hydrophobic monomer lauryl methacrylate (LMA). Polymerizations were conducted from a macro chain transfer agent (macro-CTA) consisting of 66% 2-hydroxyethyl methacrylate (HEMA) and 33% poly(ethylene glycol) methyl ether methacrylate FW ~ 300 Da (O300). A degree of polymerization (DP) of 50 was targeted for the macro-CTA in order to yield diblock copolymers with significantly larger 2nd blocks. From the poly(HEMA-*co*-O300) macro-CTA, diblock copolymers of poly[(HEMA-*co*-O300)-*b*-(DMAPS)] and poly[(HEMA-*co*-O300)-*b*-(LMA)] were grown *via* PISA in acetic acid. In order to maintain colloidal stability, it was necessary to conduct PISA of DMAPS at 10 wt% monomer, while LMA polymerizations maintained stability at 20 wt% monomer. M_n*vs.* conversion plots for both DMAPS and LMA show linear increases in molecular weight over the course of the polymerizations. Analysis of the molecular weight distributions revealed a progressive narrowing throughout the polymerization from an initial bimodal state. Copolymers of DMAPS and LMA were also synthesized over a large range of comonomer feed ratios. These materials show composition-dependent sizes in buffered solutions between 11 nm for the copolymer containing 80% by mol DMAPS to 75 nm for the copolymer containing 40 mol% DMAPS. PISA in acetic acid was then used to prepare copolymers of DMAPS with a range

of hydrophobic polymerizable prodrug monomers as well as a polymerizable peptide macromonomer. The resultant copolymers had narrow molecular weight distributions and were readily soluble in saline solutions.

4.1 Introduction

Despite their widespread clinical use, liposomal drug delivery systems suffer from a number of limitations including low drug loading efficiencies, rapid drug release, storage instability, and the need for complex formulation procedures.[1] For these reasons, there has been considerable interest in the development of polymeric prodrugs in which the therapeutic agents are covalently conjugated to hydrophilic macromolecular scaffolds *via* degradable linkages.[2–6] This strategy has been shown to substantially increase the solubility and stability of the parent drug while also enhancing drug circulation half-lives and reducing immunogenicity.[7–9] A variety of polymeric prodrugs have been developed based on post polymerization conjugation of therapeutic agents to polymers derived from natural sources (*e.g.* albumin, chitosan, and heparin).[10–12] Nanomedicines based on synthetic polymers such as poly(ethylene glycol) (PEG) and poly(2-hydroxypropyl methacrylamide) (HPMA) have also been developed.[13]

Polymeric prodrugs can also be prepared directly *via* the reversible deactivation radical polymerization (RDRP) of therapeutic agents that have been reversibly conjugated to suitable vinyl functionality.[14–17] This versatile approach allows for one or more therapeutic agents to be incorporated into the final polymer at predetermined ratios without the need for additional conjugation and purification steps.[16,18]

The synthetic versatility provided by the combination of RAFT polymerization with polymerization induced self-assembly (PISA) has greatly expanded the scope of functional nanostructures that can be synthesized under economically relevant conditions.[19–21] This pairing also has the potential to revolutionize the development of sophisticated multifunctional drug delivery based on the use of polymerizable prodrug monomers.[22] PISA is most commonly conducted using the RAFT process because of the large number of functional monomers that are amenable to the RAFT technique, as well as the wide range of compatible reaction conditions including the use of both aqueous and organic solvents.[23–25]

In the RAFT-PISA process a soluble macro chain transfer agent (macro-CTA) is chain-extended with a second monomer in a suitable solvent. Growth of the 2nd block then proceeds in solution from the macro-CTA until it exceeds a critical micelle degree of polymerization (CMDP). Beyond this point the amphiphilic block copolymer chains begin to aggregate inducing phase separation. Stabilization of the resultant nanostructures by the macro-CTA allows polymerization to continue *via* either dispersion or aqueous emulsion polymerization. Often, the onset of micellar nucleation during nanoparticle formation is also associated with an increase in the rate of polymerization.[26] This phenomenon is thought to result from diffusion of unreacted monomer into the nanoparticle cores leading to a higher local monomer concentration. Additionally, PISA allows for the final copolymer morphology to be controlled through simple manipulation of the two block copolymer segments, and can be conducted at high solids. The use of the RAFT-PISA approach has been shown to be a facile route for synthesizing a diverse array of block copolymer nanoparticle morphologies including spheres,[27] worms,[28,29] vesicles,[30] lamellae,[28] framboidal vesicles,[31]spaced concentric vesicles,[32] and yolk/shell particles.[33]

To date PISA has primarily been employed as a means of making well-defined nanostructures; however, this technique could also be used to facilitate the synthesis of zwitterionic copolymers from monomers that lack a common aqueous solvent or that precipitate upon polymerization. While the RDRP of zwitterionic monomers has been reported under homogenous aqueous conditions,[34–36] their copolymerization with hydrophobic monomers remains a significant challenge. This difficulty arises because of the low solubility of hydrophobic monomers in aqueous media combined with the poor solubility of zwitterionic polymers in organic solutions. These solubility constraints are particularly problematic in drug delivery applications, where the objective is to integrate prodrug monomers that may contain hydrolytically unstable linkages into a zwitterionic polymer scaffold.

Recently, we described the use of acetic acid as a solvent for the RAFT polymerization of ciprofloxacin prodrug monomers containing hydrolytically unstable phenyl ester linkages.[16] Kinetic studies demonstrated that these polymerizations are well controlled and show negligible degradation of the labile prodrug linkages. Because

of the ability of acetic acid to dissolve highly polar monomers and nonpolar monomers it was selected as a polymerization medium to investigate the copolymerization of zwitterionic and hydrophobic monomers *via* PISA.

Herein, we describe a simple method for preparing zwitterionic copolymers containing hydrophobic comonomers *via* RAFT PISA in acetic acid. The scope of this technology is demonstrated by evaluating the kinetics for zwitterionic monomer 2-(*N*-3-sulfopropyl-*N*,*N*-dimethyl ammonium)ethyl methacrylate (DMAPS), the hydrophobic monomer lauryl methacrylate (LMA), and copolymers of these monomers over a large range of comonomer feed ratios. PISA in acetic acid is then used to synthesize copolymers of DMAPS with a range of hydrophobic polymerizable prodrug monomers as well as a polymerizable peptide macromonomer directly without the need for amine protecting groups.

4.2 Experimental details

4.2.1 Materials

Chemicals and all materials were supplied by Sigma-Aldrich unless otherwise specified. 4-((((2-Carboxyethyl)thio)carbonothioyl)thio)-4-cyanopentanoic acid (CCC) was kindly donated by Boron Molecular. Dt-SMA, BioHEMA, and CPM were synthesized as described previously.[16,42] The peptide macromonomer containing 12 amino acids connected to a methacrylamide group *via* an aminohexanoic acid linker (Mam-AhxWSGPGVWGASVK) was synthesized using standard solid phase peptide synthesis based on previous studies. MEM was synthesized as described previously.[43]

4.2.2 Size exclusion chromatography

Absolute molecular weights and molar mass dispersity indices for polymerizations of DMAPS were determined using PolySep-SEC GFC-P 3000, LC Column 300 × 7.8 mm (Phenomenex Inc.) connected to an Agilent 1200 Series Liquid Chromatography System (Santa Clara, CA) and Wyatt Technology miniDAWN TREOS, 3 angle MALS light scattering instrument and Optilab TrEX, refractive index detector (Santa Barbara,

CA). HPLC-grade water containing 0.150 M NaCl and acetate buffer 100 mM acetate buffer pH 4.4 was used as the mobile phase at a flow rate of 0.5 mL min^{-1}.

4.2.3 Molecular weights and molar mass dispersity indices for polymerizations of LMA

SEC was performed on a Waters Alliance system equipped with an Alliance 2695 Separations Module (integrated quaternary solvent delivery, solvent degasser and autosampler system), a Waters column heater module, a Waters 2414 RDI refractive index detector, a Waters PDA 2996 photodiode array detector (210 to 400 nm at 1.2 nm) and 4× Agilent PL-Gel columns (3× PL-Gel Mixed C (5μm) and 1× PL-Gel Mixed E (3 μm) columns), each 300 mm × 7.8 mm^2, providing an effective molar mass range of 200 to 2 × 10^6). Tetrahydrofuran (THF) high purity solvent (HPLC grade) was pre-filtered through aluminium oxide (90 active neutral, 70–230 mesh) with 0.45 μm filter, and 0.1 g L^{-1} 2,6-di-*tert*-butyl-4-methylphenol (BHT) was added as inhibitor. The filtered THF containing BHT was purged slowly with nitrogen gas and used as an eluent with a flow rate of 1 mL min^{-1} at 30 °C. Number (M_n) and weight average (M_w) molar masses were evaluated using Waters Empower-3 software. The SEC columns were calibrated with low dispersity polystyrene (PSt) standards (Polymer Laboratories) ranging from 580 to 7 500 000 g mol^{-1}, and molar masses are reported as PSt equivalents. A 3rd-order polynomial was used to fit the log M_p *vs*. time calibration curve, which was near linear across the molar mass ranges.

4.2.4 Synthesis of the poly(HEMA-co-O300) macro-CTA

To a 250 mL tube was added CCC (0.60 g, 1.95 mmol), ABCVA (13.7 mg, 48.8 μmol), HEMA (8.47 g, 65 mmol), O300 (9.76 g, 32.5 mmol), and Dioxane 72.9 mL. The solution was septa sealed then vortexed until homogenous. The polymerizations solutions was then purged with nitrogen for 60 minutes and then allowed to react in a water bath preheated to 70 °C for 8 hours. The resultant polymer was then isolated by repeated precipitation from acetone into 20 times excess of diethyl ether. The polymer was then dried overnight under high vacuum. Copolymer composition was determined *via* ^{1}H NMR in $CDCl_3$ by comparison of the O300

OCH_3 resonance at 3.0–3.2 ppm (3H O300) to the combined backbone methylene resonances (2H HEMA + 2H O300) at 1.45–2.00 ppm. The final M_n and $Đ$ values were determined to be 7300 and 1.15 respectively *via* SEC analysis in DMF as detailed above.

4.2.5 Kinetic evaluation of the RAFT dispersion polymerization of DMAPS

Kinetic evaluation of DMAPS was conducted with poly(HEMA-*co*-O300) and ABCVA as the RAFT macro-CTA and initiator, respectively, in acetic acid at 70 °C. The initial monomer to CTA to initiator ($[M]_0$:$[CTA]_0$:$[I]_0$) ratio was 200:1:0.05. To understand the influence of the degree of polymerization (DP) on the evolution of molecular weight, RAFT polymerizations of DMAPS were conducted under similar reaction conditions with ratios of 50, 100, 200, and 400 for 18 h. Individual polymerization solutions were transferred to a septa-sealed vial and purged with nitrogen for 20 minutes. After the allotted time, the polymerization vials were transferred to a preheated water bath at 70 °C and allowed to polymerize for the indicated time. Following polymerization, the individual vials were quenched by exposure to oxygen by opening the septa seal and immersing the vials in ice. The polymerizations were evaluated for monomer conversion *via* ^{1}H NMR by preparing 5% (by mass) solutions of the aliquots in D_2O/0.5 M NaCl containing 1% pyridine and 1% trifuloracetic acid (by volume) as an internal standard. Monomer conversion as a function of time was determined by comparison of the combined vinyl resonances (5.6 and 6.0 ppm) normalized to the pyridine + TFA internal standard resonances (8.3–8.9 ppm) to those for the time zero sample.

Polymers were purified *via* dialysis against 0.5 M NaCl at 5 °C followed by deionized water and then isolated by lyophilization. A representative procedure is as follows: to a 50 mL tube was added poly(HEMA-*co*-O300) (M_n = 7300, $Đ$ = 1.15) (0.561 g, 76.9 μmol), ABCVA (1.08 mg, 3.85 μmol), DMAPS ((4.30 mg, 15.38 mmol)), and acetic acid 38.7 mL. The solution was then vortexed until homogenous and then transferred to individual septa sealed vials. The polymerizations solutions were then purged with nitrogen for 20 minutes and then allowed to react in a water bath preheated to 70 °C for the desired time. The individual aliquots were then quench by rapid cooling and exposure to oxygen.

4.2.6 Kinetic evaluation of the RAFT dispersion polymerization of LMA

Kinetic evaluation of LMA was conducted with poly(HEMA-*co*-O300) and ABCVA as the RAFT macro-CTA and initiator, respectively, in acetic acid at 70 °C. The initial monomer to CTA to initiator ($[M]_0$:$[CTA]_0$:$[I]_0$) ratio was 200:1:0.1. In order to understand the influence of the degree of polymerization (DP) on the evolution of molecular weight, RAFT polymerizations of DMAPS were conducted under similar reaction conditions with ratios of 50, 100, 200, and 400 for 24 h. Individual polymerization solutions were transferred to a septa-sealed vial and purged with nitrogen for 20 minutes. After the allotted time, the polymerization vials were transferred to a preheated water bath at 70 °C and allowed to polymerize for the indicated time. Following polymerization, the individual vials were quenched by exposure to oxygen by opening the septa seal and immersing the vials in ice. The polymerizations were evaluated for monomer conversion*via* ^{1}H NMR by preparing 5% (by mass) solutions of the aliquots in $CDCl_3$ containing 1% $CHCl_3$ (by volume) as an internal standard. Monomer conversion as a function of time were determined by comparison of the combined vinyl resonances (normalized to the $CHCl_3$ internal standard resonance at δ = 7.2 ppm) at δ = to those for the time zero sample. Polymers were purified *via*repeated precipitation from CH_2Cl_2 into a 10× excess of methanol and then dried under high vacuum overnight.

A representative procedure is as follows: to a 50 mL tube was added poly(HEMA-*co*-O300) (M_n = 7300, $Đ$ = 1.15) (0.561 g, 76.9 μmol), ABCVA (2.16 mg, 7.69 μmol), LMA (3.91 g, 15.38 mmol), and acetic acid 35.2 mL. The solution was then vortexed until homogenous and then transferred to individual septa sealed vials. The polymerizations solutions were then purged with nitrogen for 20 minutes and then allowed to react in a water bath preheated to 70 °C for the desired time. The individual aliquots were then quench by rapid cooling and exposure to oxygen.

4.2.7 Copolymerization of DMAPS with Dt-SMA, CPM, BioHEMA, LMA, and Mam-AhxWSGPGVWGASVK

Copolymerizations of the hydrophobic comonomers illustrated in Scheme 2 with DMAPS from a poly(HEMA-*co*-O300) macro-CTA in acetic acid were conducted at 15 wt% monomer targeting a DP of 200 with a $[CTA]_0$:$[I]_0$ of 10. Polymerizations were purged with nitrogen and then heated at 70 °C for 24 h. A representative procedure for the copolymerization of equimolar quantities of LMA and DMAPS from a poly(HEMA-*co*-O300) (M_n = 7300, $Đ$ = 1.15) macro-CTA is a follows: to a 10 mL round bottom flask was added poly(HEMA-*co*-O300) (0.112 g, 15.38 μmol), ABCVA (0.43 mg, 1.54 μmol), DMAPS (0.430 g, 1.54 mmol), LMA (0.391 g, 1.54 mmol) and acetic acid 7.39 mL. The solution was then septa sealed and then vortexed until homogenous and. The polymerization solution was then purged with nitrogen for 25 minutes and then allowed to react in a water bath preheated to 70 °C for 24 h. The individual aliquots were then quench by rapid cooling and exposure to oxygen. Polymers were purified *via* dialysis against acetone at 5 °C followed by deionized water and then isolated by lyophilization. The copolymer composition was determined*via* ^{1}H NMR by preparing 5% (by mass) solutions TFA containing 5% (by volume) d_6 DMSO.

4.2.8 Synthesis of the poly(MEM-co-O300) macro-CTA

To a 10 mL round bottom flask was added CCC (20.5 mg, 66.7 μmol), ABCVA (0.75 mg, 2.67 μmol), MEM (0.487 g, 1.67 mmol), O300 (0.5 g, 1.67 mmol), and acetic acid 3.95 mL. The solution was septa sealed then vortexed until homogenous. The polymerizations solutions was then purged with nitrogen for 30 minutes and then allowed to react in a water bath preheated to 70 °C for 8 hours. The resultant polymer was then isolated by dialysis against deionized water at 5 °C followed by lyophilization. Copolymer composition was determined *via* ^{1}H NMR in $CDCl_3$ by comparison of the O300 OCH_3 resonance at 3.0–3.2 ppm (3H O300) to the MEM anomeric resonance (1H) at 4.6 ppm yielding. Based on this analysis the molar copolymer composition was determined to be 40% MEM and 60% O300. The final M_n and $Đ$ values were determined to be 13500 g mol^{-1} and 1.13.

4.2.9 Synthesis of the poly[(MEM-co-O300)-b-(DMAPS-co-CTM)] from a poly[(MEM-co-O300)] macro-CTA

To a 10 mL round bottom flask was added poly[(MEM-*co*-O300) (56 mg, 4.00 μmol), ABCVA (0.06 mg, 0.02 μmol), DMAPS (100 mg, 0.36 mmol), CTM (30 mg, 0.04 mmol), and acetic acid 1.18 mL. The solution was septa sealed then vortexed until homogenous. The polymerizations solutions was then purged with nitrogen for 30 minutes and then allowed to react in a water bath preheated to 70 °C for 14 hours. The resultant polymer was then isolated by dialysis against deionized water at 5 °C followed by lyophilization. The final M_n and $Đ$ values were determined to be 42000 g mol^{-1} and 1.15.

4.3 Results and discussion

4.3.1 Synthesis and characterization of a poly(HEMA-co-O300) macro-CTA

While acetic acid is a good solvent for both LMA and DMAPS the resultant polymers are poorly soluble in this medium and precipitate even at low monomer conversions. In contrast, polymerization of these materials from a stabilizing macro-CTA could undergo PISA rather than precipitation. In order to investigate this hypothesis a macro-CTA stabilizer was first synthesized as shown in Scheme 1a. A relatively small degree of polymerization (DP) of 50 was targeted for the macro-CTA so that diblock copolymers with large block asymmetries could be synthesized. This design maximizes the molecular weight contribution of the 2nd block copolymer segment, which in these studies is designed to incorporate the hydrolytically unstable prodrug residues or cell-targeting component. The poly(HEMA-*co*-O300) macro-CTA was prepared using an initial molar feed ratio of 2:1 for the 2-hydroxyethyl methacrylate (HEMA) to poly(ethylene glycol) methyl ether methacrylate (O300) comonomers respectively. This composition was selected in order to yield a neutral hydrophilic copolymer with biocompatible hydroxyl residues and good solubility in a wide range of solvents from commercially available and inexpensive starting materials. The O300 comonomer was added as a minor component to the feed to enhance the aqueous solubility of the macro-CTA, while minimizing molecular weight and steric bulkiness of the self-assembled corona segments.

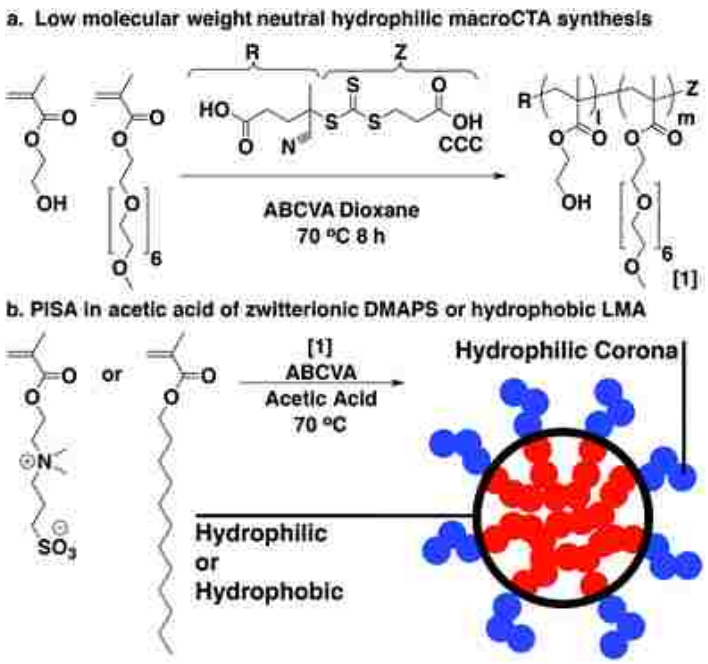

SCHEME 4.1. Synthetic strategy for the synthesis of poly(HEMA-*co*-O300) macro-CTA, and subsequent block copolymerization with DMAPS or LMA *via* RAFT PISA in acetic acid.

Copolymerization of the two monomers was conducted in dioxane at 70 °C for 8 hours in the presence of a trithiocarbonate-based RAFT agent and 4,4′-azobis(4-cyanovaleric acid) (ABCVA). The high degree of control observed for the copolymerization of HEMA and O300 under these conditions is evidenced by the narrow and symmetric molecular weight distribution (**Fig. 4.1A**). Analysis of the macro-CTA *via* a combination of ^{1}H NMR and SEC yielded a molecular weight, $Đ$, and copolymer composition of 7300 g mol^{-1}, 1.15, and 70:30 HEMA:O300, respectively (**Fig. 4.1B**). Based on these values the copolymers are expected to contain an average of 26 HEMA and 12 O300 residues per chain.

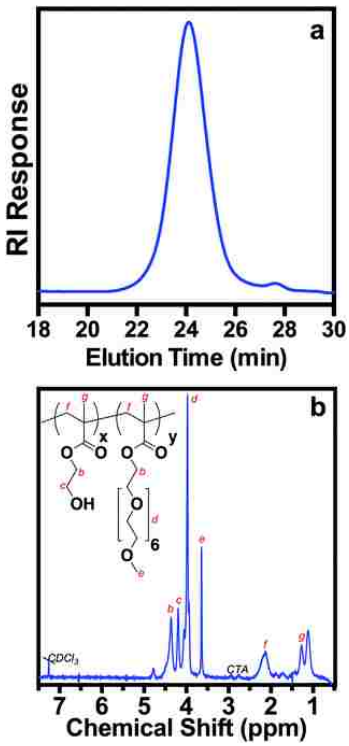

FIGURE 4.1. Characterization of the poly(HEMA-*co*-O300) macro-CTA synthesized with CCC and ABCVA as the RAFT agent and radical initiator, respectively. (a) SEC chromatogram showing the narrow and symmetric molecular weight distribution. (b) ^{1}H NMR of poly(HEMA-*co*-O300) in $CDCl_3$ with assignment of the characteristic resonances associated with the comonomer residues. The molecular weight, *Đ*, and copolymer composition was determined to be 7300 g mol^{-1}, 1.15, and 70:30 (HEMA:O300), respectively.

4.3.2 Kinetic analysis of hydrophilic DMAPS and hydrophobic LMA from poly(HEMA-co-O300) in acetic acid

In order to establish the ability of RAFT-PISA to facilitate the synthesis of hydrophobic, hydrophilic, and amphiphilic copolymers, we first investigated the homopolymerizations of DMAPS and LMA (**Scheme 4.1B**). Due to the low solubility of DMAPS in organic solvents and our desire to copolymerize the monomer with hydrophobic comonomers containing hydrolytically sensitive functionality, we decided to evaluate acetic acid as a polymerization medium. Acetic acid is a versatile high boiling solvent that is capable of dissolving a wide range of polar and nonpolar compounds. Recently, we demonstrated that acetic acid readily dissolves polymerizable ciprofloxacin derivatives that are practically insoluble across a range of common laboratory solvents. Subsequent kinetic analysis of the RAFT polymerizations of these monomers confirmed the stability of the trithiocarbonate moieties in acetic acid at 70 °C for at least 24 h.[16]

In order to maintain colloidal stability throughout the polymerization, it was necessary to conduct polymerizations of DMAPS at 10 wt% monomer while LMA polymerizations maintained colloidal stability at 20 wt% monomer. Shown in **Fig. 4.2A-B,** are the pseudo-first order rate plots for the polymerizations of DMAPS and LMA targeting a DP of 200. DMAPS polymerizations reached near quantitative conversion within 6 hours with greater than 70% conversion reached by 3 hours at an initial $[\text{macro-CTA}]_0/[\text{I}]_0$ ratio of 20. Under these conditions, the pseudo-first order rate plot was observed to be linear throughout the entire course of the polymerization. This result suggests that termination reactions remain low even at high monomer conversion. In comparison, polymerization of LMA in acetic acid proceeded to less than 30% conversion over the course of 24 hours at a $[\text{macro-CTA}]_0/[\text{I}]_0$ molar ratio of 20 (data not shown). For this reason, subsequent kinetic studies were conducted at a $[\text{macro-CTA}]_0/[\text{I}]_0$ ratio of 10. Here 84% conversion was reached at 24 hours, while still maintaining good polymerization control (*vide infra*). Some deviation from linearity is observed in the pseudo-first order rate plot of LMA at extended polymerization times (beyond 12 hours) possibly as a result of increased primary radical termination of the bulky poly(LMA) segments.

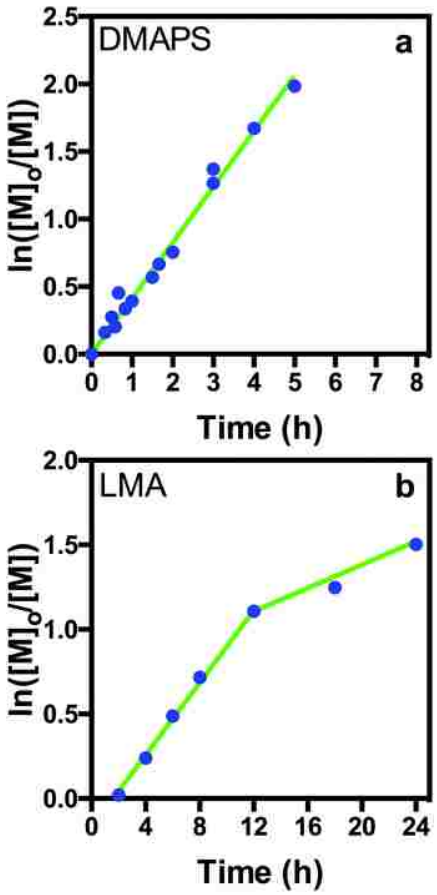

FIGURE 4.2. Pseudo-first-order kinetic plot for the poly(HEMA-*co*-O300) macroCTA mediated hompolymerizations of (a) DMAPS and (b) LMA *via* PISA in acetic acid at 70 °C.

Analysis of the evolution of M_n and $Đ$ *vs.* conversion plots for the polymerizations of DMAPS and LMA show linear increases in molecular weight over the course of the polymerizations (**Fig. 4.3A-D**). Good agreement between the theoretically determined molecular weights and the experimental values is observed for the DMAPS polymerizations (**Fig. 4.3B**). For example, DMAPS polymerizations yielded experimental/theoretical molecular weights of 27[illegible]600/27[illegible]400 and 53[illegible]400/52[illegible]400 at 37% and 81% monomer conversion, respectively. A moderate deviation from theoretical molecular weight values was observed for LMA polymerizations with experimental values that are consistently low (**Fig. 4.3D**). This deviation could be a result of the use of polystyrene standards to determine LMA molecular weights, whereas absolute molecular weights were determined for DMAPS *via* inline laser light scattering. In both cases, however, the $Đ$ values remain quite low even at moderate to high monomer conversions (**Fig. 4.3A and 4.3C**).

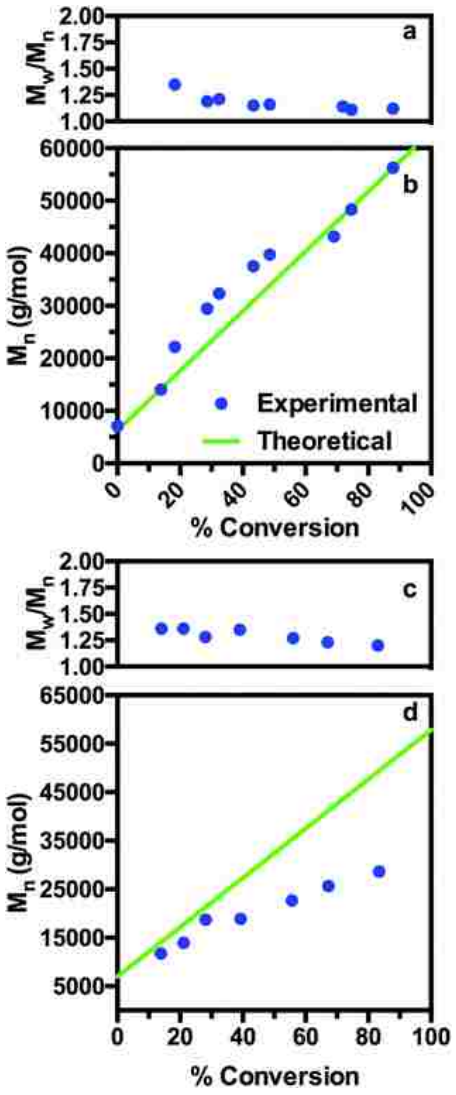

FIGURE 4.3. M_n and $Đ$ *vs.* conversion plots for the PISA of DMAPS (a, b) and LMA (c, d) from poly(HEMA-*co*-O300) at 70 °C. Theoretical values were determined based on the equation $M_n = [M]_0/[mCTA]_0 \times p \times FW_{mon} + M_n$ mCTA, where p is the monomer conversion determined by ^{1}H NMR. Absolute molecular weight values for DMAPS were determined *via* SEC analysis with inline laser light scattering in 0.150 mM NaCl SEC analysis of LMA samples was conducted in THF with molecular weight values based on polystyrene standards. Conversion values were determined by ^{1}H NMR analysis of aliquots that were diluted in D_2O + 0.5 M NaCl for DMAPS and $CDCl_3$ for LMA.

An interesting aspect of the polymerizations conducted in these studies is the presence of bimodal molecular weight distributions at low monomer conversions that become progressively unimodal as the polymerizations proceed to higher conversion. This phenomenon can be observed in an overlay of the molecular weight distributions (MWD) for polymerizations of both DMAPS and LMA (**Fig. 4.4A-B**). As can be seen in **Fig. 4.4A**, polymerization of DMAPS yields a bimodal MWD at approximately 20% monomer conversion that narrows substantially throughout the course of the polymerization. This narrowing also manifests in the $Đ$ values, which

narrow from 1.44 at 23% conversion to 1.11 at 98% conversion. A similar but less pronounced asymmetry in the MWDs is observed for LMA polymerizations (**Fig. 4.4B**). Here an initial asymmetry in the MWD is observed following a 2 h polymerization time, which corresponds to 21% monomer conversion. After 4 hours, a substantial narrowing of the MWD is observed, which continues to narrow as the polymerization proceeds to higher monomer conversion. Nevertheless, narrow MWDs are maintained for both polymer species as the polymerizations near complete monomer conversion.

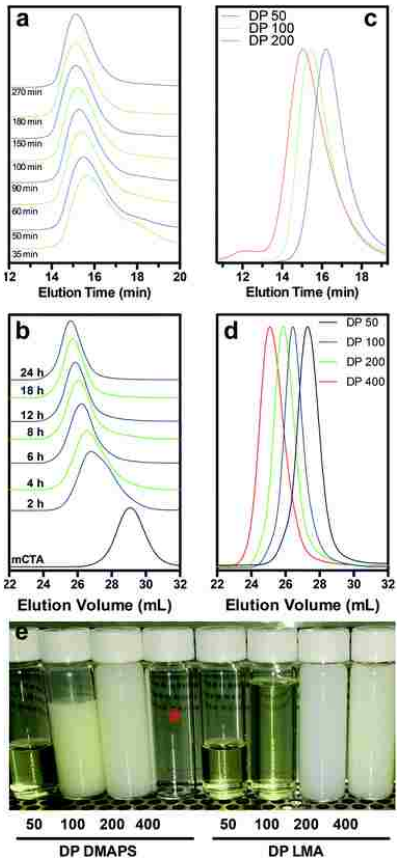

FIGURE 4.4. Overlay of SEC chromatograms traces (RI channel) showing the evolution of molar mass with time for (a) DMAPS and (b) LMA with $[M]_0$:[mCTA]$_0$:[I]$_0$ equal to 200:1:0.05 and 200:1:0.1, respectively. Molecular weight distributions for the PISA of (c) DMAPS and (d) LMA conducted at initial $[M]_0/[mCTA]_0$ ratios of 50, 100, 200, and 400. (e) Photographs of polymer solutions following the PISA of DMAPS or LMA from a poly(HEMA-*co*-O300) macro-CTA in acetic acid. Target DPs for both monomers were 50, 100, 200 and 400. *DMAPS samples targeting a DP of 400 were observed to phase separate, forming a white colloid oily phase and a clear acetic acid phase upon polymerization.

4.3.3 Evaluation of target DP for homopolymerization of DMAPS and LMA from poly(HEMA-co-O300) in acetic acid

The ability of RAFT PISA in acetic acid to control the polymerization of DMAPS and LMA over a range of molecular weights was established by investigating the polymerization behavior as a function of target DP. In these studies, the poly(HEMA-*co*-O300) macro-CTA was employed for polymerizations targeting an initial monomer to initial macro-CTA ratio ($[M]_0/[\text{macro-CTA}]_0$) of 50, 100, 200, 400. Similar to the kinetic studies, DMAPS polymerizations were observed to proceed rapidly with a high degree of control under these conditions. In all cases quantitative conversion was reached over the course of the 18 h polymerization period with molecular weights that are in good agreement with theoretical values (**Fig. 4.4C**). The polymerizations of DMAPS in acetic acid for $[M]_0$:[macro-CTA]$_0$ = 50, 100, 200 yielded symmetric and narrow molecular weight distributions (**Fig. 4.4C**) with *Đ*values around 1.10. Polymerizations of DMAPS targeting a DP of 400 were observed to phase separate forming a white colloid phase and a clear acetic acid phase upon polymerization. Good control was also observed for the polymerization of LMA in acetic acid (**Fig. 4.4D**). In contrast to the DMAPS polymerizations, LMA polymers targeting a DP of 400 were not observed to phase separate even at double the initial monomer concentration. The formation of assembled structures with DMAPS or LMA cores stabilized in acetic acid by the poly(HEMA-*co*-O300) can clearly be seen in photographs of the polymerization (**Fig. 4.4E**). Solutions were observed to become progressively more turbid as the length of the 2nd core-forming block was increased at a fixed macro-CTA length.

4.3.4 Copolymerization of prodrug monomers with DMAPS from poly(HEMA$_{co}$ O300) in acetic acid

The ability to control the copolymerization of zwitterionic sulfobetaine monomers with a range of poorly soluble, but biologically relevant, comonomers was demonstrated as depicted in **Scheme 4.2**. In these studies, DMAPS was employed as the hydrophilic and biocompatible scaffold with which hydrophobic monomers were copolymerized. In order to produce copolymers that are readily soluble in aqueous saline solutions, polymerizations were fixed at 15% (by mass) of the hydrophobic comonomer relative to DMAPS. This corresponds to between 2.2 and 8.0 mol% for the comonomers shown in Scheme 2. It should be noted that much higher ratios are possible, however, we have observed that the serum hydrolysis rates of prodrug residues are

dramatically suppressed as the polymer scaffold becomes more hydrophobic.[16,18] The accessibility of targeting residues such as biotin or macromolecular peptide monomers to cell surface receptors are also significantly reduced when these residues are sequestered within hydrophobic environments. The biologically relevant monomers outlined in **Scheme 4.2** include prodrug monomers of ciprofloxacin (CTM), a clinically relevant antibiotic, and dasatinib (DtSMA), a widely employed chemotherapeutic, as well as a cell receptor targeting/protein binding monomer (BioHEMA), and a peptide macromonomer.

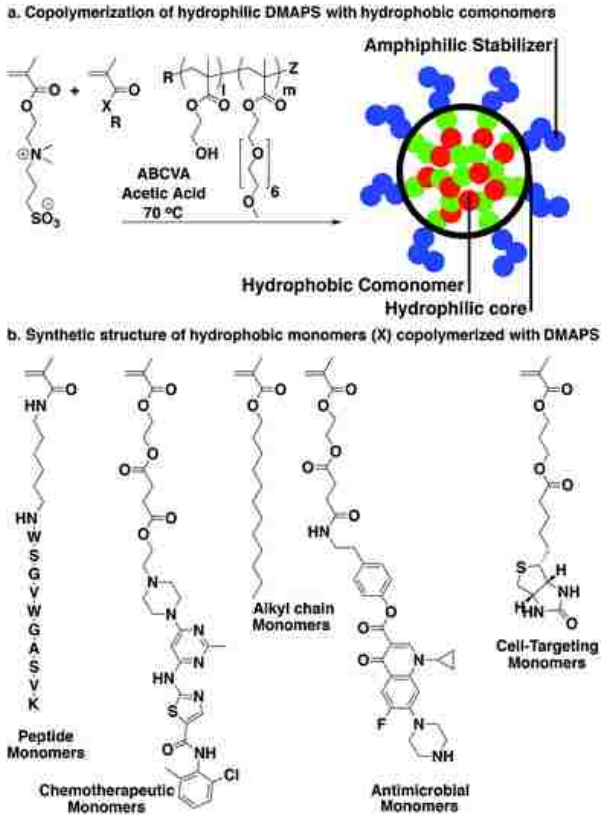

SCHEME 4.2 Synthetic scheme for the preparation copolymers block segments consisting of DMAPS and a hydrophobic comonomer *via* RAFT PISA in acetic acid.

As can be seen in **Fig. 4.5A**, the molecular weight distributions for the copolymerization of DMAPS and the hydrophobic comonomers depicted in **Scheme 4.2** are narrow and symmetric. In all cases the $Đ$ values remained below 1.20, however, some low molecular weight tailing, possibly resulting from primary radical termination of growing chains, along with a low molecular weight species is observed for poly(DMAPS-*co*-CTM). Given the high degree of control observed for comonomers with similar structures it is possible that these species are an analytical artifact produced by the amine residues present on CTM interacting with the size-

exclusion column. RAFT copolymerizations in acetic acid are also beneficial in that they allow amine-functional prodrug monomers (*e.g.* CTM) as well as peptide-macromonomers, such as the 12 amino acid methacrylamide macromonomer employed in these studies, to be polymerized directly without the need for amine protecting groups or acidic buffers. The latter conditions are particularly deleterious for copolymers that employ hydrolytically degradable linkages as part of their structure. Here the acetic acid is thought to protonate primary and secondary amines reducing their reactivity towards the thiocarbonyl thio groups.[37,38]

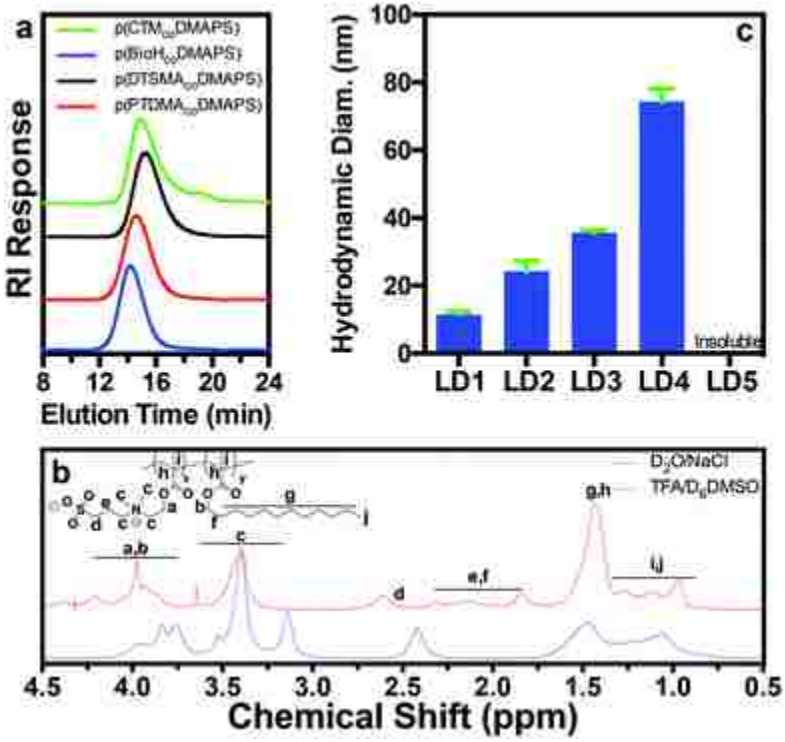

FIGURE 4.5. (a) Overlay of the aqueous SEC chromatograms for poly(DMAPS-*co*-BioHEMA), poly(DMAPS-*co*-CPM), poly(DMAPS-*co*-DtSMA), and poly(DMAPS-*co*-Mam-AhxWSGPGVWGASVK). The $[M]_0$:[macro-CTA]$_0$:$[I]_0$ ratio was 200:1:0.05 with DMAPS and hydrophobic comonomer feeds of and 15 wt% and 85 wt% respectively. (b) ^{1}H NMR spectrums for poly(LMA-*co*-DMAPS) in D_2O + NaCl and TFA/d_6 DMSO. (c) Hydrodynamic diameters for the poly(DMAPS-*co*-LMA) series in 150 mM phosphate buffered saline at pH 7.4.

4.3.5 Copolymerization of LMA with DMAPS from poly(HEMA-co-O300) in acetic acid targeting a wide range of compositions

In order to establish the ability to synthesize copolymers containing both hydrophilic and hydrophobic comonomers over a wider range of comonomer feed ratios, LMA and DMAPS were copolymerized at molar feed

ratios 20:80, 40:60, 50:50, 60:40, and 80:20 (LD1-LD5 respectively) (**Fig. 4.5B and C**). Shown in **Fig. 4.5A**, is an overlay of the ^{1}H NMR spectrums for poly(LMA-*co*-DMAPS) in D_2O + 0.5 M NaCl and trifluoroacetic acid (TFA)/d_6 DMSO. Evaluation of ^{1}H NMR spectrum conducted in TFA/d_6DMSO, where both comonomer residues are soluble, clearly shows resonances associated with both LMA and DMAP. In contrast, ^{1}H NMR analysis of the copolymer in D_2O + 0.5 M NaCl, where the DMAPS residues are soluble but the hydrophobic LMA residues are desolvated, shows the large methylene peak at 1.5 ppm to be strongly attenuated. This result suggests the formation of nanostructures where the hydrophobic LMA residues are stabilized in solution by the zwitterionic DMAPS residues. The amphiphilic nature of the resultant copolymers prevented SEC analysis determination of the molecular weight and *Đ* values. It is interesting to note that while polymerizations of both DMAPS and LMA from the poly(HEMA-*co*-O300) macro-CTA in acetic acid show substantial turbidity with the formation of the core-forming segment, statistical copolymers prepared from these monomers were observed to have low turbidity (not shown).

The resultant copolymers have amphiphilic structures in water that incorporate both zwitterionic and hydrophobic residues into a single macromolecular scaffold. Phosphatidylcholines, which are typically the most abundant lipid in animal and plant membranes, have a similar amphiphilic structure in which a zwitterionic phosphobetaine headgroup is connected to hydrophobic diacyl fatty acid tails. The widespread use of phosphatidylcholines to prepare liposomes suggests that synthetic copolymers prepared from a combination of zwitterionic and long chain hydrophobic monomers (*e.g.* lauryl methacrylate, cholesterol methacrylate, stearyl methacrylate) could be used to prepare similar nanostructures at a fraction of the cost. Indeed, analysis of the average particle diameters *via* DLS for copolymers (LD1-LD5) showed that increases in LMA content resulted in progressively larger diameters (**Fig. 4.5C**). For example, copolymers of LMA and DMAPS prepared at an initial molar feed of 20:80, respectively, have aqueous particle sizes of 11 nm, while copolymers prepared at 60:40 have particle sizes of 75 nm. Copolymers with the highest LMA feed (80% by mol) were insoluble in PBS. While a detailed analysis of the resultant morphologies is beyond the scope of the current study, these results

highlight the potential of RAFT-PISA in acetic acid to directly synthesize surface-active materials with sulfobetaine polar groups.

4.3.6 Synthesis of mannose-targeted polymeric prodrugs via RAFT PISA in acetic acid

The ability to incorporate cell-targeting functionality into the stabilizing macro-CTA from which a hydrophilic polymeric prodrug segment could be grown was demonstrated by replacing the poly(HEMA-*co*-O300) HEMA residues with mannose ethyl methacrylate (MEM). We have shown previously that polymers containing MEM residues can be employed to efficiently target polymers and nanoparticles to carbohydrate cell surface receptors, which are highly expressed on alveolar macrophages.[39,40]Invasive intracellular pathogens such as *F. tularensis* can selectively reside within these cells leading to significant morbidity and mortality.[41] As shown in **Scheme 4.3**, MEM was first copolymerized with O300 in acetic acid to prepare a poly(MEM-*co*-O300) macro-CTA. An initial molar feed ratio of 50% MEM and 50% O300 was employed with $[M]_0$:$[CTA]_0$:$[I]_0$ of 50:1:0.04 This composition was selected in order to yield a macro-CTA stabilizer with high mannose group density while also retaining good aqueous and organic solvent solubility. From the mannose-functional macro-CTA the RAFT copolymerization of prodrug monomer CTM with DMAPS was conducted in acetic acid using the PISA conditions outlined above. This approach allows the hydrophobic prodrug monomer residues to be incorporated within the hydrophilic polymer scaffold and prevents hydrolytic cleavage of the phenyl ester-link ciprofloxacin residues during polymerization.

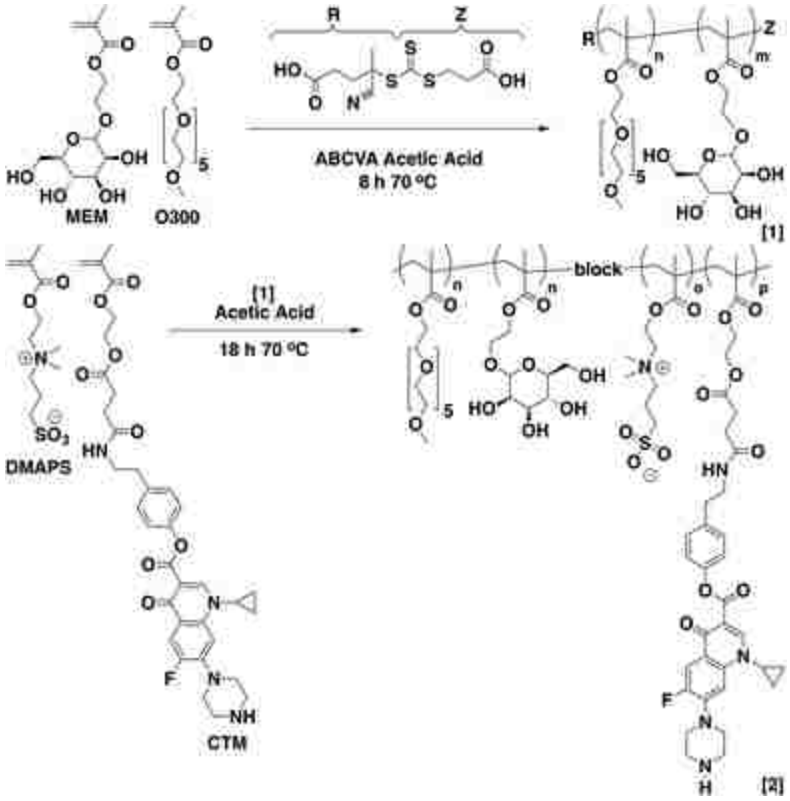

Scheme 4.3 Synthetic scheme for the preparation of mannose-targeted polymeric prodrugs containing the antibiotic ciprofloxacin. RAFT copolymerization of MEM and O300 were conducted in acetic acid with CCC and ABCVA as the RAFT agent and initiator respectively. The resultant poly(MEM-*co*-O300) macro-CTA was then chain extended with DMAPS and CTM *via* PISA in acetic acid.

Shown in Fig. 6a and b are the ^{1}H NMR spectra for the poly(MEM-*co*-O300) macro-CTA as well as the poly[(MEM-*co*-O300)-*block*-(DMAPS-*co*-CTM)] diblock copolymer. ^{1}H NMR analysis was conducted in a mixture of TFA containing 5% DMSO because poly(DMAPS) is not soluble in other organic solvents. While the final diblock copolymer is readily soluble in aqueous saline solutions, NMR analysis under these conditions resulted in significant attenuation of the CTM resonances (not shown). In contrast, NMR analysis of the copolymer in the TFA d_6–DMSO solvent systems shows sharp resonances for all of the comonomer residues as can be clearly visualized in **Fig. 4.6A and B**. Copolymer composition of the poly(MEM-*co*-O300) macro-CTA was determined by comparison of the MEM anomeric proton at 4.6 ppm to the O300 methoxy protons at 3.0–3.2 ppm. This analysis yields a copolymer composition of 40% MEM and 60% O300, which is relatively close to the initial comonomer feed composition. Shown in **Fig. 4.6B** is the ^{1}H NMR spectrum for the poly[(MEM-*co*-O300)-*block*-(DMAPS-*co*-CTM)] diblock copolymer prepared *via* RAFT-PISA in acetic acid. Because of the

convoluted nature of the ^{1}H NMR spectrum reverse phase HPLC was used to determine the copolymer composition (not shown).[16] These measurements indicate that the copolymers contain 12.3 wt% CTM, which is in good agreement with the feed. Analysis of the copolymers depicted in **Scheme 4.3** *via* dynamic light scattering in phosphate buffered saline (150 mM NaCl, 20 mM phosphate pH 7.4) shows hydrodynamic diameters that are below 7 nm. This size is consistent with a molecularly soluble unimeric species and supports the formation of random copolymers of DMAPS with the hydrophobic comonomers.

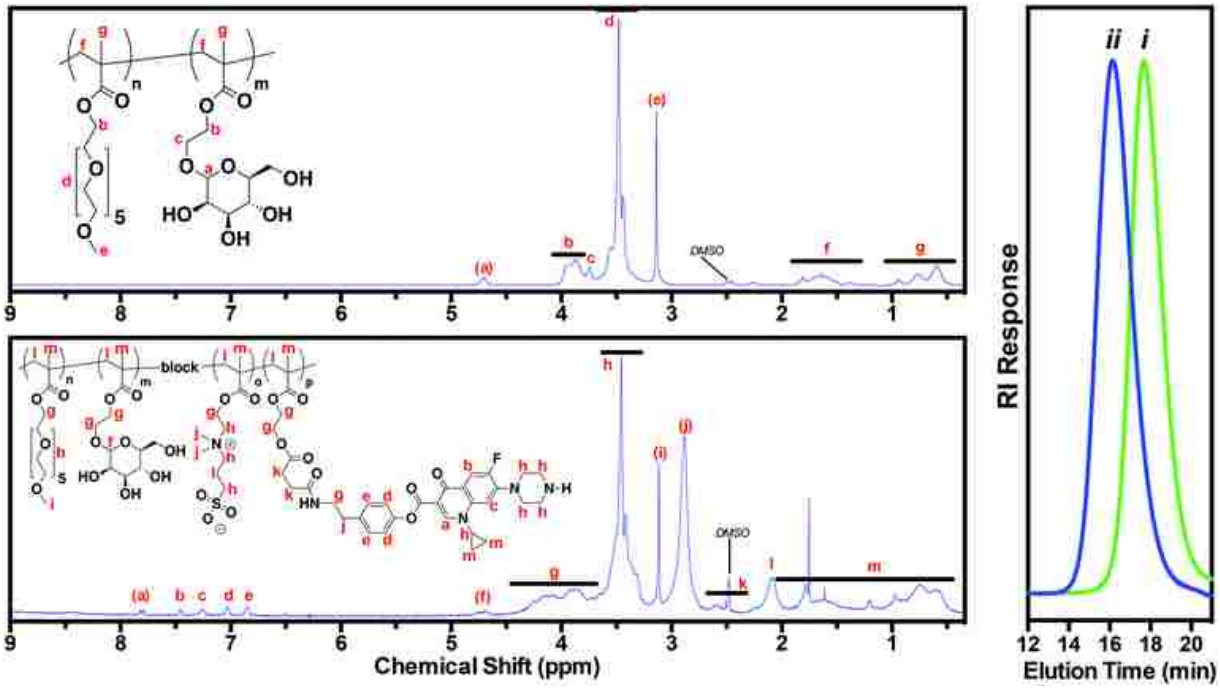

FIGURE 4.6. ^{1}H NMR spectra of (a) poly(MEM-*co*-O300) and (b) of poly[(MEM-*co*-O300)-*block*-(DMAPS-*co*-CTM)] conducted at 500 mHz with 5 wt% polymer in TFA containing 5% by volume d_6 DMSO. (c) Overlay of the aqueous SEC chromatograms for the poly(MEM-*co*-O300) macro-CTA (i) and resultant poly[(MEM-*co*-O300)-*block*-(DMAPS-*co*-CTM)] (ii). The $[M]_0$:$[macro\text{-}CTA]_0$:$[I]_0$ ratio was 200:1:0.05 with DMAPS and hydrophobic comonomer feeds of and 15 wt% and 85 wt% respectively.

Shown in **Fig. 4.6C** are the molecular weight chromatograms for the poly(MEM-*co*-O300) macro-CTA as well as the resultant poly(MEM-*co*-O300)-*b*-(DMAPS-*co*-CTM) diblock copolymer. The high polymerization control imparted under these conditions can be seen by the narrow molecular weight distributions which clearly move to shorter elution times upon the addition of the second poly-(DMAPS-*co*-CTM) segment. Absolute

molecular weights and $Đ$ values for the macro-CTA and diblock copolymer were determined to be 13 500 g mol^{-1}/1.13 and 42 000 g mol^{-1}/1.15 respectively.

4.4 Conclusions

PISA from a small neutral hydrophilic macro-CTA in acetic acid was employed to homopolymerize the hydrophilic sulfobetaine monomer DMAPS and hydrophobic monomer lauryl methacrylate LMA. Kinetic analysis of these polymerizations suggests that well-defined block copolymers can be synthesized under these conditions. Analyses of the MWDs for both polymerizations show a progressive narrowing of the chromatograms throughout the polymerization from an initial bimodal state. Copolymerizations of DMAPS with hydrophobic prodrug monomers yield copolymers with narrow and symmetric MWDs, and compositions that are controllable by the feed. These materials are readily soluble in saline solutions with hydrodynamic diameters that are consistent with molecularly dissolved unimers. The preparation of a polymeric prodrug containing macrophage-targeting mannose groups was also demonstrated by synthesizing a mannose-functional macro-CTA from which the zwitterionic prodrug segment was grown. Copolymerization of DMAPS with LMA over a wider composition range yielded polymers with composition-dependent aqueous solution properties such that an increase in polymer hydrophobicity led to the formation of large particle sizes. Given the ability of PISA in acetic acid to easily copolymerize monomers with disparate solubilities and the tremendous clinical significance of polymer-drug conjugates, it is expected that the conditions outlined in this report could lead to a new generation therapeutic copolymers and nanoparticles. We believe the use of acetic acid in these studies as a polymerization medium, which has largely been absent from the RAFT literature, is also significant given the desirable properties of this solvent (*e.g.* low cost, high boiling point, water miscibility, environmentally renewable).

4.5 Acknowledgements

This work was funded by the Defense Threat Reduction Agency (Grant #HDTRA1-13-1-0047). We would like to thank Boron Molecular for the gift of the CCC RAFT agent.

4.6 REFERENCES

1. T. M. Allen and P. R. Cullis, Adv. Drug Delivery Rev., 2013, 65, 36–48.
2. H. Ringsdorf, J. Polym. Sci., Polym. Symp., 1975, 51, 135– 153.
3. H. G. Batz, G. Franzmann and H. Ringsdorf, Angew. Chem., Int. Ed. Engl., 1972, 11, 1103–1104.
4. S. Eliasof, D. Lazarus, C. G. Peters, R. I. Case, R. O. Cole, J. Hwang, T. Schluep, J. Chao, J. Lin, Y. Yen, H. Han, D. T. Wiley, J. E. Zuckerman and M. E. Davis, Proc. Natl. Acad. Sci. U. S. A., 2013, 110, 15127–15132.
5. J. Cheng, K. T. Khin, G. S. Jensen, A. Liu and M. E. Davis, Bioconjugate Chem., 2003, 14, 1007–1017.
6. H. Han and M. E. Davis, Mol. Pharm., 2013, 10, 2558–2567.
7. K. Cho, X. Wang, S. Nie, Z. G. Chen and D. M. Shin, Clin. Cancer Res., 2008, 14, 1310–1316.
8. M. E. Davis, Z. G. Chen and D. M. Shin, Nat. Rev. Drug Discovery, 2008, 7, 771–782.
9. R. K. Jain and T. Stylianopoulos, Nat. Rev. Clin Oncol., 2010, 7, 653–664.
10. F. Kratz, J. Controlled Release, 2008, 132, 171–183.
11. E. Lee, J. Lee and S. Jon, Bioconjugate Chem., 2010, 21, 1720–1723.
12. Y. Wang, D. Xin, K. Liu, M. Zhu and J. Xiang, Bioconjugate Chem., 2009, 20, 2214–2221.
13. Y. Gu, Y. Zhong, F. Meng, R. Cheng, C. Deng and Z. Zhong, Biomacromolecules, 2013, 14, 2772–2780.
14. M. B. L. Kryger, A. A. A. Smith, B. M. Wohl and A. N. Zelikin, Macromol. Biosci., 2014, 14, 173–185.
15. M. B. L. Kryger, B. M. Wohl, A. A. A. Smith and A. N. Zelikin, Chem. Commun., 2013, 49, 2643–2645.
16. D. Das, S. Srinivasan, A. M. Kelly, D. Y. Chiu, B. K. Daugherty, D. M. Ratner, P. S. Stayton and A. J. Convertine, Polym. Chem., 2016, 7, 826–837.
17. M. C. Parrott, M. Finniss, J. C. Luft, A. Pandya, A. Gullapalli, M. E. Napier and J. M. DeSimone, J. Am. Chem. Soc., 2012, 134, 7978–7982.
18. H. N. Son, S. Srinivasan, J. Y. Yhee, D. Das, B. K. Daugherty, G. Y. Berguig, V. G. Oehle, S. H. Kim, K. Kim, I. C. Kwon, P. S. Stayton and A. J. Convertine, Polym. Chem., 2016, 7, 4494–4505.
19. N. J. Warren and S. P. Armes, J. Am. Chem. Soc., 2014, 136, 10174–10185.
20. B. Karagoz, L. Esser, H. T. Duong, J. S. Basuki, C. Boyer and T. P. Davis, Polym. Chem., 2014, 5, 350–355.
21. W.-M. Wan, C. Y. Hong and C.-Y. Pan, Chem. Commun., 2009, 39, 5883–5885.
22. M. J. Derry, L. A. Fielding and S. P. Armes, Prog. Polym. Sci., 2016, 52, 1–18.
23. C. L. McCormick and A. B. Lowe, Acc. Chem. Res., 2004, 37, 312–325.
24. D. Roy, G. Y. Berguig, B. Ghosn, D. D. Lane, S. Braswell, P. S. Stayton and A. J. Convertine, Polym. Chem., 2014, 5, 1791–1799.
25. G. Moad, Y. K. Chong, A. Postma, E. Rizzardo and S. H. Thang, Polymer, 2005, 46, 8458–8468.
26. S. L. Canning, G. N. Smith and S. P. Armes, Biomacromolecules, 2016, 49, 1985–2001.
27. M. Yu, J. Tan, J. Yang and Z. Zeng, Polym. Chem., 2016, 7, 3756–3765.

28. J. Tan, Y. Bai, X. Zhang and L. Zhang, Polym. Chem., 2016, 7, 2372–2380.
29. B. Karagoz, C. Boyer and T. P. Davis, Macromol. Rapid Commun., 2014, 35, 417–421.
30. W.-M. Wan, X. L. Sun and C.-Y. Pan, Macromol. Rapid Commun., 2010, 31, 399–404.
31. P. Chambon, A. Blanazs, G. Battaglia and S. P. Armes, Biomacromolecules, 2012, 45, 5081–5090.
32. W.-J. Zhang, C. Y. Hong and C.-Y. Pan, Macromolecules, 2014, 47, 1664–1671.
33. W. M. Wan and C. Y. Pan, Biomacromolecules, 2010, 43, 2672–2675.
34. M. S. Donovan, B. S. Sumerlin, A. B. Lowe and C. L. McCormick, Biomacromolecules, 2002, 35, 8663–8666.
35. K. E. B. Doncom, N. J. Warren and S. P. Armes, Polym. Chem., 2015, 6, 7264–7273.
36. M. S. Donovan, A. B. Lowe, T. A. Sanford and C. L. McCormick, J. Polym. Sci., Part A: Polym. Chem., 2003, 41, 1262–1281.
37. D. B. Thomas, A. J. Convertine, R. D. Hester, A. B. Lowe and C. L. McCormick, Macromolecules, 2004, 37, 1735– 1741.
38. D. B. Thomas, A. J. Convertine, L. J. Myrick, C. W. Scales, A. E. Smith, A. B. Lowe, Y. A. Vasilieva, N. Ayres and C. L. McCormick, Macromolecules, 2004, 37, 8941–8950.
39. E.-H. Song, M. J. Manganiello, Y.-H. Chow, B. Ghosn, A. J. Convertine, P. S. Stayton, L. M. Schnapp and D. M. Ratner, Biomaterials, 2012, 33, 6889–6897.
40. J. Chen, H.-N. Son, J. J. Hill, S. Srinivasan, F.-Y. Su, P. S. Stayton, A. J. Convertine and D. M. Ratner, Nanomedicine, 2016, 12, 2031–2041.
41. P. C. F. Oyston, A. Sjöstedt and R. W. Titball, Nat. Rev. Microbiol., 2004, 2, 967–978.
42. G. Y. Berguig, A. J. Convertine, S. Frayo, H. B. Kern, E. Procko, D. Roy, S. Srinivasan, D. H. Margineantu, G. Booth, M. C. Palanca-Wessels, D. Baker, D. Hockenbery, O. W. Press and P. S. Stayton, Mol. Ther., 2015, 23, 1–11.
43. E.-H. Song, M. J. Manganiello, Y.-H. Chow, B. Ghosn, A. J. Convertine, P. S. Stayton, L. M. Schnapp and D. M. Ratner, Biomaterials, 2012, 33, 6889–6897.

CHAPTER 5. A synthetic macromolecular antibiotic platform for inhalable therapy against aerosolized intracellular alveolar infections*

*Provided as published: Das D., Chen J., Srinivasan S., Kelly A.M., Lee B., Son H., Radella F., West T.E., Ratner D.M, Convertine A.J., Skerrett S.J., Stayton P.S. *Molecular Pharmaceutics.* 14(6);1988-97 (2017).

ABSTRACT

Lung-based intracellular bacterial infections remain one of the most challenging infectious disease settings. For example, the current standard for treating *Franciscella tularensis* pneumonia (tularemia) relies on prolonged administration of oral and intravenous antibiotics that poorly achieve and sustain pulmonary drug bioavailability. Inhalable antibiotic formulations are approved and in clinical development for upper respiratory infections, but sustained drug dosing from inhaled antibiotics against alveolar intracellular infections remains a current unmet need. To provide an extended therapy against alveolar intracellular infections, we have developed a macromolecular therapeutic platform that provides sustained local delivery of ciprofloxacin with controlled dosing profiles. Synthesized using RAFT polymerization, these macromolecular prodrugs characteristically have high drug loading (16-17 wt.% drug), tunable hydrolysis kinetics mediated by drug linkage chemistry (slow-releasing alkyllic vs. fast-releasing phenolic esters), and in general represent new fully synthetic nano-therapeutics with streamlined manufacturing profiles. In aerosolized and completely lethal *F.t. novacida* mouse challenge models, the fast-releasing ciprofloxicin macromolecular prodrug provided high cure efficiencies (75% survival rate under therapeutic treatment), and the importance of release kinetics was demonstrated by the inactivity of the similar but slow-releasing prodrug system. Pharmacokinetics and biodistribution studies further demonstrated that the efficacious fast-releasing prodrug retained drug dosing in the lung above the MIC over a 48h period with corresponding C_{max}/MIC and $AUC_{0\text{-}24h}$/MIC ratios being greater than 10 and 125, respectively – the thresholds for optimal

bactericidal efficacy. These findings identify the macromolecular prodrug platform as a potential therapeutic system to better treat alveolar intracellular infections such as *F. tularensis*, where positive patient outcomes require tailored antibiotic pharmacokinetic and treatment profiles.

5.1 Introduction

Alveolar intracellular bacterial infections remain a major global health challenge across the developed and developing world. The public health costs of diseases such as tuberculosis, anthrax, tularemia, and meliodosis are high, and the present and growing threat of drug resistance is well established.[1-3] For example, *Franciscella tularensis* is a highly invasive intracellular bacterium that causes tularemia, a debilitating and sometimes life-threatening disease.[4-6] Inhalation of gram-negative *F. tularensis* can result in a severe form of the disease that is associated with a low infectious dose (10-40 colony-forming units) and high morbidity and mortality.[5] Without immediate medical intervention, respiratory tularemia has a fatality rate of up to 30%.[4,7] For these reasons alone, potential aerosolization of this pathogen can have devastating impact on public health and has led to the classification of *F. tularensis* by the U.S. Centers for Disease Control and Prevention as a Tier 1 biothreat agent of concern.[6,8] Current treatment for wild-type *F. tularensis* strain infections include rigorous oral and IV antibiotic therapies with aminoglycoside, tetracycline, and/or fluoroquinolone drugs.[9-11] For example, recent microbiological and clinical data have shown the utility of ciprofloxacin, a commonly prescribed fluoroquinolone, for the treatment of respiratory tularemia.[12-15] However, many antibiotics administered orally or through IV injection are associated with systemic toxicity, poor pharmacokinetics, and low drug biodistribution to the lungs.[9,12,16] Direct pulmonary drug delivery offers an alternative, convenient, and non-invasive strategy for drug administration that can enhance therapeutic efficacy against

respiratory infections by localizing antibiotics to the site of bacterial persistence.[16-18] The U.S. Food and Drug Administration has recently approved the use of inhalable forms of antibiotics such aztreonam and tobramycin for treating severe upper respiratory *Pseudomonas aeruginosa* infections in cystic fibrosis patients.[18]

Several pharmaceutical carrier technologies are currently being developed that utilize various excipients to address shortcomings of free drug formulations, such as poor drug solubility and rapid drug clearance from the pulmonary space.[16,19,20] Liposomal carriers have been utilized to improve the therapeutic potential of a drug by increasing drug residence times, and reducing drug dosing and systemic toxicity.[21,22] For example, Wong *et al*. delivered liposome-encapsulated ciprofloxacin *via* pulmonary aerosolization and prolonged survival rates in mice against a live vaccine strain of *F. tularensis* compared to treatment with IV and aerosolized, un-encapsulated drug.[23] Liposomal delivery systems can be limited to still rapid drug release profiles, low drug encapsulation, and complex formulation procedures that can affect scalability and reproducibility.[22,24] Alternatively, polymeric carriers have been developed as dispersal-based formulations or as polymer-drug conjugates.[25-29] They have also faced challenges with burst and/or rapid drug release profiles, low drug incorporation ratios, and scale-up and manufacturing difficulties.

Here, we demonstrate the clinical and translational significance of a fully synthetic nano-therapeutic platform termed "drugamers" that addresses previous limitations of dispersal formulations and polymer-drug conjugates. Prodrug monomers are first synthetically constructed with linker and drug couplings that can be conducted in solvents and with acids/bases/catalysts that could not previously be exploited in post-synthetic polymer-drug conjugations.[30-34] The ability to then control the polymerization with other functional monomers via Reversible addition-

fragmentation chain-transfer polymerization (RAFT) synthesis provides additional opportunities to incorporate targeting moieties, sterically stabilizing compositions, and the ability to engineer block or branched architectures.[35] Recently, we utilized RAFT to copolymerize a hydrophilic stabilizer, polyethylene glycol methacrylate (PEGMA O950), and two polymerizable prodrug monomers of ciprofloxacin.[32] These drug monomers contain either an alkyllic (HBC) or phenolic ester (CPM) linkage capable of hydrolyzing and releasing drug at slow and fast rates, respectively. The resulting polymeric prodrugs were unique in their ability to achieve high drug loading, promote sustained and controlled drug release, and maintain *in vitro* antimicrobial efficacy.

In this paper, we demonstrate for the first time the ability of the drugamers to generate effective antibiotic pharmacokinetic (PK) profiles in the lung. These drug profiles correlate with strong bactericidal properties in the aerosolized *Franciscella novicida* challenge model. The *F. tularensis* subsp. *novicida* shares 98% nucleotide identity and is highly lethal with similar virulence as *F. tularensis* in animals.[36-38] Only a fast-releasing drugamer design could achieve high cure efficiencies and relevant drug concentrations in the lung, while a slow-releasing equivalent drugamer was ineffective. The results demonstrate the potential of the drugamer platform for alveolar intracellular infection therapy.

5.2 Experimental details

5.2.1 Mice.

C57BL/6 age matched (6-8 weeks) female mice were purchased from Jackson Lab and used throughout the experiments. The experiments did not use a method of randomization. The investigators were not blinded to allocation during experiments and outcome assessment. All animal work was conducted in accordance to the University of Washington's Institutional Animal Care and Use Committee, and

Department of Defense's ACURO office guidelines. Experimental group sizes were approved by the regulatory authorities for animal welfare after being defined to balance statistical power, feasibility, and ethical aspects. All mice were kept in accordance with federal and state policies on animal research at the University of Washington.

5.2.2 In vivo toxicity and biocompatibility of ciprofloxacin copolymers

Comprehensive *in vivo* polymer toxicity panels were carried out using female C57Bl/6 mice (6-8wks old). The mice were anesthetized with 5% isoflurane for 5 min before administration of 50 uL per mouse of PBS only (Corning 21-040-CV), or 20 mg/kg ciprofloxacin (45 and 43 mg/mL HBC and CPM copolymer, respectively; n = 4 for each polymer) and 40 mg/kg ciprofloxacin (90 and 86 mg/mL HBC and CPM copolymer, respectively; n = 5 for each polymer) as polymer formulations in PBS, pH 7.4. All solutions were filtered (0.2 µm) and administered *via* endotracheal aerosolization using a Microsprayer® aerosolizer designed for use on mice (Penn-Century MSA-250-M, PA, USA). Mice were dosed as above once every 24 hours for three-day consecutive dosing studies. 24 hours after the final administration, mice were weighed, and then sacrificed by CO_2 asphyxiation and lavaged by cannulating tracheas with a 22G soft catheter (Exel International 14-841-10) prior to a 1 mL PBS flush and followed by three 0.8 mL flushes. Approximately 3 mL of lavage fluid was recovered per mouse. Lungs were removed, weighed, and placed into 1 mL PBS on ice. Lung tissues were mechanically homogenized with a Qiagen TissueRuptor (9001271) before addition of 1 mL of lysis buffer [PBS+1% Triton X-100 and 1 protease tablet/10 mL (Roche 1836153001)]. Bronchoalveolar lavage (BAL) fluid was spun at 1,000 g for 15 min to pellet lavage cells. BAL cells were re-suspended into 0.5 mL RPMI 1640+10% FBS, mounted onto microscopy slides with a Cytospin centrifuge at 46 g for 5 min,

and then stained with Hemacolor (EMD Millipore 65044) prior to cytology analysis. Stained slides were analyzed for macrophage to neutrophil ratios with a minimum of 200 cells counted per slide. Cell-free BAL fluid and lung tissue homogenate (LTH) TNF-α concentration was assayed using Biolegend's paired TNF-α ELISA kit (430902).

5.2.3 Preparation of tritium-labeled ciprofloxacin copolymers

To study pharmacokinetics and biodistribution properties of drug containing copolymers, radioactive [^{3}H]*N*-succinimidyl propionate was used for post-polymerization conjugation to the secondary reactive amine (position *N*-4 of the piperazinyl group) present on polymer-bound ciprofloxacin. To a scintillation vial, 125 mg (9.62 μmoles) of either poly(O950-co-HBC) or poly(O950-co-CPM) was added at 25 mg/mL in $CHCl_3$ to two equivalents (19.23 μmoles) of TEA. Samples were vortexed until solutions were clear before reacting with [^{3}H]*N*-succinimidyl propionate (77 μCi, 1 nmol) for 24 h at 25 ˚C. Double PD-10 desalting columns were used for PBS buffer exchange and removal of unreacted radiolabel. The specific reactivity of resulting [^{3}H]-poly(O950-co-HBC) (0.74 μCi/mg) and [^{3}H]-poly(O950-co-CPM) (0.73 μCi/mg) was measured on a scintillation counter (LS 6500, Beckman Coulter) with ULTIMA GOLD (Perkin Elmer) scintillation fluid.

5.2.4 Biodistribution and blood clearance of radiolabeled delivery systems

In vivo pharmacokinetics and biodistribution of conjugated [^{3}H]-ciprofloxacin polymeric prodrugs were evaluated in 6 wk. old C57BL/6 female mice. Mice were anesthetized by isoflurane inhalation before administration of endotracheal aerosols using a microsprayer (Penn-Century MSA-250-M, PA, USA). Polymer solutions of either [^{3}H]-poly(O950-*co*-HBC) or [^{3}H]poly(O950-

co-CPM) dissolved in PBS was administered at 0.95 µCi (20 mg/kg ciprofloxacin with the addition of unlabeled polymer) per mice as a single dose (50 µL). Whole blood samples were drawn (n = 5) over time (0, 2, 8, 18, 24, and 48 hours) using cardiac puncture, and immediately transferred to microcontainers with lithium heparin to prevent clotting. Blood solutions of 100 µL were sequentially treated with 200 µL of solvable, 20 µL of 0.1 M EDTA di-sodium salt solution, and 60 µL of 30% hydrogen peroxide in 20 µL aliquots to reduce coloring and quenching. Samples were reacted for 30 min at 25 ˚C before ULTIMA GOLD scintillation fluid was added, vortexed, and allowed to equilibrate for 1 h. [H^3] activity was measured by scintillation counting with the help of an automated deconvolution program for radioactive signal to determine percent (%) injected dose per mL (% ID/mL) of blood. Similarly, at the various times (0, 2, 8, 18, 24, and 48 hours) mice lungs, livers, spleens, kidneys, and stomachs (n = 5 for each tissue) were harvested, weighed, dissolved in Solvable (5 mL/g) and processed as recommended by manufacturer (Perkin Elmer). Solutions were diluted into ULTIMA GOLD, vortexed, reacted overnight at 25 ˚C, and run on a scintillation counter to determine the % injected dose per gram (% ID/g) of tissue.

5.2.5 Measuring in vivo polymer released and aerosolized free ciprofloxacin concentrations

To understand the *in vivo* pharmacokinetics and biodistribution properties of released drug from the polymer prodrugs, unmodified poly(O950-co-HBC), poly(O950-co-CPM) or unconjugated free drug were dosed *via* endotracheal aerosolization at 20 mg/kg ciprofloxacin in 6 wk. old C57BL/6 female mice. As before, mice were anesthetized by isoflurane inhalation before administering single doses of either polymer solutions in PBS or free drug in sodium acetate buffer (pH 5.5) using a microsprayer. *In vivo* drug concentrations in the various tissues and blood were analyzed against calibration standards using analytical liquid chromatography coupled with

tandem triple quadrupole mass spectrometry detection. Whole blood (cardiac puncture) and organ samples (n = 5) were collected over time (0, 2, 8, 18, 24, and 48 hours for polymers and 30 min, 1, 6, 18, 24, and 48 hours for free drug) and homogenized. Resulting homogenates (30 uL) were sequentially diluted 10x with de-ionized water and added to 5 ng/mL (10 uL) of deuterated ciprofloxacin-d8 internal standard (CDN Isotopes Inc., Quebec, Canada). A single step extraction was performed using 2x dilution of acetonitrile, and samples were then vortexed and spun at 17,000 g for 15 min before supernatants isolated for analysis. Analytes were injected into a XSelect UPLC HSS PFP 2.1 by 75 mm (3.5 µm) analytical column (Waters Corporation, Milford, MA, USA) and separated using a gradient method of water and acetronitrile with 10 mM formic acid. Calibration standards were prepared ranging from 40 ng/mL to 3.5 ug/mL in tissue and blood homogenates, and then were combined and diluted with deuterated ciprofloxacin internal standard and acetonitrile, respectively. Separate quality control solutions were prepared similarly at concentrations of 100 ng/mL, 500 ng/mL, and 2 ug/mL. The liquid chromatography system was composed of an I-Class Acquity UPLC (Waters Corporation, Milford, MA, USA) with a direct infusion syringe pump and temperature-controlled 96 vial auto-sampler maintained at 4 ˚C. The chromatographic system was coupled to a Waters Xevo TQ-S tandem quadrupole mass spectrometer (Waters Corporation, Milford, MA, USA) with a Micromass ZsprayTM Atmospheric Pressure Ioniation (API) Source. The LC–MS/MS system and data analysis was carried out using MassLynx® software (version 4.1) (Waters Corporation, Milford, MA, USA).

5.2.6 In vivo aerosolization of Franciscella novicida

F. novicida U112 was originally obtained from Francis Nano (University of Victoria, Victoria, Canada). A stock was prepared from overnight growth in trypticase soy broth with 0.1%

L-cysteine at 37°C with aeration. Bacteria were harvested in stationary phase, diluted in 20% glycerol, aliquoted, flash-frozen, and stored at -80°C, yielding a post-thaw titer of 10^9 CFU/ml. For each experiment, an aliquot was thawed, diluted 1:50 in PBS, and 6 ml were transferred to a Heart Mini-hi-flow nebulizer (Westmed, Arizona, USA) for aerosolization. Mice from all three treatment groups were simultaneously exposed to aerosolized bacteria using a Biaera whole-body exposure chamber (Biaera Technologies, Maryland, USA), with total airflow through the chamber maintained at 19.5 L/min during a 20 min exposure. To determine bacterial deposition in the lungs, 4 mice were euthanized immediately after exposure with pentobarbital (300 mg/kg intraperitoneally) followed by exsanguination. The left lungs were harvested, homogenized in PBS, and quantitatively cultured on trypticase soy agar supplemented with 0.1% L-cysteine.

5.2.7 In vivo prophylactic and therapeutic delivery of ciprofloxacin copolymers

Prophylactic and therapeutic antibiotic activity *in vivo* of poly(O950-co-HBC) and poly(O950-co-CPM) was conducted using endotracheal aerosolization dosed every 24 hours for three consecutive days. Female C57BL/6 mice, 6-8 wks. old, were anesthetized with 5% isoflurane with O_2 at one L/min exposure after filling the chamber for one min. Using a mouse laryngoscope (Penn-Century LS-2, LS-2M, PA, USA), and an endotracheal microsprayer (Penn-Century MSA-250-M, PA, USA), 50 uL of either PBS (n = 8), poly(O950-co-HBC) (n = 8) or poly(O950-co-CPM) (n = 8) was administered prophylactically or therapeutically at 20 mg/kg or 40 mg/kg ciprofloxacin concentrations. Specifically, three treatment cycles were carried out to vary the relative dosing schedule in relation to bacterial infection. Prophylactic regimens were initiated at three days (treatment cycle (I) -3, -2, and -1) and one day (treatment cycle (II) -1, 0, and +1) before infection, while a complete therapeutic regimen was started on the day of infection (treatment

cycle (III) 0, +1, and +2). Day zero was classified as the time point for bacterial infection, and mice received corresponding doses one hour before infection. The microsprayer was cleaned in between experimental groups using a series of washes with 70% alcohol, dd-H_2O, and PBS, while the sprayer tip was externally wiped with 70% alcohol and briefly air-dried.

Measurements of health were catalogued by monitoring the appearance, temperature, behavior, and body weight of each mouse daily. The mice were scored using a standard appearance-chart where high health values represented normal reactive behaviors, while their body temperatures and weights were quantified using an IR surface thermometer and digital scale, respectively. Mice that had an appearance score above 6, a body weight loss of over 20%, or temperature below 25 ˚C were euthanized. Experimental endpoint was 14 days after bacterial infection at which point any surviving mice were also euthanized.

5.2.8 Statistical analysis

All results are expressed as the mean ± SD or the mean ± SEM as indicated. Biological replicates were used in all experiments unless otherwise stated. Data were analyzed using two-way analysis of variance (ANOVA) and Tukey post-hoc tests when more than two groups were compared. Survival benefits were determined using a Mantel Cox test. All analyses were performed using GraphPad Prisim 5.0 (GraphPad Software, USA, 2007). Statistical significance was assigned for $P < 0.001$. No statistical methods were used to pre-determine the sample size of the experiments.

5.3 Results

5.3.1 Engineering ciprofloxacin macromolecular prodrugs

Ciprofloxacin was chemically linked to the polymerizable methacrylate moiety through either a slow-releasing alkyllic ester (HBC) or a fast releasing phenolic ester (CPM) linkage (**Fig. 5.1**). RAFT Polymerization of the prodrug monomers with a solubilizing polyethylene glycol methyl ether methacrylate (FW ~950 Da, O950) was achieved with precise control and reproducibility over final polymer molecular weight distributions and compositions, as characterized by GPC and ^{19}F-NMR, respectively (**Table 5.1**).[32] Both polymers were synthesized with predicted molecular weights and drug compositions (13.1 kDa and 16 wt.% ciprofloxacin for poly(O950-co-HBC) and 11.8 kDa and 16.7 wt.% ciprofloxacin for poly(O950-co-CPM) based on initial feeds of the respective comonomers, and monomer to RAFT chain transfer agent to initiator ratios ($[M]_o$:$[CTA]_o$:$[I]_o$). As previously shown, the polymeric hydrolysable ester linkers were designed to demonstrate tunable drug release kinetics, with poly(O950-co-HBC) releasing drug considerably slower ($t_{1/2}$ ~ 21 days) than poly(O950-co-CPM) ($t_{1/2}$ ~ 5 days).[32]

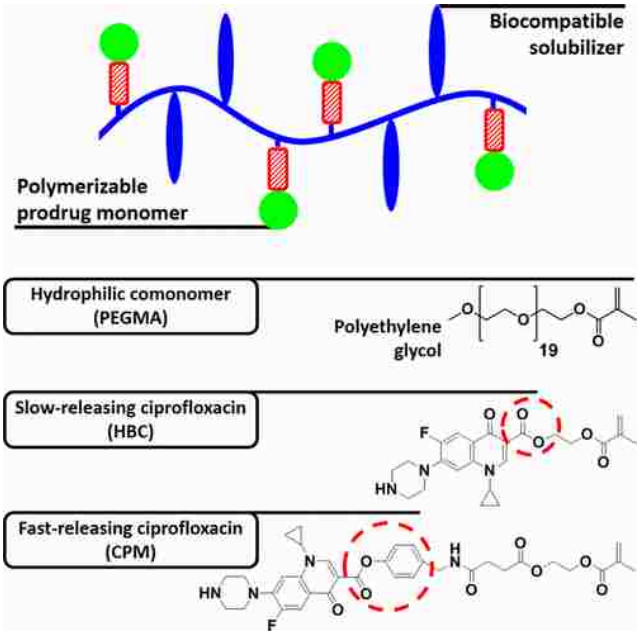

FIGURE 5.1. Schematic representation of ester-functionalized ciprofloxacin polymeric prodrugs. The synthesis of inhalable ciprofloxacin containing polymers utilized RAFT polymerization of a biocompatible polyethylene glycol methacrylate (PEGMA O950) hydrophilic comonomer, and two variants of the prodrug monomer: (1) a slow-releasing alkyllic ciprofloxacin ester (HBC) and (2) a fast-releasing phenolic ciprofloxacin ester (CPM). These esters linked the active drug compound to the polymer backbone via hydrolyzable moieties.

5.3.2 Acute lung safety of ciprofloxacin delivery systems

In order to determine the *in vivo* biocompatibility of the polymeric prodrugs after pulmonary administration, the lung toxicity of endotrachaelly delivered poly(O950-co-HBC) and poly(O950-co-CPM) was evaluated using the metrics of animal weight change, tumor necrosis factor alpha (TNF-α) concentration in lung tissue homogenate (LTH) and bronchoalveolar lavage fluid (BALF), and neutrophil infiltration into the lungs. Using an endotracheal microsprayer, copolymers were dosed at either 40 mg/kg (**Fig. 5.2**) or 20 mg/kg ciprofloxacin (**Fig. 5.3**) once every 24 hours for three-consecutive days. The data demonstrate no statistical differences ($P \leq 0.1$) across all observed toxicity markers at either drug dose for the poly(O950-co-HBC) and poly(O950-co-CPM) drugamers compared to PBS controls. For example, administration of either HBC or CPM copolymer systems at 40 mg/kg (**Fig. 5.2B**) in consecutive doses resulted in lavage fluids containing 4.9 ± 2.8% and 5.12 ± 2.7% neutrophils, respectively, whereas PBS controls exhibited 4.6 ± 2.3% neutrophils. Similarly, TNF-α concentrations in both the LTH and BALF for both HBC and CPM copolymers at 40 mg/kg (**Fig. 5.2C-D**) and 20 mg/kg (**Fig. 5.3C-D**) remained low and comparable to PBS control administrations.

Table 5.1. Summary of Cipro polymeric prodrug composition, molecular weight, and molar mass dispersity.

Polymer	O950 (feed)	O950 (exp.)	HBC (feed)	HBC[a] (exp.)	CPM (feed)	CPM[a] (exp.)	M_n[b] (kDa)	Đ[b]	Drug (wt.%)
Poly(O950-*co*-HBC)	74	65	26	35	-	-	13.1	1.08	16
Poly(O950-*co*-CPM)	80	64	-	-	20	36	11.8	1.09	16.7

a. Determined by ^{19}F NMR with a sodium trifluoroacetate internal standard in DMSO
b. Measured by gel permeation chromatography

5.3.3 Pharmacokinetics and biodistribution of endotrachaelly delivered [^{3}H]-Ciprofloxacin copolymers

To follow the polymer biodistribution kinetic profiles, a tritium radiolabel was conjugated to the *N*-4 piperazinyl group on ciprofloxacin, and subsequently purified of unreacted label. The resulting [^{3}H]-poly(O950-co-HBC) and [^{3}H]-poly(O950-co-CPM) were mixed with unlabeled polymers, and administered *via* endotracheal aerosolization as a single dose at 20 mg/kg and 0.95 μCi per mouse. As a function of time, whole blood and organs were harvested, homogenized, and all data was normalized to

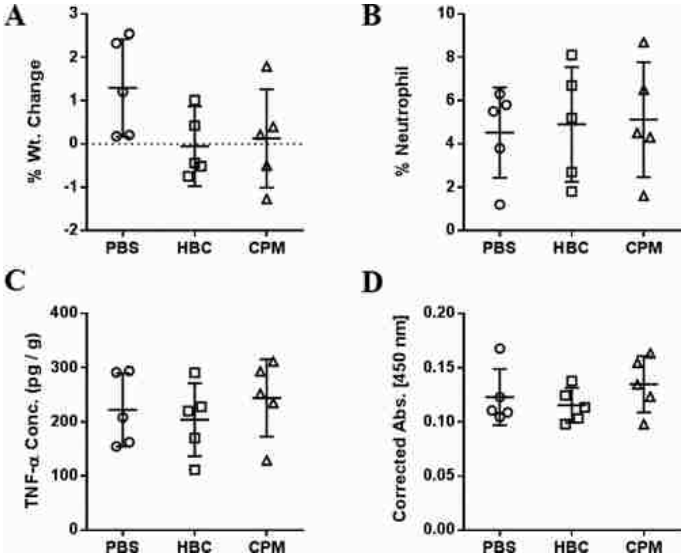

FIGURE 5.2. Pulmonary toxicity of endotracheally delivered polymeric prodrugs dosed at 40 mg/kg ciprofloxacin. Evaluation of *in vivo* toxicity of poly(O950-*co*-HBC) and poly(O950-*co*-CPM) via endotracheal aerosolization (50 μL) at 40 mg/kg ciprofloxacin dosed every 24 h over three-consecutive days. Multiple metrics of acute lung toxicity were examined in female C57Bl/6 mice (6–8wks old) and compared to PBS negative controls (n = 5 per group). (A) Animal weights measured prior to treatment and 24 h after the final treatment were ratioed to calculate percent (%) weight change per mice. (B) The % of neutrophils within the alveolar space was determined by differential cell counting of mounted and stained cells from bronchoalveolar lavage fluid (BALF). Values were calculated as [neutrophil count/(neutrophil + macrophage + lymphocytes)] × 100%. Tissue necrosis factor alpha (TNF-α) levels were measured by sandwich ELISA from (C) lung tissue homogenates (LTH) and (D) BALF. Concentration values of TNF-α from LTH were adjusted to mass of the harvested lungs, while BALF TNF-α levels were not within the linear region of a standard curve, so are presented as absorbance values corrected to total volume of harvested fluid. No statistically significant differences were observed using two-way ANOVA and a Tukey posthoc test between polymer treated and PBS treated mice within dose groups ($P \leq 0.1$). Error bars represent mean ± SEM.

mass (g) of tissue or volume (mL) of blood retrieved. The % injected-dose (I.D.)/time of the radiolabeled ciprofloxacin polymer conjugates is shown in **Fig. 5.4A**. The pulmonary distribution (α) and elimination (β) rate constants of the drugamers were found to be (k_α) 0.05 h^{-1} (95% confidence interval [CI] 0.04 – 0.06) and (k_β) 0.045 h^{-1} (95% CI 0.04 – 0.05) for the [^{3}H]-poly(O950-co-HBC), and k_α 0.1 h^{-1} (95% CI 0.07 – 0.12) and k_β 0.08 h^{-1} (95% CI 0.06 – 0.11) for [^{3}H]-poly(O950-co-CPM). In addition, the lung half-life ($t_{1/2}$) of the ^{3}H-HBC drugamer system was 15.3 h (95% CI 13.74 – 18.31), while the $t_{1/2}$ for ^{3}H-CPM system reduced to 8.2 h (95% CI 6.21 – 10.83). Similarly, the blood $t_{1/2}$ of the ^{3}H-HBC and ^{3}H-CPM drugamer system was 17.3 h (95% CI 15.83 – 20.14) and 10.4 h (95% CI 8.56 – 13.21), respectively. Radioactivity from ^{3}H-HBC and ^{3}H-CPM copolymer systems accumulated over a time-span of 24 h in the liver (**Fig. 5.5A**), spleen (**Fig. 5.5B**), and kidneys (**Fig. 5.5C**) before being eliminated by 48 h after delivery.

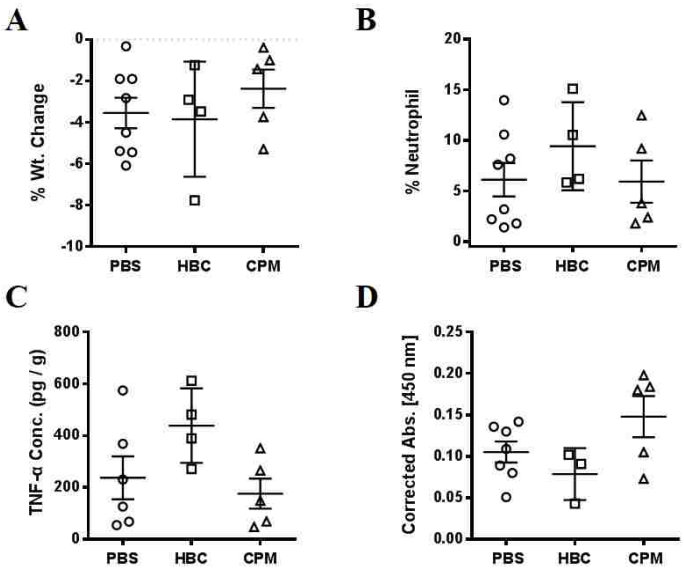

FIGURE 5.3. Pulmonary toxicity of copolymers administered as an aerosol at 20 mg/kg ciprofloxacin. Comprehensive toxicity panel establishing relative biocompatibility of alkyllic ciprofloxacin ester (HBC) and phenolic ciprofloxacin ester (CPM) statistical copolymers following endotracheal delivery at 20 mg/kg ciprofloxacin single dose (50 uL) every 24 hours for three-consecutive days. Markers for acute lung toxicity were evaluated by observing (**A**) changes in mice body weight (n = 8 PBS; n = 4 HBC; n = 5 CPM), quantifying (**B**) percent (%) neutrophil populations within lung endothelial cell-linings (n = 8 PBS; n = 4 HBC; n = 5 CPM), and measuring tissue necrosis factor alpha (TNF-α) levels in (**C**) lung tissue homogenates (LTH) (n = 6 PBS; n = 4 HBC; n = 5 CPM) and (**D**) bronchoalveolar lavage fluid (BALF) (n = 7 PBS; n = 3 HBC; n = 5 CPM). Animal weight loss was recorded 24 hours after final treatment and ratioed to weights prior to treatment. Differential cell counting of mounted and stained cells from BALF was utilized to calculate % neutrophil present using [neutrophil count/(neutrophil + macrophage + lymphocytes)]. Levels of TNF-α were measured using ELISA; reported (**C**) concentrations were adjusted to mass of the harvested lungs and (**D**) absorbance values were corrected for total volume isolated BALF. Analytical two-way ANOVA with Tukey post-hoc test was utilized to establish no statistical significance between treatment groups ($P \leq 0.1$). Error bars are presented as mean ± SEM.

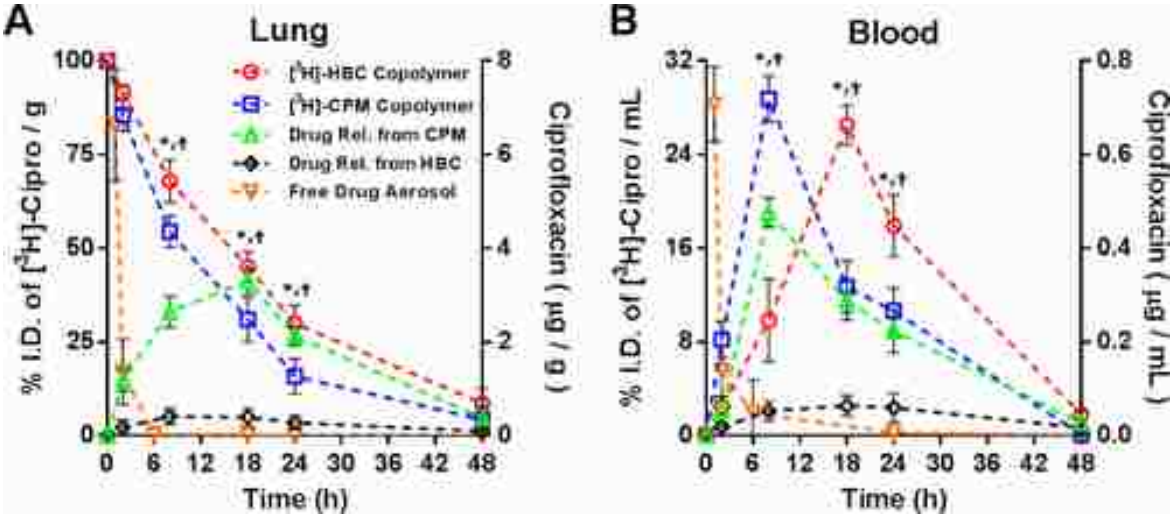

FIGURE 5.4. Investigation of lung and blood pharmacokinetics and biodistribution properties of endotracheally delivered poly(O950-*co*-HBC) and poly(O950-*co*-CPM) copolymers. Radiolabeled polymers were first synthesized using [^{3}H] NHS-propionate for post-polymerization conjugation to the *N*-4 position of the piperazinyl group found on ciprofloxacin. Both copolymers dissolved in PBS were dosed (50 µL) via endotracheal aerosolizations at 0.95 µCi and 20 mg/kg ciprofloxacin per mice as a function of time. Whole blood and lung tissues (n = 5 per polymer per time) were harvested, processed with Solvable, and analyzed with a scintillation counter. Disintegrations per minute were measured with the help of an automated deconvolution program for [^{3}H] radioactivity and used to determine percent (%) injected dose (I.D.) in mice (A) lungs and (B) blood (left *y*-axis). In a separate experiment, unmodified polymers were similarly dosed at 20 mg/kg ciprofloxacin per mouse, and as a function of time, whole blood and lung tissues (n = 5 per polymer per time) were harvested, homogenized, and analyzed for polymer-released drug concentrations using quantitative LC–MS. In addition, free ciprofloxacin formulated at 20 mg/kg in sodium acetate buffer (pH 5.5) was endotracheally administered via microsprayer and analyzed similarly over time for PK and distribution properties in the lung and blood (n = 5). Deuterated ciprofloxacin (-d_8) was used as an internal standard with calibration curves to evaluate amounts of available release or free drug in mice (A) lungs and (B) blood (right *y*-axis). Values were normalized against weight of lung (% I.D./g) or volume of blood (% I.D./mL) retrieved. Two-way ANOVA analysis with a Tukey posthoc test was utilized to establish statistical significance between the tritium-labeled polymers (*) and concentration of released-drug (†) at various time points; $^{*/\dagger}P < 0.001$. Data represents mean ± SD.

5.3.4 Pharmacokinetics and biodistribution of polymer-released ciprofloxacin

In vivo PK and biodistribution of polymer-released and free-endotrachaelly delivered ciprofloxacin was evaluated using an analytical LC-MS technique after a single endotracheal administration of unmodified polymeric prodrugs at 20 mg/kg drug. All data was normalized to mass of tissue or volume of blood retrieved. Results demonstrate that the fast-releasing poly(O950-co-CPM) drugamer released significantly (P<0.001) more drug in the lung (**Fig. 5.4A**), blood (**Fig. 5.4B**), and organs (**Fig. 5.5**). of mice as a function of time compared to the slow-releasing

poly(O950-co-HBC) drugamer. Lung antibiotic concentrations from the phenolic ester-modified ciprofloxacin polymer peaked from (mean ± SD) 1.1 ± 0.2 µg/g at 2 h to 3.4 ± 0.2 µg/g at 18 h (**Table 5.2**). In comparison, drug released from the alkyllic ester HBC prodrug only increased from 0.17 ± 0.15 µg/g at 2 h to 0.23 ± 0.12 µg/g by 18 h (**Table 5.2**). This profile of hydrolytic release and increasing drug dosing over time is notably distinct from the rapid immediate release and subsequent elimination profiles of liposomal or free drug. Levels of ciprofloxacin in the lungs from both prodrugs decreased from 18 h to 48 h after endotracheal administration, and was similar to the observed clearance profiles of the drugamers (**Fig. 5.4A**).

Table 5.2. Summary of lung and blood pharmacokinetic/pharmacodynamic parameters from endotrachaelly delivered polymeric prodrugs

Drug Rel. from Poly.	$AUC_{0\text{-}24}$ (95% CI)[a] (µg x h / g –or– / mL)	C_{max} ± SD[a] (µg / g –or– / mL)	t_{max} (h)	C_{max} / MIC^2	$AUC_{0\text{-}24h}$ / MIC[b] (h)	Organ
CPM copolymer	58.6 (56.4 – 60.8)	3.4 ± 0.2	18	113.7	1953.5	Lung
HBC copolymer	3.1 (2.4 – 4.7)	0.23 ± 0.12	18	7.62	103.5	
CPM copolymer	7.0 (6.8 – 7.2)	0.48 ± 0.03	8	15.9	233.4	Blood
HBC copolymer	1.1 (0.96 – 1.4)	0.06 ± 0.02	18	2.1	39.3	

a. Determined by GraphPad Prisim 7 analytical software; lung and blood normalized to g or mL, respectively
b. Minimum inhibitory concentration (MIC) determined to be 0.03 µg/mL from literature *(36)*

The pulmonary $t_{1/2}$ of released ciprofloxacin was measured to be 9.3 h (95% CI 7.82 – 11.38) and 15.6 h (95% CI 13.73 – 17.46) for the fast-releasing phenolic ester and slow-releasing alkyllic ester drugamer, respectively. In comparison, endotrachaelly administered free ciprofloxacin is rapidly cleared, k_{el} of 0.7 h^{-1} (95% CI 0.54 – 0.83), from the lungs into the blood with a pulmonary $t_{1/2}$ of 0.9 h (95% CI 0.8 – 1.2) (**Fig. 5.4A**). Additionally, no redistribution of ciprofloxacin from

circulation into the lungs was observed as evidenced by a consistent and rapid decrease in drug concentration during pulmonary elimination as well as the lack of detectable drug levels in the lung after clearance. We believe that the body acts as a sink and rapidly absorbs any available active drug first from the lungs and then from the blood, and that any recirculating drug has minimal influence on the total pulmonary drug concentration. Similar pulmonary pharmacokinetics have been observed by Cipolla et al. after intranasal instillation of free ciprofloxacin where the drug was observed to have comparable characteristic pulmonary half-life and rapid elimination kinetic without increases in drug concentration due to circulatory redistribution.[39] Moreover, lung PK profiles spanning up to 24 h have been reported for various liposomal ciprofloxacin formulations ($t_{1/2}$ 7.4 h) administered as intranasal instillations or aerosolizations in murine models. The key difference is that these liposomes release much of the drug (>70%) within 2-4 h of administration.[23,39,40] Blood concentrations of ciprofloxacin released from the fast-releasing phenolic ester prodrug peaked from 0.06 ± 0.02 µg/mL at 2 h to 0.48 ± 0.03 µg/mL at 8 h before being cleared by 48 h after dosing (**Table 5.2**). This was statistically (P<0.001) different from the drug release and accumulation profile for the slow-releasing alkyllic ester variant where maximum drug concentrations only reached 0.06 ± 0.02 µg/mL by 18 h (**Fig. 5.4B**). Accordingly, the area under the blood concentration *vs.* time curves from 0-24 h ($AUC_{0\text{-}24h}$) for the fast-releasing phenolic ester prodrug in the lung and blood was quantified to be 58.6 µg x h/g (95% CI 56.4 – 60.8) and 7.0 µg x h/mL (95% CI 6.8 – 7.2), respectively, while that for the slow-releasing polymer was 3.1 µg x h/g (95% CI 2.4 – 4.7) in the lung and 1.1 µg x h/mL (95% CI 0.96 – 1.4) in the blood (**Table 5.2**). Furthermore, peak drug concentrations in the liver (**Fig. 5.5A**), spleen (**Fig. 5.5B**), and kidneys (**Fig. 5.5C**) from the fast-releasing poly(O950-co-CPM) copolymer were greater than those achieved from administering the slow-releasing HBC variant,

and were measured to be 2.26 ± 0.2 µg/g (18 h), 2.0 ± 0.4 µg/g (24 h), and 6.4 ± 0.6 µg/g (24 h), respectively. Polymer-released ciprofloxacin from both constructs was cleared from these organs within 48 h after endotracheal delivery.

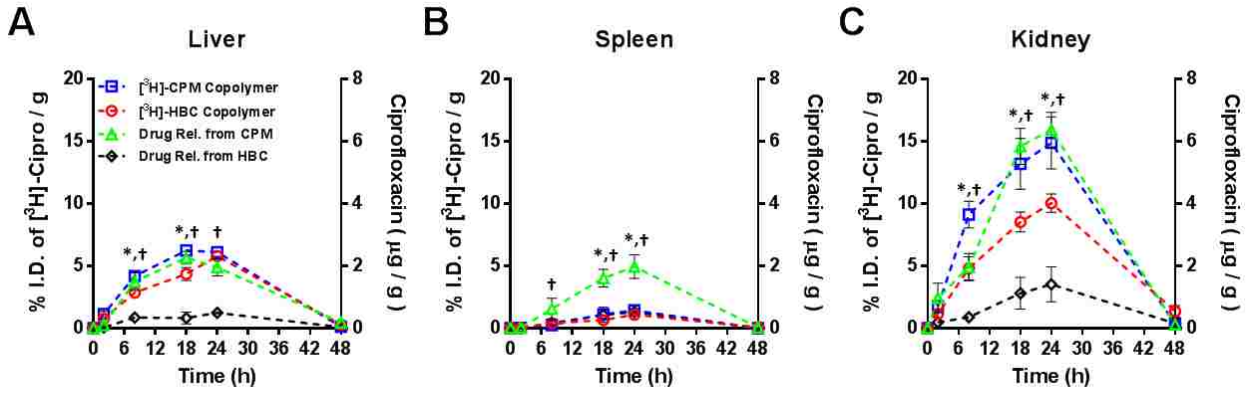

FIGURE 5.5. The pharmacokinetics and biodistribution of endotracheally delivered HBC and CPM copolymers in mice liver, spleen, and kidney. Radiolabeled copolymers were dosed at 0.95 µCi and 20 mg/kg ciprofloxacin per mice as a function of time. Organ tissues (n = 5 per polymer per time) were harvested, processed, and analyzed with a scintillation counter to determine percent (%) injected dose (I.D.) in mice (**A**) liver, (**B**) spleen, and (**C**) kidney. In a separate experiment, analytical LC-MS was used to evaluate released drug concentrations after endotracheal administration of un-modified polymers at a dose of 20 mg/kg ciprofloxacin. Corresponding mice (**A**) liver, (**B**) spleen, and (**C**) kidney tissues (n = 5 per polymer per time) were harvested, homogenized, and quantified for polymer-released drug using a deuterated ciprofloxacin (-d8) internal standard. Values were normalized against weight of organ (% I.D. / g) retrieved. Two-way ANOVA analysis with Tukey post-hoc test was utilized to establish statistical significance between the radiolabeled polymers (*) and concentration of released-drug (†) at various time points; (*,†) $P < 0.001$. Data represents mean ± SD.

5.3.5 Prophylactic and therapeutic bioactivity of ciprofloxacin polymeric prodrugs

Evaluation of dose response, treatment regimen, and overall bactericidal efficacy of the drugamers was conducted in the *F. novicida* aerosol challenge model. Polymers were administered using an endotracheal microspayer either with a prophylactic alone treatment at -3, -2, and -1 day (cycle I; 20 mg/kg ciprofloxacin), combination of prophylactic and therapeutic treatment at -1, 0, and +1 days (cycle II; 20 mg/kg ciprofloxacin), or therapeutic at 0 (one hour prior to infection), +1, and +2 days (cycle III; 40 mg/kg ciprofloxacin). In all experiments, mice were lethally infected by the aerosol route with approximately 10 LD50s of *F. novicida* (71 ± 18 cfu/mouse for cycle I, 53 ± 11 cfu/mouse for cycle II, and 161 ± 23 cfu/mouse for cycle III; average ± SEM). Animal

survival was monitored until mice qualified for euthanasia or reached the experimental end-point (14 days post-bacterial exposure). Mice treated with a purely prophylactic regimen (cycle I) at 20 mg/kg ciprofloxacin for all treatment groups did not survive to the experimental end-point; however, the CPM copolymer extended survival by three days compared to the HBC copolymer

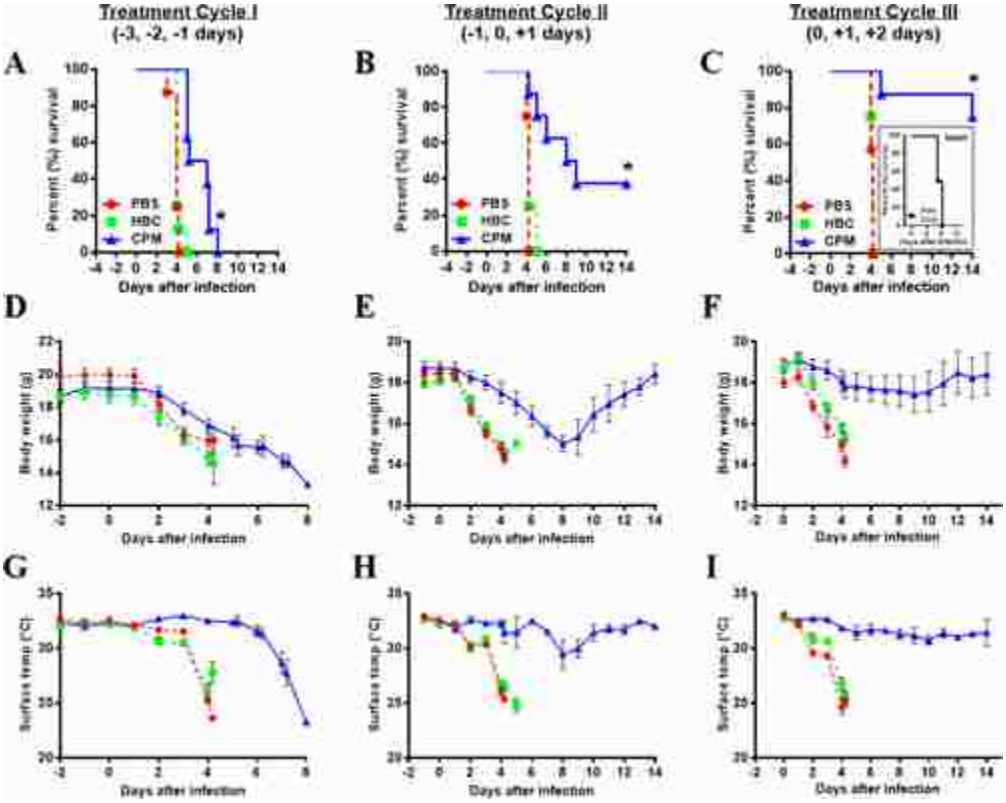

FIGURE 5.6. Determination of *in vivo* antimicrobial efficacy of ciprofloxacin polymeric prodrugs using aerosolized, highly virulent *Franciscella novicida* (strain U112). In this lethal mice challenge model, copolymer systems containing alkyllic (HBC) and phenolic (CPM) ester-functionalized ciprofloxacin were administered either prophylactically or therapeutically (50 µL aerosolization) at (A) −3, −2, and −1 day with 20 mg/kg ciprofloxacin (Cycle I), (B) −1, 0, and 1 day with 20 mg/kg ciprofloxacin (Cycle II), and (C) 0, 1, and 2 days with 40 mg/kg (Cycle III) (n = 8 for each treatment group per cycle). To evaluate the therapeutic efficacy of unconjugated drug, in a separate animal challenge experiment, ciprofloxacin at 40 mg/kg was administered to mice on days 0, 1, and 2 after infection (inset). All bacterial inoculation occurred 1 h after treatment on day 0. Measurements of health were recorded by monitoring changes in mice (D–F) body weight and (G–I) surface temperature. Mice that had a body weight loss of 20% or surface temperature below 25 °C were classified as irrecoverable and consequently euthanized. The challenge end-point was marked at 14 days post-bacterial exposure at which point any surviving mice were euthanized. A log-rank (Mantel Cox) test was used to determined statistical significance (*P < 0.001) for the Kaplan–Meier survival plots. Each treatment cycle represents separate studies. Body weight and surface temperature measurements are presented as mean ± SEM.

and PBS control (**Fig. 5.6A**). A transition from a prophylactic (cycle I) to a predominantly therapeutic (cycle III) treatment schedule, and a shift from 20 mg/kg to 40 mg/kg ciprofloxacin,

increased the survival rate of mice treated with poly(O950-co-CPM) from 0% (n = 0/8) (**Fig. 5.6A**) to 37.5% (n = 3/8) (**Fig. 5.6B**) to 75% (n = 6/8) (**Fig. 5.6C**). Mice treated with endotrachaelly delivered free ciprofloxacin at 20 mg/kg (cycle II) and 40 mg/kg (cycle III) demonstrated limited survival extension with all treated animals succumbing to the bacterial infection (n = 0/8) within five to 10 days (data no shown[41]). In general, the slow releasing poly(O950-co-HBC) was unable to provide any improvement in survival regardless of the treatment cycle or drug concentration. This trend between the two ciprofloxacin variants was also reflected in morbidity metrics of body weights (**Fig. 5.6D-F**) and surface temperatures (**Fig. 5.6G-I**) as a function of dosing schedule. For example, body weights of animals that were treated with PBS or poly(O950-co-HBC) dropped approx. 20% over 4 days after infection (**Fig. 5.6D-F**), while for poly(O950-co-CPM), animals dosed with cycle II or III recovered (**Fig. 5.6E**) or retained (**Fig. 5.6F**) their body weights, respectively. The therapeutic treatment cycle (III) provided enhanced survival of mice treated with the CPM copolymer, as suggested by the high survival rate (**Fig. 5.6C**), associated body weights (**Fig. 5.6F**), surface temperatures (**Fig. 5.6I**), and overall health scores based on appearance/behavior (**Fig. 5.7**).

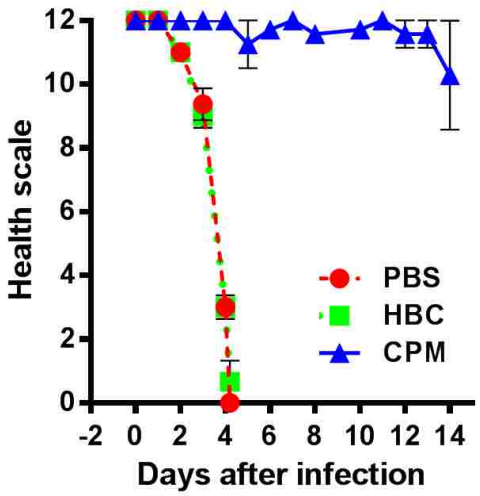

FIGURE 5.7. Morbidity measurements after therapeutic treatment with polymeric prodrugs of ciprofloxacin. Representative changes in health-metrics for mice administered with poly(O950-co-CPM) polymeric prodrugs (n = 6) at 40 mg/kg ciprofloxacin for the therapeutic treatment cycle (0, 1, and 2 days). The health of the mice after bacterial inoculation was evaluated by monitoring the appearance of each mice using an appearance chart a pre-determined scoring rubric. Mice with high health scores display high general activity, cleanliness, regular breathing, normal posture, and clear and open eyes. Lethargic, sickly mice have low scores associated to poor responsiveness during interaction and stimulation. Data is presented as mean ± SEM.

5.4 Discussion

Historically, clinical treatment of respiratory bacterial infections has focused on oral and IV standards of care; however, these strategies limit drug biodistribution and pharmacokinetics to the lungs.[12,16] The pulmonary route of administration offers a unique advantage in increasing drug concentrations at the site of bacterial persistence.[17] Recent advances in pulmonary drug delivery have stemmed from developing inhalable free-drug dispersions and liposomal formulations that provide improved therapy compared to oral and IV intervention strategies.[42,43] Hamblin *et al.* utilized aerosol delivery of liposomal ciprofloxacin in human clinical trials for upper respiratory infections and demonstrated increased survival rates in mice against a *F. tularensis* Schu4 strain.[40,44] Others have also demonstrated that oral ciprofloxacin does not provide prolonged treatment and protection against respiratory forms of *Francisella* infections.[45] In addition,

aerosolized un-encapsulated ciprofloxacin is rapidly absorbed within 1-2 h after administration, and consequently fails to clear pulmonary *Francisella* infections.[39,40] It is clear that new therapeutic systems are needed to better control the required PK profiles of antibiotics to effectively combat alveolar intracellular infections.

Polymeric prodrugs synthesized using polymerizable drug monomers offer an attractive alternative to traditional free-drug or liposomal delivery approaches. Higher drug weight percentages can be achieved compared to traditional polymer-drug conjugates since the steric constraints of post-synthetic conjugations are minimized. The solubility and other physical properties of antibiotics becomes only minimally important in this formulation approach because they are synthetically solubilized at the monomer and polymer synthesis stage with a wide range of compatible solvent choices. In related work with a stable drug linkage, Turos *et al*. synthesized polyacrylate nanoparticles in which a *N*-thiolated β-lactam antibiotic was covalently conjugated onto the polymer network by microemulsion polymerization of backbone (alkyllic) ester-modified acrylated antibiotic.[29] Our prodrug approach opens an array of hydrolytic, redox, and enzyme-sensitive linkers with broad release kinetic properties that were not previously as accessible for post-synthetic, aqueous conjugations. This provides a unique and new capability to rationally design Cmax, AUC to minimum inhibitory concentration (MIC) ratios, time above MIC, and other PK properties. The ability to then control the polymerization with other functional monomers provides further opportunities to incorporate targeting agents to maximize uptake in alveolar macrophages. Lastly, the synthetic nature of this drugamer platform is designed to achieve scale-up, reproducibility, and chemistry-based analytics that rapidly advance candidates to GMP manufacturing status.

The unique ability to tune the lung PK profiles and subsequent efficacy against highly lethal aerosolized *F. novicida* infections in mice has been demonstrated here. Synthesis of the polymeric prodrugs was achieved *via* the RAFT copolymerization of ciprofloxacin-functionalized methacrylate monomers and a solubilizing comonomer, polyethylene glycol methyl ether methacrylate (O950).[32] These copolymers consisted of a functionalized slow-releasing alkyllic ester ciprofloxacin (HBC) or a fast-releasing phenolic ester ciprofloxacin (CPM) to create drug-rich, soluble polymer therapeutics (**Fig. 5.1**). As suggested by toxicity screening factors such as neutrophil infiltration[46] and TNF-α concentrations in mice LTH and BALF[47], the nano-therapeutics displayed favorable safety profiles at doses relevant for *in vivo* bioactivity (40 mg/kg ciprofloxacin, **Fig. 5.2**, and 20 mg/kg ciprofloxacin**, Fig. 5.3**). Animal challenge with poly(O950-co-HBC) and poly(O950-co-CPM) demonstrated enhanced efficacy of the phenolic ester ciprofloxacin prodrug (CPM). Differences in survival rate between mice treated with poly(O950-co-CPM) and those treated with poly(O950-co-HBC) was magnified as dosing schedules were adjusted from purely prophylactic (Cycle I) to include therapeutic administrations (Cycle II) at the same drug concentration (20 mg/kg) (**Fig. 5.6B**). Importantly, doubling the dose (from 20 to 40 mg/kg ciprofloxacin) and shifting to a complete therapeutic regimen (Cycle III) did not improve the survival rate of mice treated with slow-releasing poly(O950-co-HBC) (**Fig. 5.6C**) nor those treated with endotrachaelly administered free ciprofloxacin (data not shown[41]). The poor therapeutic efficacy (n = 0/8 survival rate) of unconjugated ciprofloxacin can be correlated to the rapid clearance of the drug from the pulmonary compartment with $t_{1/2}$ of approximately 1 h (**Fig. 5.4A**). In addition, these studies demonstrate the PK/pharmacodynamics (PD) relationships underlying the efficacious $AUC_{0\text{-}24}$ and C_{max} values achieved by the fast releasing but not slow releasing drugamers (**Table 5.2**). Fluoroquinolones, such as ciprofloxacin, exhibit a concentration-

dependent killing with a prolonged post-antibiotic effect such that optimal bactericidal efficacy is associated with achieving a C_{max}/MIC of >10 and an AUC_{0-24}/MIC ratio of >125 against strains of *Francisella*.[48,49] Analysis of *in vivo* released-drug concentrations demonstrated that our slow-releasing poly(O950-co-HBC) maintains suboptimal pulmonary and blood C_{max}/MIC and AUC_{0-24}/MIC ratios (**Table 5.2**). In contrast, the fast-releasing, phenolic ester-modified ciprofloxacin prodrug appears by survival and morbidity measurements to have cured 75% of mice due to optimal PK/PD parameters (**Table 5.2**).

A combination strategy exploiting tritium radiolabeling of the copolymers with separate quantitative LC-MS analysis of polymer-released ciprofloxacin was utilized to understand variations in PK and biodistribution properties associated with the two drug-ester modified polymers. These studies suggest that polymer elimination from the lungs is correlated to the elimination and distribution of free drug to various organs. Thus, we anticipate that by enhancing pulmonary retention of our drugamers we can further improve the dosing and observed efficacy profile. Repeated aerosolization every 24 h of the macromolecular prodrug into the lungs would increase the concentration of released drug in the pulmonary space. To this extent, the fast-releasing CPM prodrug may generate more effective levels of drug in the lung compared to the slow-releasing HBC prodrug where the levels of released drug at 24 h are consistently low enough with repeated dosing that we do not observe antibacterial activity.

Respiratory infections of *F. tularensis* and other CDC classified Tier 1 pathogens, such as *Burkholderia thailandensis*, require immediate medical intervention with preferred localized and sustained pulmonary administration of drugs. Inhalable polymeric prodrugs utilizing hydrolysable drug monomers represent a creative approach for pulmonary drug delivery. Accordingly, drug linkage chemistry is an important parameter for achieving antibiotic efficacy, and can also influence the PK and biodistribution properties of the resulting constructs. Improved survival rates from animals therapeutically treated with the

faster-releasing ciprofloxacin polymer conjugate serve as an engineering guideline for developing future iterations of these polymeric prodrugs for clinical application. The expected distribution of released ciprofloxacin from the lung back into the bloodstream and subsequently to other organs may be advantageous in infective settings where the bacterial infection rapidly disseminates from the lung to the blood and other organs. Additionally, *Francisella* is an intracellular pathogen that selectively resides and replicates within alveolar macrophages.[7] Targeting drugs to particular cell types such as the alveolar macrophage may further enhance and extend the residence times of the inhaled antibiotics, which would be beneficial in improving PK/PD parameters (e.g. C_{max} and AUC/MIC ratios). Moreover, these targeted delivery systems could provide dose sparing properties and minimize drug resistance by focusing intracellular drug dosing at key bacterial reservoir sites. Our group and others have previously shown alveolar macrophage targeting through the use of mannosylated polymers. [50-52] These targeting approaches may provide future routes for improving pharmaceutical properties of these polymeric prodrug therapeutics for alveolar intracellular infection treatments. The preliminary studies shown in this paper not only demonstrate the promising clinical utility of RAFT polymerized ciprofloxacin prodrugs, but also help to address key barriers in pulmonary drug delivery using an inhalable prodrug system.

5.5 Acknowledgements

We thank Dr. David Danley (Department of Bioengineering, University of Washington, Seattle WA) for his assistance with the assessment of the preliminary pharmacokinetic and biodistribution studies of the copolymers. **Funding:** This work was funded by the Defense Threat Reduction Agency (Grant #HDTRA1-13-1-0047).

5.6 REFERENCES

1. Gagneux, S.; Long, C.D.; Small, P.M.; Van, T.; Schoolnik, G.K.; Bohannan, B.J.M. The competitive cost of antibiotic resistance in Mycobacterium tuberculosis. *Science* **2006**, *312*, 1944-1946.

2. Cosgrove, S.E. The relationship between antimicrobial resistance and patient outcomes: mortality, length of hospital stay, and health care costs. *Clin. Infect. Dis.* **2006**, *42*, S82-89.
3. Eliopoulos, G.E. The impact of antimicrobial resistance on health and economic outcomes. *Clin. Infect. Dis.* **2003**, *36*, 1433-1437.
4. Oyston, P.C.F.; Sjöstedt, A.; Titball, R.W. Tularaemia: bioterrorism defense renews interest in Francisella tularensis. *Nat. Rev. Microbiol*. **2004**, ***2***, 967-978.
5. Karpoff, S.P.; Antononoff, N.I. The spread of tularemia through water as a new factor in its epidemiology. *J. Bacteriol.* **1936**, *32*, 243-258.
6. Dennis, D.T.; Inglesby, T.V.; Henderson, D.A.; Bartlett, J.G.; Ascher, M.S.; Eitzen, E.; et al. Tularemia as a biological weapon – medical and public health management. *JAMA.* **2001**, ***285***, 2763-2773.
7. Golovliov, I.; Baranov, V.; Krocova, Z.; Kovarova, H.; Sjöstedt, A. An attenuated strain of the facultative intracellular bacterium Francisella tularensis can escape the phagosome of monocytic cells. *Infect. Immun.* **2003**, *71*, 5940-5950.
8. Hopla, C.E. The ecology of tularemia. *Adv. Vet. Sci. Comp. Med.* **1974**, *18*, 25-53.
9. Ellis, J.; Oyston, P.C.F.; Green, M.; Titball, R.W. Tularemia. *Clin. Microbiol. Rev.* **2002**, *15*, 631-646.
10. Tarnvik, A. Protective immunity to Francisella tularensis. *Rev. of Infect. Dis.* **1989**, *2*, 440-451.
11. Anthony, L.S.; Morrissey, P.J.; Nano, F.E. Growth inhibition of Francisella tularensis live vaccine strain by IFN-gamma-activated macrophages is mediated by reactive nitrogen intermediates derived from L-arginine metabolism. *J. Immunol.* **1992**, *148*, 1829-1834.
12. Maurin, M.; Mersali, N.F.; Raoult, D. Bactericidal activities of antibiotics against intracellular Francisella tularensis. *Antimicrob. Agents Chemother.* **2000**, *44*, 3428-343.
13. Syrjala, H.; Schildit, R.; Raisainen, S. In vitro susceptibility of Francisella tularensis to fluoroquinolones and treatment of tularemia with norfloxacin and ciprofloxacin. *Eur. J. Clin. Microbiol.* **1991**, *10*, 68-70.
14. Johansson, A.; Berglund, L.; Gothefors, L.; Sjöstedt, A.; Tarnvik, A. Ciprofloxacin for treatment of tularemia in children. *Pediatr. Infect. Dis. J.* **2000**, *19*, 449-453.
15. Tarnvik, A.; Berglund, L. Tularaemia. *Eur. Respir. J.* **2003**, *21*, 361-373.
16. Labiris, N.R.; Dolovich, M.B. Pulmonary drug delivery – part I: physiological factors affecting therapeutic effectiveness of aerosolized medications. *J. Clin. Pharmacol.* **2003**, *56*, 588-599.
17. Gelperina, S.; Kisich, K.; Iseman, M.D.; Heifets, L. The potential advantages of nanoparticle drug delivery systems in chemotherapy of tuberculosis. *Am. J. Resp. Crit. Care*. **2005**, *172*, 1487-1490.
18. O'Sullivan, B.P.; Yasothan, U.; Kirkpatrick, P. Inhaled aztreonam. *Nat. Rev. Drug Discov.* **2010**, *9*, 357-358.
19. Pilcer, G.; Amighi, K. Formulation strategy and use of excipients in pulmonary drug delivery. *Int. J. Pharm.* **2010**, 392, 1-19.
20. Cook, R.O.; Pannu, R.K.; Kellaway, I.W. Novel sustained release microspheres for pulmonary drug delivery. *J. Control. Release.* **2005**, *104*, 79-90.
21. Allen, T.M.; Cullis, P.R. Liposomal drug delivery systems: from concept to clinical applications. *Adv. Drug Deliver. Rev.* **2013**, *65*, 36-48.
22. Sharma, A.; Sharma, U.S. Liposomes in drug delivery: progress and limitations. *Int. J. Pharm.* **1997**, *154*, 123-140.
23. Wong, J.P.; Yang, H.; Blasetti, K.L.; Schnell, G.; Conley, J.; Schofield, L.N. Liposome delivery of ciprofloxacin against intracellular Francisella tularensis infection. *J. Control. Release.* **2003**, *92*, 265-273.

24. Labiris, N.R.; Dolovich, M.B. Pulmonary drug delivery – part II: the role of inhalant delivery devices and drug formulations in therapeutic effectiveness of aerosolized medications. *Brit. J. Clin. Pharmaco.* **2003**, *56*, 600-612.
25. Cho, S.H.; Kim, K.S.; Kang, J.K. Antitumor activities of poly(methacryloly-D-glucosamine) prodrugs. *Korea Polym. J.* **1998**, *6*, 188-192.
26. Kryger, M.B.L.; Smith, A.A.; Wohl, B.M.; Zelikin, A.N. Macromolecular prodrugs for controlled delivery of ribavirin. *Macromol. Biosci.* **2014**, *14*, 173-185.
27. Leonard, J.K.; Turek, D.; Sloan, K.B.; Wagener, K.B. Polyethylene prodrugs using precisely placed pharmaceutical agents. *Macromol. Chem. Phys.* **2010**, *211*, 154-165.
28. Zuwala, K.; Smith, A.A.A.; Postma, A.; Ruiz-Sanchis, C.G.; Melchjorsen, J.; Tolstrup, M.; et al. Polymers fight HIV: potent (pro)drugs identified through parallel automated synthesis. *Adv. Healthcare Mater.* **2015**, *4*, 46-50.
29. Turos, E.; Shim, J.Y.; Wang, Y.; Greenhalgh, K.; Reddy, G.S.K.; Dickey, S.; et al. Antibiotic-conjugated polyacrylate nanoparticles: new opportunities for development of anti-MRSA agents. *Bioorg. Med. Chem. Lett.* **2007**, *17*, 53-56.
30. Smith, A.A.A.; Zuwala, K.; Kryger, M.B.L.; Wohl, B.M.; Guerrero-Sanchez, C.; Tolstrup, M.; et al. Macromolecular prodrugs of ribavirin: towards a treatment of co-infection with HIV and HCV. *Chem. Sci.* **2015**, *6*, 264-269.
31. Son, H.N.; Srinivasan, S.; Yhee, J.Y.; Das, D.; Daugherty, B.K.; Berguig, G.Y.; et al. Chemotherapeutic copolymers prepared via the RAFT polymerization of prodrug monomers. *Polym. Chem.* **2016**, *7*, 4494-4505.
32. Das, D.; Srinivasan, S.; Kelly, A.M.; Chiu, D.Y.; Daugherty, B.K.; Ratner, D.M.; et al. RAFT polymerization of Ciprofloxacin prodrug monomers for the controlled intracellular delivery of antibiotics. *Polym. Chem.* **2016**, *7*, 826-837.
33. Yuan, F.; Quan, L.; Cui, L.; Goldring, S.T.; Wang, D. Development of macromomlecular prodrug for rheumatoid arthritis. *Adv. Drug. Deliv. Rev.* **2013, *64***, 1205-1219.
34. Yuan, F.; Nelson, R.K.; Tabor, D.E.; Zhang, Y.; Akhter, M.P.; Gould, K.A.; Wang, D. Dexamethasone prodrug treatment prevents nephritis in lupus prone (NZB x NZW)F1 mice without causing systemic side effects. *Arthritis Rheumatol.* **2012**, *64*, 4029-4039.
35. Keddie, D.J. A guide to the synthesis of block copolymers using reversible-addition fragmentation chain transfer (RAFT) polymerization. *Chem. Soc. Rev.* **2014**, *43*, 496-505.
36. Kingry, L.C.; Peterson, J.M. Comparative review of Francisella tularensis and Francisella novacida. *Front. Cell. Infect. Microbiol.* **2014**, *4*, 1-12.
37. Kieffer, T.L.; Cowley, S.; Nano, F.E.; Elkins, K.L. Francisella novicida LPS has greater immunological activity in mice than F. tularensis LPS, and contributes to F. novicida murine pathogenesis. *Microbes Infect.* **2003**, *5*, 397-403.
38. Anthony, L.S.; Burke, R.D.; Nano, F.E. Growth of Francisella spp. in rodent macrophages. *Infect. Immun.* **1991**, *59*, 3291-3296.
39. Cipolla, D.; Blanchard, J.; Gonda, I. Development of liposomal ciprofloxacin to treat lung infections. *Pharmaceutics*. **2016**, *8*, 1-31.
40. Hamblin, K.A.; Armstrong, S.J.; Barnes, K.B., Davies, C.; Wong, J.P.; Blanchard, J.D.; et al. Liposome encapsulation of ciprofloxacin improves protection against highly virulent Francisella tularensis strain schu S4. *Antimicrob. Agents Chemother.* **2014**, *58*, 3053-3059.
41. Chen, J.; Das, D.; Srinivasan, S.; Son, H.; Lee, Brian.; Radella, F.; et. al. Glycan targeted polymeric antibiotic prodrugs for alveolar macrophage infections. *Unpublished work* (authors granted permission).

42. Conley, J.; Yang, H.M.; Wilson, T.; Blasetti, K.; DiNinno, V.; Schnell, G.; et al. Aerosol delivery of liposome-encapsulated ciprofloxacin: aerosol characterization and efficacy against Francisella tularensis infection in mice. *Antimicrob. Agents Chemother.* **1995**, *39*, 2104-2111 (1995).
43. Norville, I.H.; Hatch, G.J.; Bewley, K.R.; Atkinson, D.J.; Hamblin, K.A.; Blanchard, J.D.; et al. Efficacy of liposome-encapsulated ciprofloxacin in a murine model of Q fever. *Antimicrob. Agents Chemother.* **2014**, *58*, 5510-5518.
44. Hamblin, K.A.; Wong, J.P.; Blanchard, J.D.; Atkins, H.S. The potential of liposome-encapsulated ciprofloxacin as a tularemia therapy. *Front. Cell. Infect. Microbiol.* **2014**, *4*, 26-30.
45. Steward, J.; Piercy T.; Lever, M.S.; Simpson, A.J.H.; Brooks, T.J.G. Treatment of murine pneumonic *Francisella tularensis* infection with gatifloxacin, moxifloxacin or ciprofloxacin. *Int. J. Antimicrob. Agents.* **2006**, *27*, 439-443.
46. Izbicki, G.; Segel, M.J.; Christensen, T.G.; Conner, M.W.; Breuer, R. Time course of bleomycin-induced lung fibrosis. *Int. J. Exp. Path.* **2002**, *83*, 111-119.
47. Khanh, L.N.P.; Channabasappa, S.; Hossain, M., Liu, L.; Singh, B. Leukocyte-specific protein 1 regulates neutrophil recruitment in acute lung inflammation. *Am. J. Physiol. Lung Cell Mol. Physiol.* **2015**, *309*, 995-1008.
48. Craig W.A. Pharmacokinetic/pharmacodynamic parameters: rationale for antibacterial dosing of mice and men. *Clin. Infect. Dis.* **1998**, *26*, 1-10.
49. Peterson, J.W.; Moen, S.T.; Healy, D.; Pawlik, J.E.; Taormina, J.; Hardcastle J.; et al. Protection afforded by fluoroquinlones in animal models of respiratory infection with Bacillus anthracis, Yersinia pestis, and Francisella tularensis. *Open Microbiol. J.* **2010**, *4*, 34-46.
50. Chen, J.; Son, H.; Hill, J.J.; Srinivasan, S.; Su, F.; Stayton, P.S.; et al. Nanostructured glycopolymer augmented liposomes to elucidate carbohydrate-mediated targeting. *Nanomed. Nanotech. Biol. Med.* **2016**, *12*, 2031-2041.
51. Chono, S.; Tanino, T.; Seki, T.; Morimoto, K. Efficient drug targeting to rat alveolar macrophages by pulmonary administration of ciprofloxacin incorporated into mannosylated liposomes for treatment of respiratory intracellular parasitic infections. *J. Control. Release.* **2008**, *127*, 50-58.
52. Nafee, N.; Husari, A.; Maurer, C.K.; Lu, C.; Rossi, C.; Steinbach, A.; Hartmann R.W.; Lehr, C.M.; Schneider, M. Antibiotic-free nanotherapeutics: ultra-small, mucus penetrating solid lipid nanoparticles enhance the pulmonary delivery and anti-virulence efficacy of novel quorum sensing inhibitors. *J. Control. Release.* **2014**, *192*, 131-140.

CHAPTER 6. Radiant star nanoparticle prodrugs for the treatment of intracellular alveolar infections*

*Provided as a submitted publication: Das D., Srinivasan S., Brown F.D., Anika., Anika Prof., Postma A., Ratner D.M., Stayton P.S., Convertine A.J. *Polymer Chemistry.* Submitted 2017.

ABSTRACT

Radiant star nanoparticle (RSN) prodrugs were synthesized in a two-step process by first homopolymerizing RAFT transmers followed by copolymerization from the hyperbranched polymer core. Two trithiocarbonate-based transmers were synthesized containing either alkyl ester or acetal groups linking the polymerizable methacrylate group to the chain transfer agent (CTA). RAFT polymerization from the homopolymerized transmer cores yielded RSNs with linear polymer chains connected to hyperbranched cores. Hydrolysis studies conducted over a period of 30 days at 37 ^{o}C in acetate buffer showed that RSNs prepared from alkyl ester linked cores remained stable while acetal linked cores exhibited a progressive degradation into linear polymers over the same period. Macrophage targeting RSN prodrugs containing the antibiotic ciprofloxacin and mannose targeting residues were synthesized directly via RAFT polymerization of the prodrug and mannose monomers. Hydrolysis studies conducted in human serum showed that the RSNs released the covalently linked ciprofloxacin significantly faster than diblock copolymer micelles but moderately slower than soluble copolymers with comparable compositions. Flow cytometry showed substantially higher macrophage binding by the mannose-targeted RSNs while in vivo biocompatibility experiments showed no differences relative to phosphate buffer treated negative controls.

6.1 Introduction

Polymeric prodrugs have attracted considerable attention as a potential strategy for overcoming the limitations typically associated with physically encapsulating drug delivery systems.[1-4] Polymeric prodrugs consist of therapeutic agents that have been covalently conjugated to a macromolecular scaffold via a hydrolytic or enzymatically degradable linkage. This strategy has been shown to substantially increase the solubility and stability of the parent drug while also enhancing drug circulation half-lives and reducing immunogenicity.[5-8] An attractive route for the synthesis of polymeric prodrugs is the direct reversible deactivation radical polymerization (RDRP) of therapeutic agents that have been reversibly modified with suitable vinyl functionality.[9-20] These polymerizable prodrug monomers (PPMs) allow for the facile incorporation of drug moieties into the final polymer at predetermined ratios without the need for additional conjugation and purification steps.

Recently, we reported the synthesis of polymeric prodrugs using PPMs based on derivatives of the antibiotic ciprofloxacin.[11] Drug release studies conducted in human serum showed that the phenyl ester-linked antibiotic was cleaved from the polymer scaffold at significantly higher rates relative to the aliphatic-linked drug. These differences in the relative antibiotic release rates were found to strongly influence the antimicrobial activity of the polymeric prodrug with ciprofloxacin linked via phenyl esters showing significantly lower minimum inhibitory concentrations than the aliphatic ester linked drug. Subsequent animal studies have shown that that these ciprofloxacin-based polymeric prodrugs provided high cure efficiencies in a completely lethal F.t. novacida pulmonary mouse challenge models, while mice treated with free ciprofloxacin were all dead within 6 days of exposure to the bacteria.[21]

Diblock copolymer-based prodrugs that self-assemble under physiological conditions to form nanoparticles are desirable from a drug delivery perspective as they can contain the covalently linked prodrugs at a significant fraction of their total mass. These systems also typically show longer in vivo circulation times relative to analogous linear polymers and can provide preferential uptake in some cell populations, such as macrophages, because of their size and ability to display multivalent receptor-specific targeting ligands. [22] Despite these advantages, diblock copolymer based nanoparticles, where the covalently linked prodrugs are localized in the hydrophobic core, typically show low rates of drug release.[11,13] Additionally, self-assembled structures such as micelles and liposomes can interact with serum proteins in vivo resulting in partial or complete disassociation of the constituent polymer or lipids. [23] Interaction of these structures with serum proteins can also cause them to be eliminated by the mononuclear phagocytic system or, in the case of encapsulation-based drug delivery system, result in extraction of the physically bound drugs. [24]

The incorporation of PPMs into advanced polymer nanostructures has the potential to provide further enhancements in therapeutic activity while substantially reducing the cost and complexity of preparing multifunctional drug delivery systems.[2526] To date a variety of sophisticated polymeric architectures have been prepared by RAFT polymerization methodology including stars, brushes, brushed-brushes, and bottlebrushes.[27-29] Hyperbranched polymers have also been investigated for drug delivery applications. Hyperbranched polymers can be conveniently prepared by nitroxide-mediated polymerization (NMP) and atom transfer radical polymerization (ATRP) via the use of vinyl-functionalized initiators (inimers) or by RAFT using vinyl-functionalized CTAs (transmers).

Hyperbranched polymers synthesized with inimers/transmers typically have larger molar mass dispersities; however, their constituent segments are still somewhat controlled. In this approach the degree of branching can be manipulated by simple adjustment of the inimer/transmer to monomer ratio and overall monomer conversion. For example, transmers have been employed to prepare architecturally distinct antigen carriers with pH-responsive endosomal-releasing segments.[30] In these studies, dendritically branched copolymers were synthesized using a methacrylate-functionalized RAFT CTA. Antigen delivery with the hyperbranched and cross-linked polymer architecture enhanced in vitro MHC-I antigen presentation relative to free antigen, whereas the linear construct did not have a discernible effect.

To date there have been relatively few reports detailing the homopolymerization of transmers.[3132] Homopolymerization of transmers using thermal initiators generally yield hyperbranched polymers with relatively low molecular molecular weights.[333435] In contrast, concurrent ATRP/RAFT polymerization of transmers have been shown to yield hyperbranched polymers over 500 kDa.[36] Unimolecular hyperstar polymer for siRNA delivery have also been synthesized by homopolymerization of ATRP inimers in microemulsion followed by solution polymerization of DMAEMA from the multifunctional core.[37] The resultant hyperstar-siRNA complexes showed in vitro transfection efficiencies higher than the Lipofectamine control. Herein we describe the development of mannose-targeted radiant star nanoparticle (RSN) prodrugs prepared by the copolymerization of PPMs with glycan monomers from homopolymerized transmer cores linked via ester or acetal bonds.

6.2 Experimental details

6.2.1 Materials.

Chemicals and all materials were supplied by Sigma-Aldrich unless otherwise specified. 4-((((2-Carboxyethyl)thio)carbo-nothioyl)thio)-4-cyanopentanoic acid (CCC) was kindly donated by Boron Molecular. Hydroxyethyl methacrylate (HEMA) rhodamine B methacrylate (REMA)[38] and *N,N'*-dimethylacrylamide (DMA) were distilled under reduced pressure. Spectra/Por regenerated cellulose dialysis membranes (6-8 kDa cutoff) where obtained from Fisher Scientific. 4-Cyano-4-(ethylsulfanylthiocarbonyl) sulfanylvpentanoic acid (ECT) was synthesized as described previously. [39] Sephedex G-25 prepacked PD10 columns were obtained from GE Life Sciences. 4-Cyano-4-ethylsulfanylthiocarbonylsulfanyl-4-methyl-butyric acid 2-(2-methyl-acryloyloxy)-ethyl ester (hECT)[30], mannose ethyl methacrylate (MEM) [40], and ciprofloxacin (tyramine) methacrylate (CTM) [11] were synthesized as described previously.

6.2.2 Synthesis of 4-Cyano-4-ethylsulfanylthiocarbonylsulfanyl-4-methyl-butyric acid 2-{1-[2-(2-methyl-acryloyloxy)-ethoxy]-ethoxy}-ethyl ester (aECT)

To a 50 mL round bottom flask containing a magnetic stir bar was added ECT (5.0 g, 19.0 mmol, 1.0 equivalent), 4-dimethylaminopyridine (4.64 g, 38.0 mmol, 1.2 equivalents), *N*,*N*′ dicyclohexylcarbodiimide (4.7 g, 22.8 mmol, 1.2 equivalents, and 28 mL methylene chloride. To the solution was then added ethyleneglycol vinyl ether (4.01 g, 22.8 mmol, 1.2 equivalents). The round bottom flask was then capped with a rubber septa and allowed to react over ice for 1 hour and then at room temperature overnight. The solution was then transferred to a separation funnel and was 5 times with saturated sodium bicarbonate solution. The organic phase was then collected, dried over sodium sulfate, filtered through a plug of cotton, and then isolated via rotary evaporation. The product was then used for the synthesis of aECT without further purification. To a 10 mL round bottom flask was added EGVE-ECT (0.5 g, 1.5 mmol), HEMA (0.195 g, 1.5

mmol), TFA (50 μL, 653 μmol), and methylene chloride 1.0 mL. The reaction was then sealed with a septa and allowed to react overnight. The product was then isolated via silica gel column chromatography using an eluent consisting of ethyl acetate/hexanes (75:25) with 1 % triethylamine. ^{1}H NMR (500 MHz, benzene-d6, ppm) δ = 6.16 (1H, singlet, vinyl), 5.24 (1H, vinyl), 4.52 (1H, quartet, acetal), 4.19 (2H, triplet, ester), 4.08 (2H, triplet, ester), 3.28-3.56 (4H, multiplet, $OCH_2CHCH_3OCH_2$), 2.79 (2H, quartet, SCH_2), 2.0-2.4 (4H, multiplet, $C(CH_3)(CN)CH_2CH_2$), 1.85 (3H, singlet, vinyl-methyl), 1.32(3H, singlet, $C(CN)CH_3$), 1.13 (3H, doublet, acetal-methyl), and 0.82 (3H, triplet, SCH_2CH_3) (for the labeled ^{1}H NMR spectrum see supporting information). ^{13}C NMR (125 MHz, benzene-d6, ppm) δ = 216.9, 170.8, 136.6, 125.1, 118.7, 99.3, 63.9, 63.7, 62.6, 62.3, 33.8, 31.0, 29.5, 24.1, 19.2, 18.1, 12,2.

6.2.3 Synthesis of poly(hECT) and poly(aECT)

To a 5 mL conical bottom flask was added either hECT (mg, mmol) or aECT (mg, mmol), ABCVA (mg, mmol), and 4 mL of anhydrous DMSO. The flask was then sealed with a rubber septa and then purged with nitrogen for 30 minutes. The solution was then transferred to a preheated oil bath at 70 ºC and allowed to polymerize for 18 h. The polymers were then isolated by the polymerization solution to 45 mL of diethyl ether in 50 ml conical tubes. After vortexing the solutions were centrifuged at 4200 rpm for 5 minutes. After this time the ether solution was decanted and yellow polymer oil was diluted 1 to 1 with acetone and reprecipitated into ether as described above (x6).

6.2.4 Synthesis of DMA RSNs from poly(hECT) and poly(aECT)

Polymerization of DMA was conducted in DMSO in the presence of either poly(hECT) or poly(aECT) and ABCVA. The initial molar feed percentages of the Dt-SMA and O950 monomers were both 50 %. The $[M]_o$:$[CTA]_o$:$[I]_o$) was 200:1:0.025 at an initial monomer concentration of 25 wt. %. To a 10 mL conical bottom flask was added poly(hECT) (20 mg, 53 mmol) or poly(aECT) (25 mg, 53 mmol), DMA (1.06 g, 10.7 mmol), ABCVA (0.373 mg, 1.3 mmol) and 3.17 mL DMSO. The polymerization solutions were then septa sealed and then purged with nitrogen for 30 minutes. After this time, the polymerization solution was transferred to a preheated oil bath at 70 ^oC and allowed to polymerize for 4 hours. The copolymer was isolated by adding the polymerization solution to 45 mL of diethyl ether in 50 ml conical tubes. After vortexing the solutions were centrifuged at 4200 rpm for 5 minutes. After this time the clear ether solution was decanted and yellow polymer oil was diluted 1 to 1 with acetone and reprecipitated into ether as described above (x6).

6.2.5 Kinetic evaluation of the RAFT polymerization of DMA from poly(hECT)

The initial monomer ($[M]_o$) to CTA equivalents to initiator ($[I]_o$) ratio was 350:1:0.025 respectively. Individual polymerization solutions were transferred to a septa-sealed vial and purged with nitrogen for 30 minutes. After this time, the polymerization vials were transferred to a preheated oil bath at 90 ^oC and allowed to polymerize for the prescribed time period. In order to determine monomer conversion 50 L of the polymerization solutions were first diluted into 900 L of $CDCl_3$. The molar fraction of DMA converted to polymer was then determined by comparison of the total vinyl resonances (3H) (A) between 5.0-6.5 ppm to the total backbone resonances between 0.5-1.5 ppm (B) using the equation: % DMA conversion = [(A+B)-(A)]/(A+B)]*100.

6.2.6 Synthesis of poly(mannose-co-CTM) RSN from poly(hECT)

Copolymerization of MEM and CTM from poly(hECT) was conducted with an initial monomer $[M]_o$:$[CTA]_o$:$[I]_o$ ratio was 100:1:0.05 at an initial overall monomer concentration of 20 % m/v. To a 5 mL conical bottom flask was added poly(hECT) (3.06 mg, 8.15 μmol), MEM (0.2 g, 0.684 mmol), CTM (0.1 g, 0.131 mmol), REMA (7.75 mg, 13.1 μmol), V70 (0.125 mg, 0.408 μmol) as 100 μL of 1.25 mg mL^{-1} solution in dioxane, and 1.2 mL of DMSO. The polymerization solution was then septa-sealed purged with nitrogen for 30 minutes. After this time, the polymerization vials were transferred to a preheated oil bath at 30 ^oC and allowed to polymerize for 18 hours. After this time the polymerization solution was transferred to a solution to 45 mL of diethyl ether in 50 ml conical tubes. After vortexing the solution was centrifuged at 4200 rpm for 5 minutes. The ether solution was decanted and yellow polymer oil was diluted to a final volume of 25 mL in 0 .5 M phosphate buffer pH 7.4. The aqueous solution was then dialyzed against deionized water at 5 ^oC using spectra/Por regenerated cellulose dialysis membranes (6-8 kDa cutoff) and then isolated by lyophilisation. The lyophilized polymer was then redisolved in deionized water and then purified by double Sephedex G-25 prepacked PD10 columns according to the manufactures instructions.

6.2.7 Synthesis of poly(DMA-co-CTM RSN from poly(hECT)

Copolymerization of DMA and CTM from poly(hECT) was conducted with an initial monomer $[M]_o$:$[CTA]_o$:$[I]_o$ ratio was 100:1:0.05 at an initial overall monomer concentration of 20 % m/v. To a 5 mL conical bottom flask was added poly(hECT) (8.06 mg, 21.5 μmol), DMA (0.2 g, 2.02 mmol), CTM (0.1 g, 0.131 mmol), REMA (7.75 mg, 13.1 μmol), V70 (0.331 mg, 1.07 μmol) as 100 μL of 3.31 mg mL^{-1} solution in dioxane, and 1.2 mL of DMSO. The polymerization

solution was then septa-sealed purged with nitrogen for 30 minutes. After this time, the polymerization vials were transferred to a preheated oil bath at 30 ^{o}C and allowed to polymerize for 18 hours. After this time the polymerization solution was transferred to a solution to 45 mL of diethyl ether in 50 ml conical tubes. After vortexing the solution was centrifuged at 4200 rpm for 5 minutes. The ether solution was decanted and yellow polymer oil was diluted to a final volume of 25 mL in 0 .5 M phosphate buffer pH 7.4. The aqueous solution was then dialyzed against deionized water at 5 ^{o}C using spectra/Por regenerated cellulose dialysis membranes (6-8 kDa cutoff) and then isolated by lyophilisation. The lyophilized polymer was then redisolved in deionized water and then purified by double Sephedex G-25 prepacked PD10 columns according to the manufactures instructions.

6.2.8 Synthesis of linear poly(mannose-co-CTM)

Copolymerization of MEM and CTM in the presence of the trithiocarbonate-based RAFT agent CCC was conducted with an initial monomer $[M]_o$:$[CTA]_o$:$[I]_o$ ratio was 100:1:0.05 at an initial overall monomer concentration of 20 % m/v. To a 5 mL conical bottom flask was added CCC (2.50 mg, 8.15 μmol), MEM (0.2 g, 0.684 mmol), CTM (0.1 g, 0.131 mmol), REMA (7.75 mg, 13.1 μmol), V70 (0.125 mg, 0.408 μmol) as 100 μL of 1.25 mg mL^{-1} solution in dioxane, and 1.2 mL of DMSO. The polymerization solution was then septa-sealed purged with nitrogen for 30 minutes. After this time, the polymerization vials were transferred to a preheated oil bath at 30 ^{o}C and allowed to polymerize for 18 hours. After this time the polymerization solution was transferred to a solution to 45 mL of diethyl ether in 50 ml conical tubes. After vortexing the solution was centrifuged at 4200 rpm for 5 minutes. The ether solution was decanted and yellow polymer oil was diluted to a final volume of 25 mL in 0 .5 M phosphate buffer pH 7.4. The aqueous

solution was then dialyzed against deionized water at 5 ^{o}C using spectra/Por regenerated cellulose dialysis membranes (6-8 kDa cutoff) and then isolated by lyophilisation. The lyophilized polymer was then redisolved in deionized water and then purified by double Sephedex G-25 prepacked PD10 columns according to the manufactures instructions.

6.2.9 Synthesis of linear poly(DMA-co-CTM)

Copolymerization of DMA and CTM in the presence of the trithiocarbonate-based RAFT agent CCC was conducted with an initial monomer $[M]_o$:$[CTA]_o$:$[I]_o$ ratio was 100:1:0.05 at an initial overall monomer concentration of 20 % m/v. To a 5 mL conical bottom flask was added CCC (6.60 mg, 21.5 μmol), DMA (0.2 g, 2.02 mmol), CTM (0.1 g, 0.131 mmol), REMA (7.75 mg, 13.1 μmol), V70 (0.331 mg, 1.07 μmol) as 100 μL of 3.31 mg mL^{-1} solution in dioxane, and 1.2 mL of DMSO. The polymerization solution was then septa-sealed purged with nitrogen for 30 minutes. After this time, the polymerization vials were transferred to a preheated oil bath at 30 ^{o}C and allowed to polymerize for 18 hours. After this time the polymerization solution was transferred to a solution to 45 mL of diethyl ether in 50 ml conical tubes. After vortexing the solution was centrifuged at 4200 rpm for 5 minutes. The ether solution was decanted and yellow polymer oil was diluted to a final volume of 25 mL in 0 .5 M phosphate buffer pH 7.4. The aqueous solution was then dialyzed against deionized water at 5 ^{o}C using spectra/Por regenerated cellulose dialysis membranes (6-8 kDa cutoff) and then isolated by lyophilisation. The lyophilized polymer was then redisolved in deionized water and then purified by double Sephedex G-25 prepacked PD10 columns according to the manufactures instructions.

6.2.10 Gel Permeation Chromatography (GPC)

Absolute molecular weights and polydisperity indices were determined using using Tosoh SEC TSK-GEL α-3000 and α-e4000 columns (Tosoh Bioscience, Montgomeryville, PA) connected in series to an Agilent 1200 Series Liquid Chromatography System (Santa Clara, CA) and Wyatt Technology miniDAWN TREOS, 3 angle MALS light scattering instrument and Optilab TrEX, refractive index detector (Santa Barbara, CA). HPLC-grade DMF containing 0.1 wt.% LiBr at 60 ^{o}C was used as the mobile phase for p(hECT), p(aECT), and poly(DMA) at a flow rate of 1 mL/min. Copolymers containing mannose were evaluated in an aqueous eluent consisting of…..

6.2.11 Dynamic Light Scattering

Particle sizes of the polymers were measured by dynamic light scattering (DLS) using a Malvern Zetasizer Nano ZS. Lyophilized polymer was dissolved phosphate buffer saline (150 mM NaCl, 20 mM phosphates, pH 7.4), at a concentration of 1 mg mL^{-1}.

6.2.12 Transmission Electron Microscopy (TEM)

A 1.0 mg mL^{-1} solution of the polymeric nanoparticles in deionized water was applied to carbon-coated copper grid for 30 min, then stained with 4% UA for 5 min and dried until analysis. The grid was stained with a 4% solution of uranyl acetate for 15 min and then dried until analysis. Transmission electron microscopy was performed on a Tecnai G2 F20, 200 kV scanning transmission electron microscope (S/TEM). The average particle size and circularity were determined using ImageJ by evaluating 100 separate nanoparticles.

6.2.13 Polymer hydrolysis studies

The hydrolytic stability of poly(DMA) RSNs polymerized from p(hECT) and p(aECT) cores was evaluated at pH 4.8 and 7.4 in 150 mM acetate and phosphate buffer respectively. Polymers were dissolved in the buffers at a concentration of 25 mg $mL^{-1}$and then incubated at 37 ^{o}C for the appropriate time period. Prior to analysis, a 200 μL aliquot was diluted into 800 μL of DMF. The sample was analyzed directly via gel permeation chromatography as described above.

6.2.14 Analysis of Cipro by high-performance liquid chromatography (HPLC)

HPLC analysis of Cipro was carried out with an Agilent 1260 Quaternary HPLC Pump, Agilent 1260 Infinity Standard Automatic Sampler, Agilent 1260 Infinity Programmable Absorbance Detector, and Agilent ChemStation software for LC system (Palo Alto, CA). Both ciprofloxacin hydrochloride and liquid Sera Human from AB blood donor were purchased and used as received. The analyte was separated at ambient temperature using a Zorbax RX-C18 (4.6 × 150 mm; 5 μm) analytical column (Agilent Technologies, CA).

The UV detector was operated at 277 nm, and the mobile phase consisted of 2% aqueous acetic acid and acetonitrile (84:16) v/v, as described elsewhere. The flow rate was set at 1.0 mL min−1 and sample injection volume at 20 μL. A stock solution of Cipro was prepared in deionized water at 10 mg mL^{-1}. Working solutions of Cipro for standard curves were diluted from stock solution using the mobile phase to the listed concentrations of 200 μg mL^{-1}, 100 μg mL^{-1}, 50 μg mL^{-1}, 25 μg mL^{-1}, 12.5 μg mL^{-1}, 6.25 μg mL^{-1}, 3.12 μg mL^{-1}, and 1.56 μg mL^{-1}. Each listed solution above was diluted with a 1:1 v/v ratio of either mobile phase:deionized water or mobile phase: human serum to create a final Cipro standards of 100 μg mL^{-1}, 50 μg mL^{-1}, 25 μg mL^{-1}, 12.5 μg mL^{-1}, 6.25 μg mL^{-1}, 3.12 μg mL^{-1}, 1.56 μg mL^{-1}, and 0.78 μg mL^{-1} for pharmaceutical and biological analysis, respectively. Both non-serum (mobile phase:deionized water) and serum

standards were subsequently treated with 50% acetonitrile (v/v) to promote protein precipitation. Serum standards were centrifuged at 12 000g for 15 minutes and supernatants were collected and filtered using a 0.45 μm low protein binding filter before HPLC analysis. Non-serum standards were analysed without the need for centrifugation. All standards were processed using a gradient HPLC elution profile, where the mobile phase transitioned to 100% acetonitrile over 15 minutes, followed by 10 minutes of column washing with acetonitrile and water and 5 minutes of equilibration with mobile phase.

6.2.15 Drug release from polymeric prodrugs

Drug release from polymeric prodrugs was carried out in serum at 37 °C at a polymer concentration of 6 mg mL−1. Sample time points were collected on a regular basis. Quantification of total ciprofloxacin in the polymeric prodrugs was measured by taking 6 mg mL^{-1} of polymer and dissolving it in 10% aq. H_2SO_4 for 48 h at 25 °C. The HPLC with a gradient elution profile was used to quantify amount of drug released using the same instrument parameters set forth for drug standards. A 1:1 dilution of serum sample to 2% aqueous acetic acid and acetonitrile (84:16) v/v was con- ducted, followed by another 1:1 dilution with acetonitrile. The resulting samples were vortexed and centrifuged at 12 000g for 15 minutes. Supernatants were collected and filtered using a 0.45 μm low protein-binding filter before running on the HPLC.

6.2.16 In vitro uptake studies

Experiments were conducted with MPI cells (passaged with 30 ng mL^{-1} murine GM-CSF) seeded at 200,000 cells/well. The cells were treated with 20 μg mL^{-1} of rhodamine labeled polymers (for 0.5 h, 2h, and 5h). To make sure equivalent fluorescence was dosed for all treatment

groups, standard curves were calculated as a function of polymer concentration. At each time point, the cells were collected, washed, and resuspended with cold PBS containing 0.2% fetal bovine serum (FBS) to remove unbound polymer. All samples were kept on ice and uptake/association was detected using the Y1 channel (rhodamine B).

Statistical analysis was performed by Student's paired t test. (*) denotes a P-value of b 0.05. (**) denotes a P-vaue of b 0.005. Error bars are reported as SDs. All samples were performed in triplicate unless noted otherwise.

6.2.17 Acute lung safety of ciprofloxacin delivery systems

In order to determine the in vivo biocompatibility of the polymeric prodrugs after pulmonary administration, the lung toxicity of endotrachaelly delivered poly(MEM-co-CTM) RSNs were evaluated using the metrics of animal weight change, tumor necrosis factor alpha (TNF-α) concentration in lung tissue homogenate (LTH) and bronchoalveolar lavage fluid (BALF), and neutrophil infiltration into the lungs. Using an endotracheal microsprayer, copolymers were dosed at 20 mg/kg once every 24 hours for three-consecutive days. The data demonstrate no statistical differences ($P \leq 0.1$) across all observed toxicity markers at either drug dose compared to phosphate buffered saline (PBS) controls.

6.3 Results and discussion

In these studies we desired to develop hydrophilic single polymer nanoparticle prodrugs that combine both the favorable uptake and circulation properties of nanoparticle-based systems with the higher drug release rates often observed for molecularly soluble polymeric prodrugs. In order to achieve this objective RAFT transmers were first homopolymerized to yield a

hyperbranched polymer core containing multiple chain transfer agents (CTAs) from which linear polymeric prodrugs could then be grown using polymerizable prodrug monomers. As shown in **Scheme 6.1**, trithiocarbonate-based transmers containing cyanovaleric acid R-groups were employed in these studies because of the ability of these CTAs to effectively control the polymerization of methacrylate monomers while also allowing relatively high $[CTA]_o/[I]_o$ ratios (e.g. 100:1) to be employed. The latter consideration is important for minimizing star-star coupling during the second polymerization step. The transmers shown in **Scheme 6.1** also contain a polymerizable methacrylate residue covalently bound to the CTA by either an alkyl ester or an acetal linkage. These linkages were hypothesized to yield hyperbranched cores that would degrade at different rates under aqueous conditions.

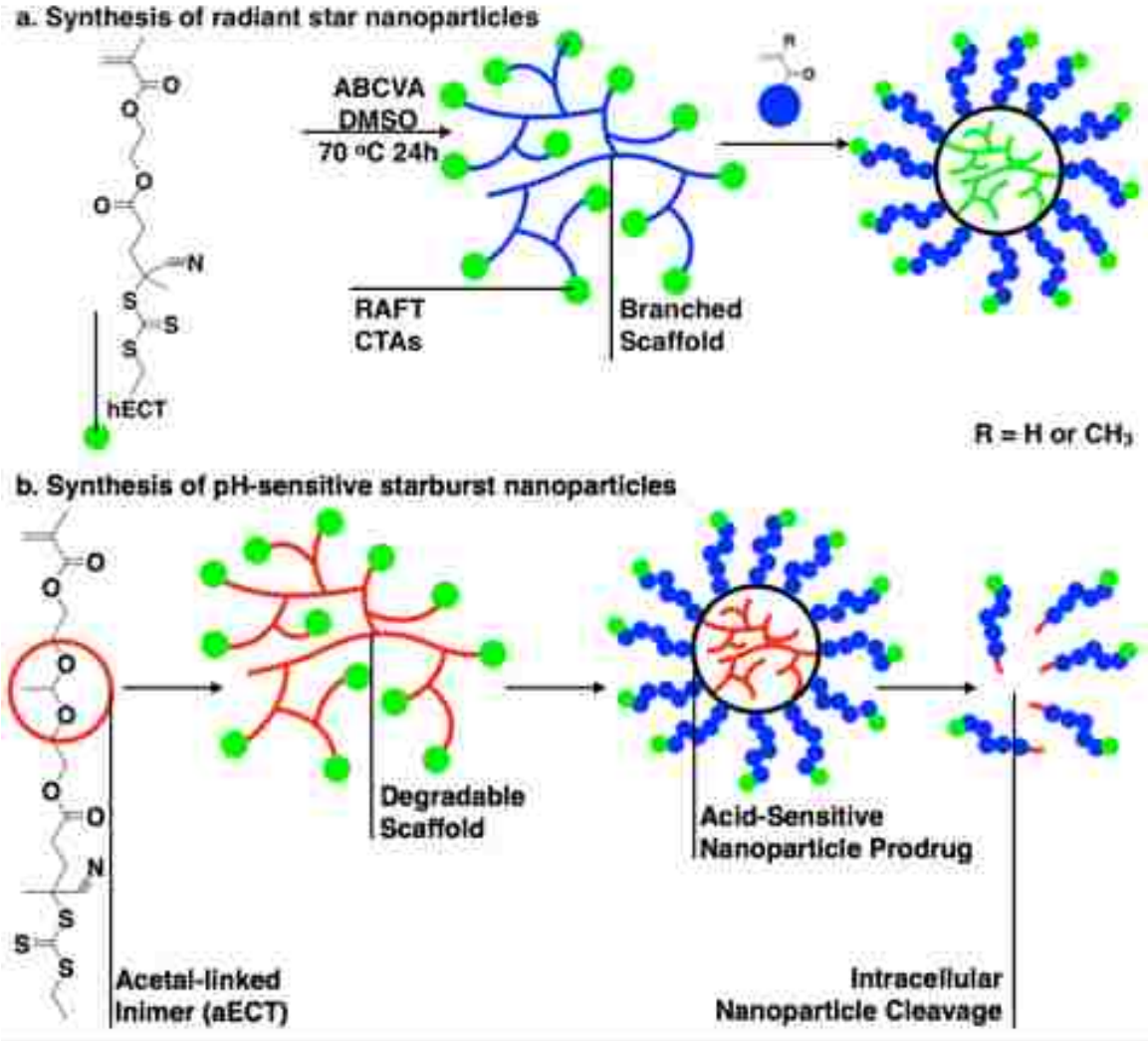

SCHEME 6.1. Overall synthetic strategy for the synthesis of radiant star nanoparticle (RSN) and starburst nanoparticle (SBN) prodrugs via RAFT polymerization from homopolymerized transmer cores.

As shown in **Fig. 6.1A**, the alkly ester-linked transmer (hECT) was conjugated to the RAFT CTA via standard carbodiimide chemistry using a DMAP catalyst as described previously. In order to synthesize the acetal inked transmer (aECT) a two step synthesis was employed where the CTA was first esterified with ethylene glycol vinyl ether which was then reacted with hydroxyethyl methacrylate in the presence of an acid catalyst to yield the desired product. Shown in **Fig. 6.2B**, is the ^{1}H NMR confirming the formation of the desired acetal-linked transmer with labeled peaks

including the characteristic acetal CH and CH_3 resonances at 1.1 and 4.5 respectively. The resultant transmers were then homopolymerized in dry DMSO at 70 ^oC for 18 h using an initial transmer to initiator ratio of 20. NMR analysis of the crude polymerization mixture indicated that these conditions led to quantitative conversion of the vinyl resonances at 6.1 and 5.2 ppm respectively (not shown). Following purification, the resultant poly(hECT) and poly(aECT) cores were then analyzed using a combination of ^1H NMR and GPC (**Fig. 62A-C**). Shown in **Fig. 6.2A,B** are the ^1H spectra for the homopolymerized transmers with the resonances labeled. Notably the peaks have broadened considerably relative to the low molecular weight precursors with the vinyl resonances and concurrent appearance of methylene and methyl resonances in the backbone region. GPC analysis of poly(hECT) and poly(aECT) (**Fig. 6.2C,D**) show molecular weight distributions that are unimodal and symmetric with molar mass dispersities around 1.30. The homo-polymerized transmers have relatively low molecular weights of 8700 Da and 9300 Da for the alkyl ester and acetal ester containing structures respectively. This corresponds to approximately 23 and 20 RAFT CTAs respectively per polymeric transmer core assuming a homogenous composition composed exclusively of the precursor transmers.

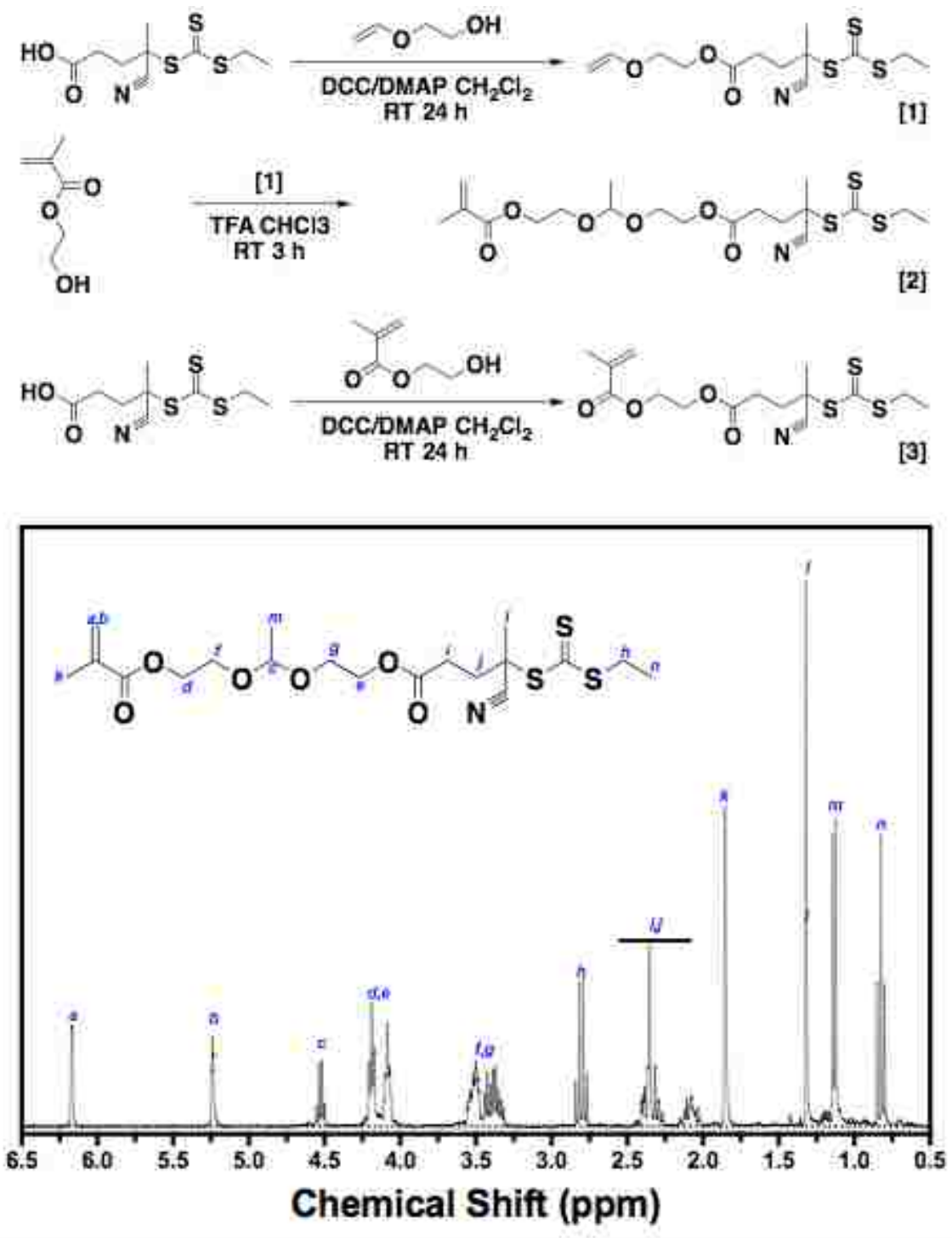

FIGURE 6.1. Fig. 1 (a) Synthetic scheme for the synthesis of alkyl ester (hECT) and acetal linked (aECT) RAFT transmers. (b) ^{1}H NMR spectrum conduct in D6 benzene for the acetal linked RAFT transmer aECT.

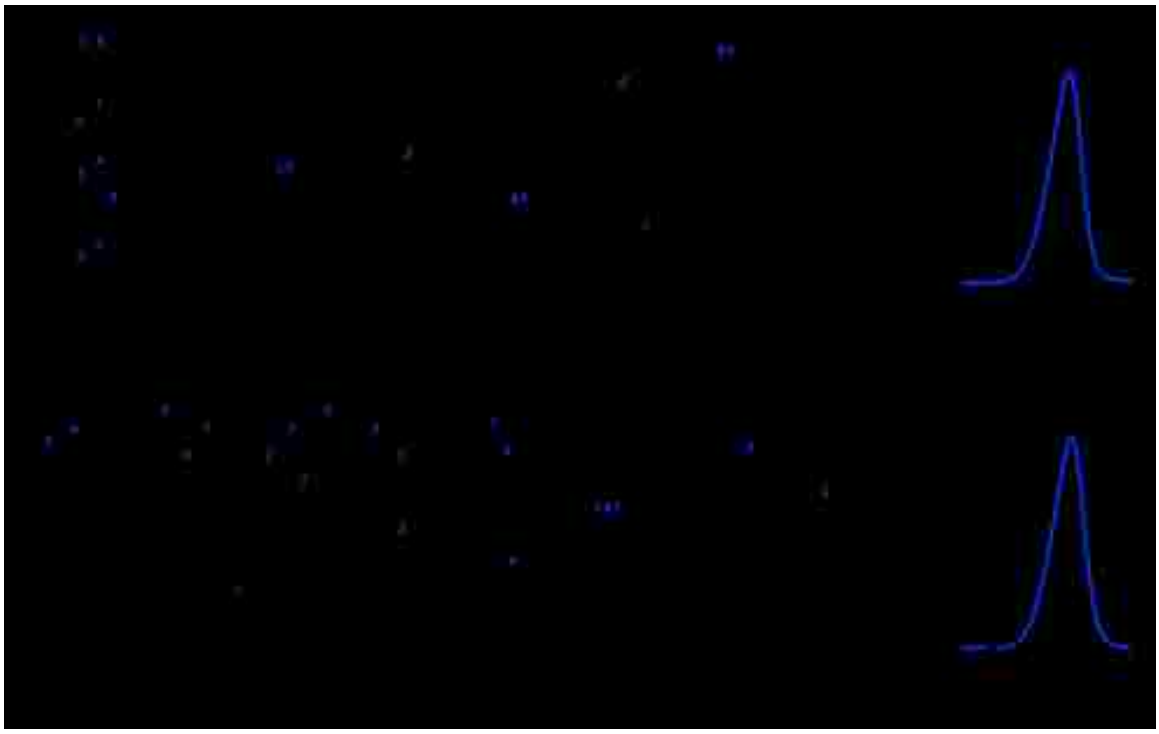

FIGURE 6.2. ^{1}H NMR and molecular weight distributions for the poly(hECT) and poly(aECT) hyperbranched transmer cores synthesized via homopolymerization of hECT and aECT.

In order to prepare nanoparticle prodrugs from the homopolymerized transmer cores we first investigated the RAFT polymerization of a range of methacrylate and acrylamide based monomers (**Fig. 6.3**). As can be seen in **Fig. 6.3A,B**, the RAFT polymerization of DMA from both transmer cores yields unimodal and symmetric molecular weight distributions that elute at much lower elution volumes. In these polymerizations a $[M]_o[CTA]_o:[I]_o$ ratio of 200:1:0.05 was targeted resulting in molecular weights and molar mass dispersities of 364 000/1.32 and 275 000/1.36 for the alkyl ester and acetal linked radiant star nanoparticles. The effect of $[M]_o/[CTA]_o$ at a fixed $[CTA]_o/[I]_o$ of 0.05 was next evaluated. As can be seen in **Fig. 6.3D**, a clean progression of molecular weights towards lower elution volumes is observed with increasing $[M]_o/[CTA]_o$ suggesting the ability to prepare RSNs with different molecular weights simply by controlling the initial reaction stoichiometry. In all cases the molecular weight distributions remained symmetric

and unimodal with moderate molar mass dispersities around 1.45. The ability to prepare methacrylate based RSNs was next evaluated by conducting RAFT polymerizations from the poly(hECT) core low molecular weight methacrylate monomers (HEMA and DMAEMA) and high molecular weight methacrylate monomers (PEGMA FW_{avg} ~ 300 and 950). As shown in **Fig. 6.3D,F**, a higher degree of control was observed for the polymerization of the smaller methacrylate monomers DMAEMA and HEMA from the polymeric transmer core. Here relatively narrow and symmetric molecular weight distributions were observed with molecular weight and molar mass dispersities of 186 300/1.39 and 401 400/1.57 respectively. In contrast, the RAFT polymerization of the sterically bulky PEGMA monomers yielded somewhat asymmetric molecular weight distributions with the presence of a high molecular weight star-star coupling peak observed for both the O300 and O950 polymerizations. Nonetheless minimal low molecular weight contamination was observed in these polymerizations suggesting that the PEGMA based RSNs might still prove to be versatile nanoparticle prodrugs despite the presence of some heterogeneity.

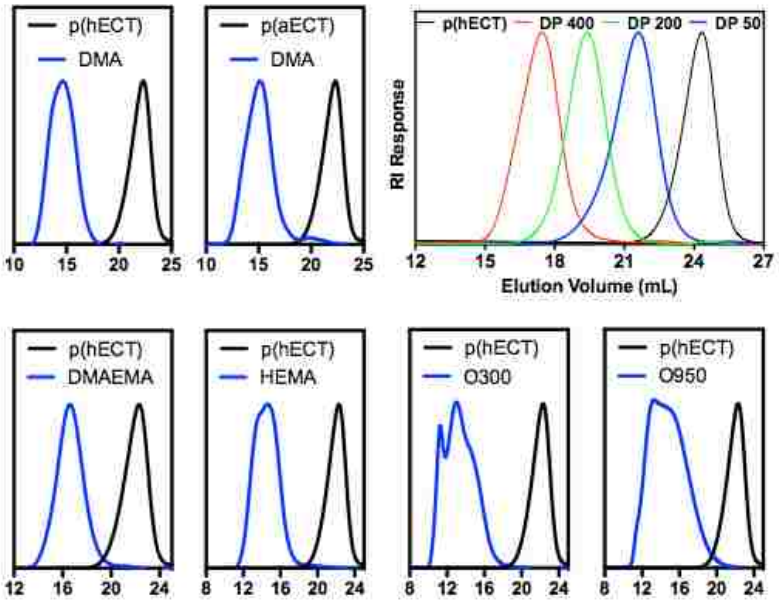

FIGURE 6.3. Molecular weight distributions for polymeric transmer cores as well as the corresponding RSN for (a) dimethyl acrylamide (DMA), (b) N,N-dimethylaminoethyl methacrylate (DMAEMA), (c) 2-hydroxyethyl methacrylate (HEMA), (d) polyethyleneglycol monomethyl ether methacrylate (FW~300 Da) (O300) and (e) polyethyleneglycol monomethyl ether methacrylate (FW~950 Da) (O950). Molecular weight and molar mass dispersity values were determined to be: poly(hECT) 8700:1.42, poly(aECT) 9300:1.43, DMA poly(hECT) 364 000:1.32, DMA poly(aECT) 275 000:1.36, DMAEMA 186 300:1.39, HEMA 401 400:1.57, O300 1 743 000:3.40, O950 3 538 000:2.30. Molecular weight distributions for poly(DMA) prepared from a poly(hECT) transmer core targeting a different degrees of polymerization. Mn/molar mass dispersity: DP 50 = 83 000:1.39, DP 200 = 155 400: 1.37, DP 400 = 525 900:1.26.

The hydrolytic stability of DMA-based RSNs derived from both the alkyl ester linked poly(hECT) and acetal poly(aECT) linked cores was evaluated. Acetals have been shown to hydrolyzed rapidly under acidic conditions such as those found in the intracellular compartment of macrophages while polymeric alkyl ester remain more stable under these conditions. Shown in **Fig. 6.4A,B**, are the GPC chromatograms for poly(DMA) polymerized from poly(hECT) and poly(aECT) cores. Here the polymers were incubated at 37 ^{o}C in 150 mM acetate buffer at pH 5.0 for the indicated time period before being diluted into DMF and analyzed via GPC. As can be seen in **Fig. 6.4A**, an overlay of the molecular weight distributions for the alkyl ester linked RSN shows no visible change between the initial polymeric nanoparticle and those incubated in buffer for 30 days. In contrast, a progressive degradation of the high molecular RSN is observed for the

acetal linked RSN over the course of the 30 day incubation period. Here the relatively broad RSN peak is seen to reduce in area with the appearance of a narrow lower molecular species that is consistent with linear polymers liberated from the central core following acetal hydrolysis. The slower rate of acetal hydrolysis observed relative to low molecular weight acetal species is hypothesized to arise from the hydrophobic environment of the central core.

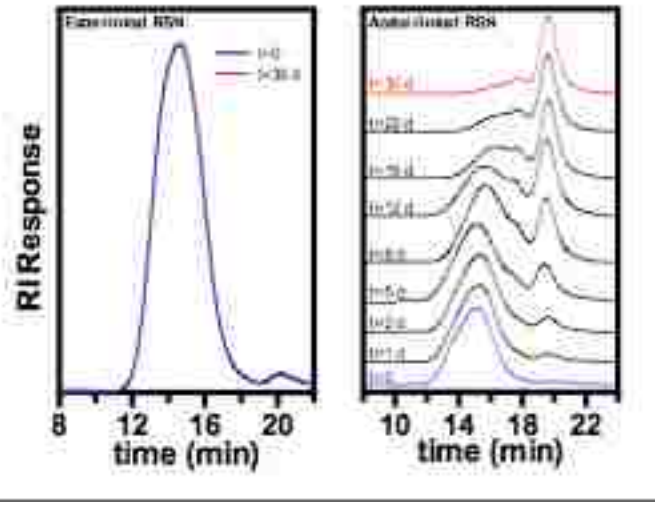

FIGURE 6.4. Molecular weight distributions for poly(DMA) polymerized from poly(hECT) and poly(aECT) transmer cores following incubation in pH 5.0 acetate buffer at 37 ºC.

Therapeutic RSN prodrugs were next synthesized, as shown in **Scheme 6.2**, by copolymerizing the ciprofloxacin prodrug monomer (CTM) with a hydrophilic mannose monomer (Man) from homopolymerized transmer cores containing either alkyl ester or acetal linkages. Phenyl ester linked prodrug polymerizable prodrug monomers were employed in these studies as we have shown previously that these species hydrolyze at significantly higher rates in human serum than the analogous alkyl ester analogue. Indeed we have recently observed high cure rates for mice treated with phenyl ester linked ciprofloxacin based polymeric prodrugs while alkyl ester

linked derivatives as well as the free ciprofloxacin controls show no protection against the completely lethal mouse model of *Francisella tularensis* infection. The mannose comonomer employed in these polymerizations functions as a biocompatible hydrophilic stabilizer while also efficiently targeting alveolar macrophages where many pathogens such as Burkholderia pseudomallei and *Francisella tularensis* are known to reside. Polymerizations were conducted with an initial mol fraction of CTM and Man of 16 % and 84 % (33 wt. % CTM) with an $[M]_o/[CTA]_o$ and $[CTA]_o/:[I]_o$ ratio of 100 and 0.05 respectively in DMSO. In order to suppress the reaction of the secondary amine present on ciprofloxacin with the polymeric chain transfer agents polymerizations were conducted at 30 ^oC. In addition to these mannose based RSNs, materials containing DMA as the hydrophilic stabilizer as well as the analgous linear copolymers were also synthesized to serve as untargeted controls (vide infra).

Shown in **Fig. 6.5A-D** are the ^1H NMR and molecular weight distributions for the poly(Man-co-CTM) and poly(DMA-co-CTM) RSNs respectively. Resonances associated with residues from CTM as well as the respective Man and DMA comonomers can be clearly observed in **Fig. 6.5A,D** respectively. Because of the complex nature of the poly(Man-co-CTM) spectrum, copolymer composition was determined by acid hydrolysis followed by reverse phase HPLC analysis of the release ciprofloxacin relative to standard curves for both materials. Based on this analysis a molar copolymer composition of 20 % CTM / 80 % Man and 19.7 % CTM / DMA 80.3 % was determined which is in relatively good agreement with the feed. These values yield RSN prodrugs with 40 wt. % CTM (17.5 % ciprofloxacin drug) and 39 wt. % CTM (17 % ciprofloxacin drug). Evaluation of the poly(Man-co-CTM) RSN via TEM (**Fig. 6.5E**) shows irregular structures that are consistent with the RSN morphology depicted in **Scheme 6.2**. TEM analysis yields RSN diameters of approximately 20-30 nm, which is close to the 24.6 nm observed via DLS.

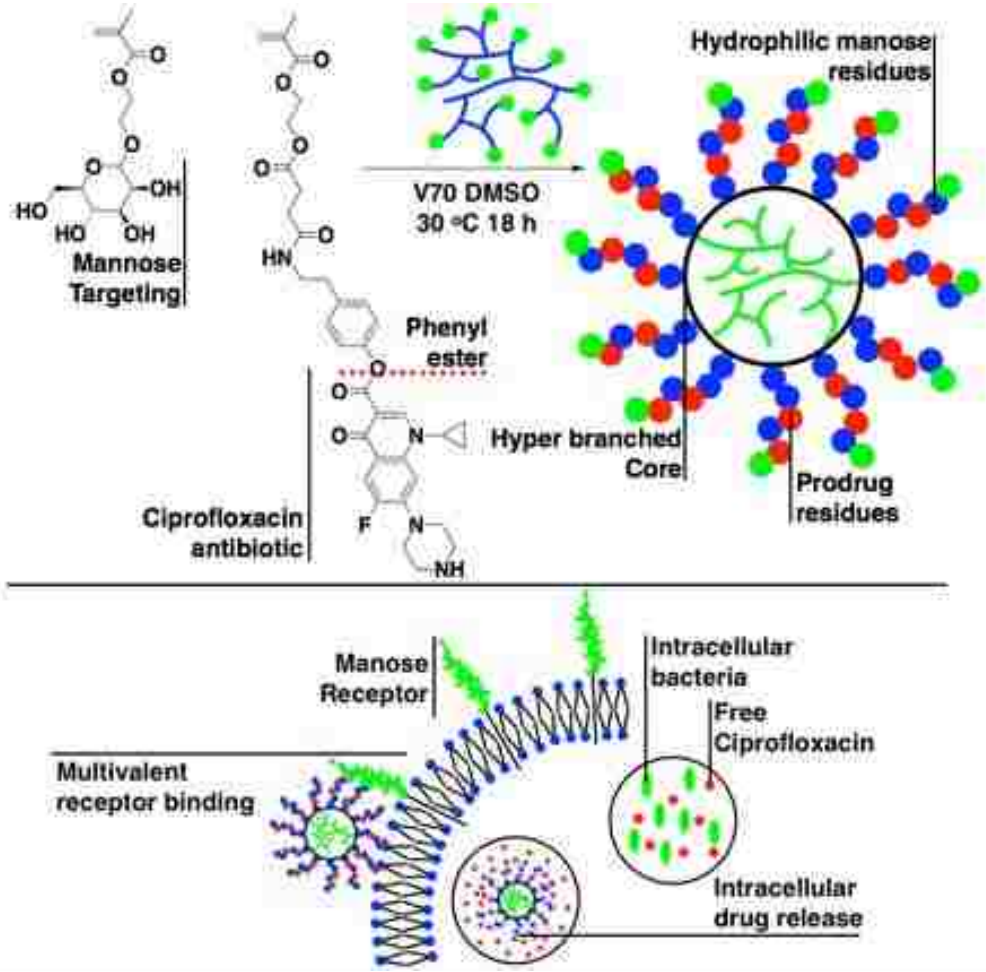

SCHEME 6.2. (a) Synthetic scheme for the preparation of mannose targeted RSNs prodrugs via direct RAFT copolymerization of glycan functionalize monomer (Man) with the phenyl ester linked ciprofloxacin monomer (CTM) from polymeric transmer cores. (b) Schematic illustration showing the mannose targeted RSN prodrug being internalized by alveolar macrophages following binding to the mannose receptor.

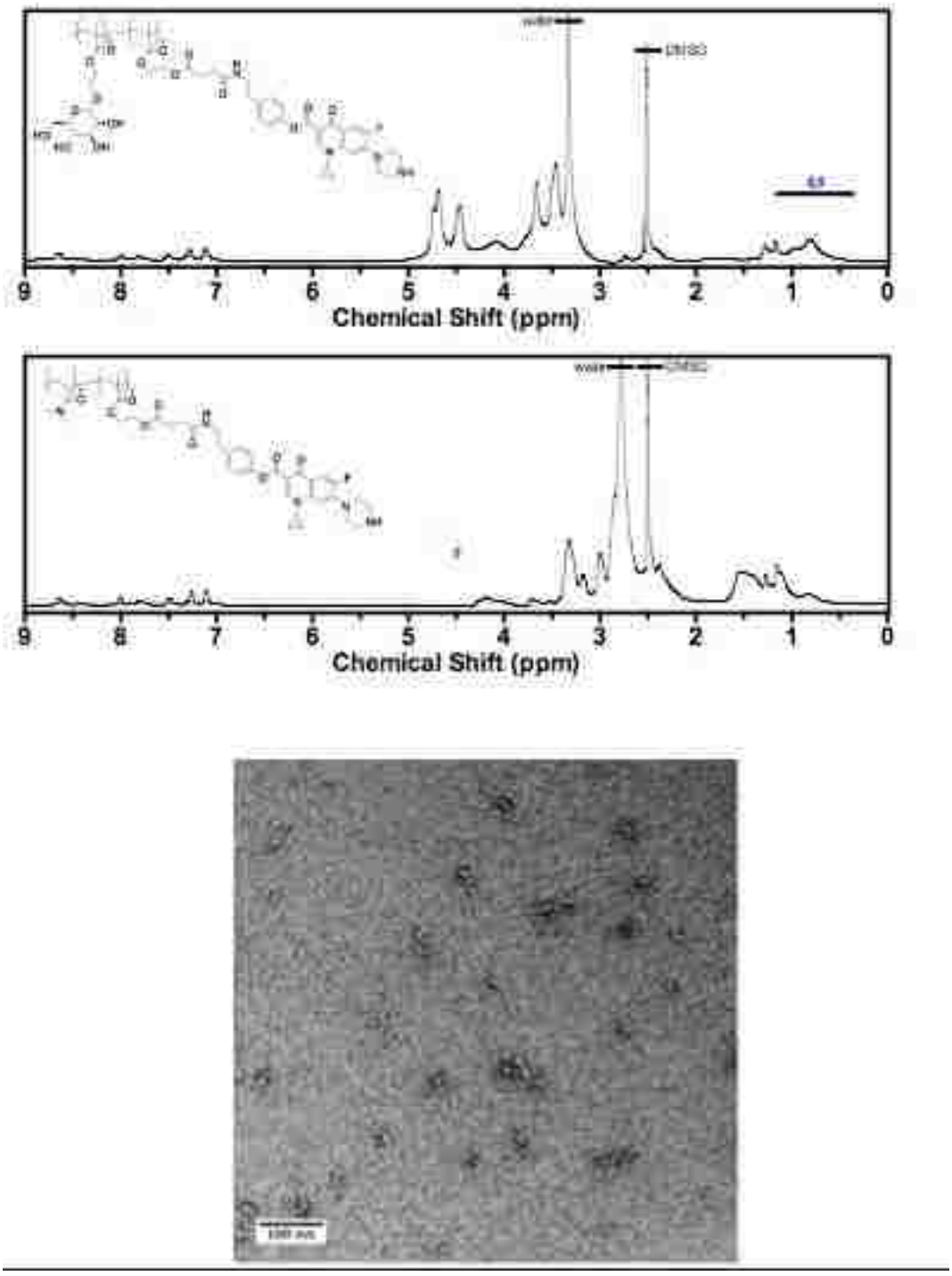

FIGURE 6.5. ^{1}H NMR spectra in D_6 DMSO for (a,b) poly(Man-co-CTM) and (c,d) poly(DMA-co-CTM) as well as the corresponding molecular weight distributions. (e) Transmission electron microscopy images for a poly(Man-co-CTM) RSN.

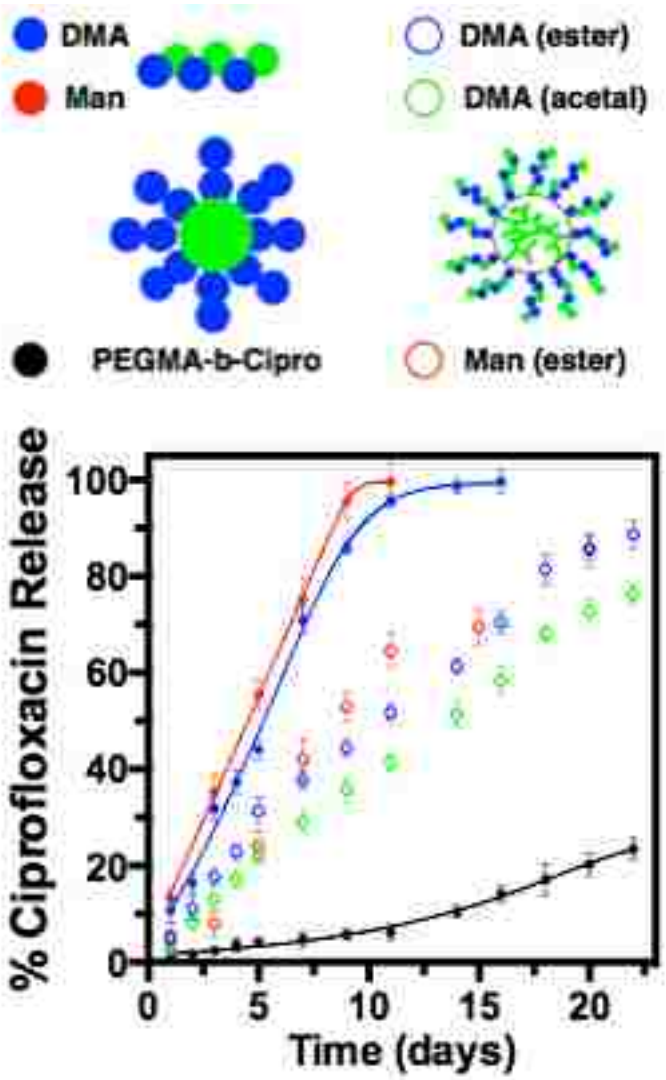

FIGURE 6.6. Ciprofloxacin release from polymers incubated in 100 % human serum at 37 ºC.

Shown in **Fig. 6.6** is the percent ciprofloxacin release as a function of time for polymeric prodrugs incubated in human serum. In this study the rate of antibiotic released via cleavage of the phenyl ester-linked drugs was evaluated as a function of polymer architecture and hydrophilic comonomer. Here the highest rates of ciprofloxacin release were observed for the poly(DMA-co-CTM) and poly(Man-co-CTM), where the amount of the hydrophobic prodrug monomer in the copolymer was limited to approximately 33 wt. %. This composition was observed to yield

copolymers that were easily dispersed in phosphate buffer at concentrations as high as 200 mg/mL with sizes that are consistent with molecularly dissolved unimers. Comparable rates of drug release were observed for both the DMA and Man based copolymers where 50 % drug release was observed at 125 and 110 hours respectively. In contrast ciprofloxacin release from poly(O950-b-CTM), where the hydrophobic prodrug residues are localized in a discrete block copolymer segment, was observed to be quite slow with less than 4 % drug release over the same time period. This result is consistent with our previous studies, where molecularly soluble copolymers of CTM and polyethylene glycol methyl ether methacrylate (FW ~ 950 Da) (O950) showed considerably higher hydrolysis rates than those observed for diblock copolymers where the hydrophobic prodrug monomer was localized in the interior of micelles under aqueous conditions at pH 7.4. Evaluation of the DMA and mannose based RSNs show hydrolysis rates that are slower than the linear copolymers at similar compositions but significantly faster than the hydrolysis rates observed for diblock copolymer micelles. For example, 31.4 hydrolysis was observed for the DMA based RSN polymerized from a poly(hECT) transmer following 120 h incubation in human serum. The corresponds to 7.3 times more ciprofloxacin released than the poly(PEGMA-b-CTM) micelles and only 12.7 % less ciprofloxacin released than the linear copolymer. No dramatic difference in drug release rates were observed between RSN prodrugs prepared from alkyl ester and acetal cores. This result likely arises from the slow rate of RSN degradation relative to the time scale of the hydrolysis experiment and moderately low differences in ciprofloxacin release between the linear and RSN prodrugs. This finding also suggests that more hydrolytically unstable transmer linkages such as hemiacetal ester may provide further enhancements in drug release from RSNs.

Previously, we have shown that primary and immortalized macrophages show distinct differences in mannose receptor expression levels with the primary cells showing significantly higher levels of the receptor. In order to evaluate the ability of the RSN prodrugs to target the macrophage mannose receptor, self-renewing, non-transformed MPI cells were first treated with 30 ng/mL murine GM-CSF to induce macrophage differentiation. Functionally, these cells have been known to closely resemble alveolar macrophages more so than immortalized cell-lines.[1] The cells were then treated with rhodamine B labeled poly(Man-co-CTM) and poly(DMA-co-CTM) RSNs as well as the analogous linear controls for 30, 60, and 120 minutes. To make sure equivalent fluorescence was dosed for all treatment groups, standard curves were produced as a function of polymer concentration. Flow cyotmetry was then employed to evaluate the amount of fluorescence for each treatment group. As shown in **Fig. 6.7A**, cells treated for 30 minutes show an initial but modest increase in fluorescence for both the linear and RSN containing mannose-targeting groups (444 and 2037 respectively) while the untargeted materials show low fluorescence close to untreated controls. Evaluation of the histograms following 120 minutes of treatment (**Fig. 6.7B**) shows a significant increase in fluorescence for mannose-targeted RSN compared to the remaining treatment groups. These differences were observed to be the most apparent at 300 minutes (**Fig. 6.7C**) where the mannose targeted RSN prodrus showed approximately 6 times the fluorescence as the other treatment groups. These results, which are plotted in **Fig. 6.7D**, suggest that the combination of mannose targeting groups with nanoparticle dimensions provide substantially enhanced macrophage binding relative to both mannose targeted linear copolymers and untargeted RSNs.

In order to determine the in vivo biocompatibility of the RSN prodrugs following pulmonary administration, the lung toxicity of endotracheally delivered poly(Man-co-CTM)

prepared from a poly(hECT) transmer core was evaluated using the metrics of animal weight change (**Fig. 6.7E**), tumor necrosis factor alpha (TNF-α) (**Fig. 6.7F**), concentration in lung tissue homogenate (LTH) (**Fig. 6.7G**) and bronchoalveolar lavage fluid (BALF) (**Fig. 6.7H**), and neutrophil infiltration into the lungs. Here mice were dosed with the RSN at 20 mg/kg ciprofloxacin once every 24 h for three-consecutive days. These data demonstrate no statistical differences ($P \leq 0.1$) across all observed toxicity markers at either drug dose for the poly(Man-co-CTM) RSN prodrug compared to PBS controls. As shown in **Fig. 6.7D-G**, three consecutive doses resulted in lavage fluids containing 5.7 ± 1.8 % neutrophils, respectively, whereas PBS controls exhibited 3.7 ± 7.0 % neutrophils. Similarly, TNF-α concentrations in both the LTH and BALF remained low and comparable to PBS control administrations.

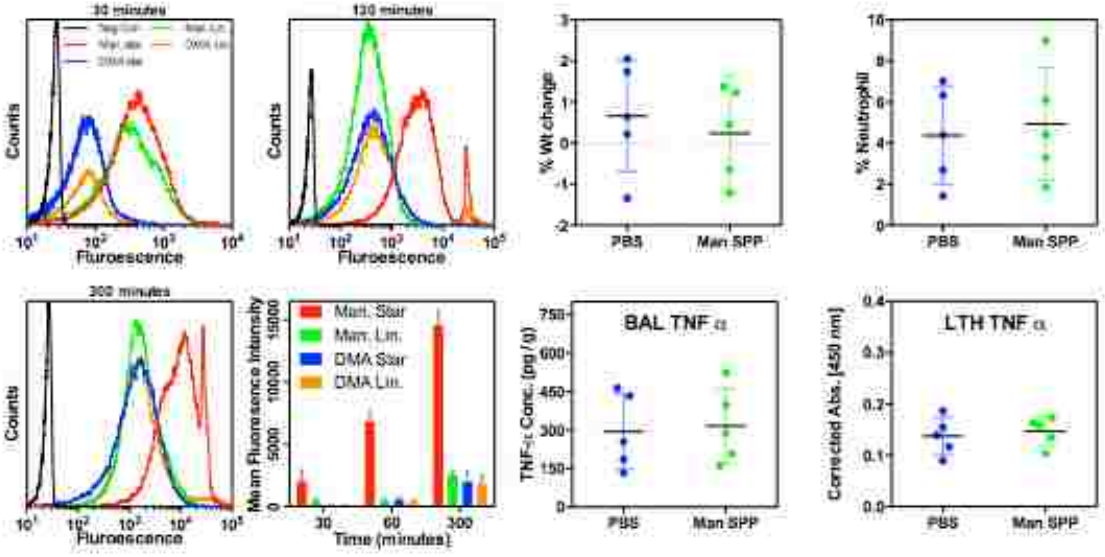

FIGURE 6.7. (a-d) Flow cytometry studies conducted in IL4 transformed RAW264.7 cells comparing the cell binding properties of mannose-targed and untargeted RSN prodrugs as well as the linear controls. (e-h) Pulmonary toxicity of endotracheally delivered poly(Man-co-CTM) RSN prodrugs dosed at 20 mg/kg ciprofloxacin every 24 h over three- consecutive days.

6.4 Conclusion

Homopolymerization of alkyl ester and acetal linked transmers yielded hyperbranched polymer cores with relatively low molecular weights and unimodal molecular weight distributions. Subsequent RAFT copolymerizations from the hyperbranched transmer cores enabled the synthesis of RSNs with high molecular weights, symmetric molecular weight distributions, and low amounts of homopolymer impurity. Hydrolysis studies conducted in acetate buffer from the alkyl ester and acetal linked cores demonstrated the high aqueous stability of the former while the latter showed a progressive degradation into unimeric species over the same period. Drug release studies conducted directly in 100 % human serum showed that the RSN prodrugs provided a substantial increase in ciprofloxacin release relative to diblock copolymer micelles with only a modest reduction in release relative to linear copolymer controls. Flow cytometry studies conducted in RAW264.7 cells induced to express the mannose receptor show significantly higher levels of cell binding for mannose-targeted RSN prodrugs relative to untargeted RSNs as well as both targeted and untargeted linear control polymers. In vivo biocompatibility studies showed no statistical differences between mice treated with mannose-targeted RSNs and phosphate buffer negative control mice. These results taken together suggest that RSNs provide a promising and simple strategy for preparing biocompatible nanoparticle prodrugs with enhanced drug release and receptor binding properties.

6.5 Acknowledgements

This work was funded by the Defense Threat Reduction Agency (Grant #HDTRA1-13-1-0047).

6.6 REFERENCES

53. T. M. Allen and P. R. Cullis, *Advanced Drug Delivery Reviews*, 2013, **65**, 36–48.
54. S. Eliasof, D. Lazarus, C. G. Peters, R. I. Case, R. O. Cole, J. Hwang, T. Schluep, J. Chao, J. Lin, Y. Yen, H. Han, D. T. Wiley, J. E. Zuckerman and M. E. Davis, *PNAS*, 2013, **110**, 15127–15132.
55. J. Cheng, K. T. Khin, G. S. Jensen, A. Liu and M. E. Davis, *Bioconjugate Chemistry*, 2003, **14**, 1007−1017.
56. H. Han and M. E. Davis, *Mol. Pharm.*, 2013, **10**, 2558–2567.
57. K. Cho, X. Wang, S. Nie, Z. G. Chen and D. M. Shin, *Clin Cancer Res*, 2008, **14**, 1310–1316.
58. M. E. Davis, Z. G. Chen and D. M. Shin, *Nat Rev Drug Discov*, 2008, **7**, 771–782.
59. R. K. Jain and T. Stylianopoulos, *Nat Rev Clin Oncol*, 2010, **7**, 653–664.
60. J. A. Alfurhood, H. Sun, C. P. Kabb, B. S. Tucker, J. H. Matthews, H. Luesch and B. S. Sumerlin, *Polym. Chem.*, 2017, **41**, 2545.
61. M. B. L. Kryger, A. A. A. Smith, B. M. Wohl and A. N. Zelikin, *Macromolecular Bioscience*, 2014, **14**, 173–185.
62. M. B. L. Kryger, B. M. Wohl, A. A. A. Smith and A. N. Zelikin, *Chemical Communications*, 2013, **49**, 2643–2645.
63. D. Das, S. Srinivasan, A. M. Kelly, D. Y. Chiu, B. K. Daugherty, D. M. Ratner, P. S. Stayton and A. J. Convertine, *Polymer Chemistry*, 2016, **7**, 826–837.
64. M. C. Parrott, M. Finniss, J. C. Luft, A. Pandya, A. Gullapalli, M. E. Napier and J. M. DeSimone, *JACS*, 2012, **134**, 7978−7982.
65. H. N. Son, S. Srinivasan, J. Y. Yhee, D. Das, B. K. Daugherty, G. Y. Berguig, V. G. Oehle, S. H. Kim, K. Kim, I. C. Kwon, P. S. Stayton and A. J. Convertine, *Polymer Chemistry*, 2016.
66. D. Das, D. Gerboth, A. Postma, S. Srinivasan, H. Kern, J. Chen, D. M. Ratner, P. S. Stayton and A. J. Convertine, *Polymer Chemistry*, 2016, **7**, 6133–6143.
67. F. Joubert, L. Martin, S. Perrier and G. Pasparakis, *Macro Letters*, 2017, **6**, 535–540.
68. J. Sun, Y. Liu, Y. Chen, W. Zhao, Q. Zhai, S. Rathod, Y. Huang, S. Tang, Y. T. Kwon, C. Fernandez, R. Venkataramanan and S. Li, *Journal of Controlled Release*, 2017, **258**, 43–55.
69. M. Danial, S. Telwatte, D. Tyssen, S. Cosson, G. Tachedjian, G. Moad and A. Postma, *Polym. Chem.*, 2016, **7**, 7477–7487.
70. Z. Duan, Y. Zhang, H. Zhu, L. Sun, H. Cai, B. Li, Q. Gong, Z. Gu and K. Luo, *ACS Appl Mater Interfaces*, 2017, **9**, 3474–3486.
71. H. B. Kern, S. Srinivasan, A. J. Convertine, D. Hockenbery, O. W. Press and P. S. Stayton, *Mol. Pharm.*, 2017, **14**, 1450–1459.
72. U. Hasegawa, A. J. van der Vlies, C. Wandrey and J. A. Hubbell, *Biomacromolecules*, 2013, **14**, 3314–3320.
73. D. Das, J. Chen, S. Srinivasan, A. M. Kelly, B. Lee, H.-N. Son, F. Radella, T. E. West, D. M. Ratner, A. J. Convertine, S. J. Skerrett and P. S. Stayton, *A synthetic macromolecular antibiotic platform for inhalable therapy against aerosolized intracellular alveolar infections*, 2017.
74. R. Duncan, *Nat Rev Drug Discov*, 2003, **2**, 347–360.
75. S. Kim, Y. Shi, J. Y. Kim, K. Park and J.-X. Cheng, *Expert Opin Drug Deliv*, 2010, **7**, 49–62.
76. A. Vonarbourg, C. Passirani, P. Saulnier and J. P. Benoit, *Biomaterials*, 2006, **27**, 4356–4373.
77. C. E. Wang, P. S. Stayton, S. H. Pun and A. J. Convertine, *Journal of Controlled Release*, 2015.
78. T. Sun, Y. S. Zhang, B. Pang, D. C. Hyun, M. Yang and Y. Xia, *Angewandte Chemie International Edition in English*, 2014, **53**, 12320–12364.
79. C. J. Hawker, *Angewandte Chemie International Edition in English*, 1995, **34**, 1456–1459.
80. T.-H. Tran, C. T. Nguyen, L. Gonzalez-Fajardo, D. Hargrove, D. Song, P. Deshmukh, L. Mahajan, D. Ndaya, L. Lai, R. M. Kasi and X. Lu, *Biomacromolecules*, 2014, **15**, 4363–4375.

81. D. D. Lane, D. Y. Chiu, F. Y. Su, S. Srinivasan, H. B. Kern, O. W. Press, P. S. Stayton and A. J. Convertine, *Polym. Chem.*, 2014.
82. J. T. Wilson, A. Postma, S. KELLER, A. J. Convertine, G. Moad, E. Rizzardo, L. Meagher, J. Chiefari and P. S. Stayton, *AAPS J*, 2015, **17**, 358–369.
83. X. Wang and H. Gao, *Polymers*, 2017, **9**, 188.
84. M. Zhang, H. Liu, W. Shao, C. Ye and Y. Zhao, *Macromolecules*, 2012, **45**, 9312–9325.
85. J. Schmitt, N. Blanchard and J. Poly, *Polym. Chem.*, 2011, **2**, 2231–2238.
86. A. P. Vogt and B. S. Sumerlin, *Macromolecules*, 2008.
87. Z. Wang, J. He, Y. Tao, L. Yang, H. Jiang and Y. Yang, *Macromolecules*, 2003, **36**, 7446–7452.
88. X. Wang, Y. Shi, R. W. Graff, X. Cao and H. Gao, *Macromolecules*, 2016, **49**, 6471–6479.
89. L. Zhao, X. Wu, X. Wang, C. Duan, H. Wang, A. Punjabi, Y. Zhao, Y. Zhang, Z. Xu, H. Gao and G. Han, *Macro Letters*, 2017, **6**, 700–704.
90. J. Chen, H.-N. Son, J. J. Hill, S. Srinivasan, F.-Y. Su, P. S. Stayton, A. J. Convertine and D. M. Ratner, *Nanomedicine: Nanotechnology, Biology and Medicine*, 2016, **12**, 2031–2041.
91. A. J. Convertine, D. S. W. Benoit, C. L. Duvall, A. S. Hoffman and P. S. Stayton, *J Control Release*, 2009, **133**, 221–229.
92. E.-H. Song, M. J. Manganiello, Y.-H. Chow, B. Ghosn, A. J. Convertine, P. S. Stayton, L. M. Schnapp and D. M. Ratner, *Biomaterials*, 2012, **33**, 6889–6897.

VITA

Debobrato Das did his undergraduate studies at the University of California, Los Angeles where he received a combined B.S./M.S. in Bioengineering in June 2013. At UCLA, Debobrato worked for Dr. Benjamin M. Wu (Dept. of Bioengineering) in tissue engineering and drug delivery. His undergraduate research focused on investigating synthetic biomimetic microenvironments to promote tissue regeneration for ligament repair. Additionally, in his M.S. thesis, Debobrato studied apatite derived nanoparticle formulations for gene delivery for applications in stem cell maturation and conditioning. After completing his studies at UCLA, Debobrato joined the Department of Bioengineering at the University of Washington where he received his Ph.D. in Bioengineering in September 2017. Under co-advisement by Dr. Patrick S. Stayton and Dr. Daniel M. Ratner (Dept. of Bioengineering), his graduate studies focused on engineering inhalable drug delivery systems against lethal pulmonary bacterial infections. Currently, Debobrato is working as a Presidential Post-Doctoral Fellow at the Novartis Institute for Biomedical Research and Massachusetts Institute of Technology exploring drug delivery into the central nervous system.